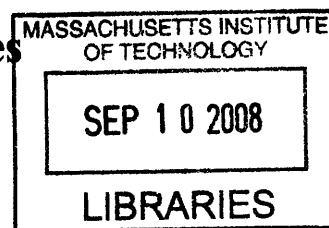# Design and Operation of Microchemical Systems for

Multistep Chemical Syntheses

by
Hemantkumar Sahoo

B. Chem. Eng., University of Mumbai, Institute of Chemical Technology (2003)
S.M. Chemical Engineering Practice, Massachusetts Institute of Technology (2005)

Submitted to the Department of Chemical Engineering
in partial fulfillment of the requirements for the degree of

Doctor of Philosophy in Chemical Engineering
at the

MASSACHUSETTS INSTITUTE OF TECHNOLOGY
September 2008

Author...   ....
Hemantkumar Sahoo
Department of Chemical Engineering
August 26, 2008

Certified by...
Klavs F. Jensen
Department Head, Chemical Engineering
Warren K. Lewis Professor of Chemical Engineering
Professor of Materials Science and Engineering
Thesis Supervisor

Accepted by..
William M. Deen
Carbon P. Dubbs Professor of Chemical Engineering
Chairman, Committee for Graduate Students

Design and Operation of Microchemical Systems
for Multistep Chemical Syntheses
by
Hemantkumar Sahoo

Submitted to the Department of Chemical Engineering on August 26, 2008,
in partial fulfillment of the requirements for the degree of
Doctor of Philosophy in Chemical Engineering

Abstract

This thesis focused on advancing the microchemical field from single device based demonstrations to systems that can perform multi-step series and parallel synthesis. Few examples of micro-separators and micro-pumps suited for miniaturized lab-on-a-chip systems for organic syntheses exist, so the first half of this thesis developed systems for these micro-unit-operations, while the second half demonstrated multistep microchemical operations enabled by these systems.

In-line continuous separation devices are developed that enabled removal of unreacted reagents/byproducts, making it possible to realize a series of reactions without leaving the microreactor environment. Differences in surface forces and preferential wettability characteristics of fluoropolymers are used for phase separation. Such microseparators are used to demonstrate 100% separation of two phase flows of hexane and water, toluene and water, dichloromethane and water, and hexane and methanol. Integrated liquid-liquid extraction devices are microfabricated that performed two-phase contacting by segmented flow, followed by separation – resulting in single stage extraction. Single stage extraction of N,N-dimethylformamide from dichloromethane to water, and from diethyl ether to water is demonstrated.

The development of separators allows microreactors to be connected to microseparators to form microreactor networks enabling reactions and separations in succession. The starting reagents are loaded in syringes and syringe pumps push fluid through the train of microdevices. However, this pumping scheme is limited by pressure constraints at the pump drives as well as the microseparators. Therefore, there is a need to develop in-line pumps to sustain the microdevice network.

Pressure-driven flow is employed for the operation of micropumps. An enclosure with the liquid is pressurized with helium gas, causing the liquid to flow. The dynamics of pressurizing and de-pressurizing an enclosure are modeled and confirmed by experiments. Active and passive control schemes to provide constant flowrate of the liquid are developed and implemented. Different schemes are developed to use the gas pressure to manipulate the flow path of liquids. In one scheme, two enclosures are used together to perform as an in-line pump. The in-line pumps also acted as a buffer to prevent any disturbance propagation, and allowed the upstream and downstream to operate at different flowrates. The pump concept is demonstrated at two scales – 1) microfabricated silicon chips of 40 microliter volume and 2) using glass shell vials of 10000 microliter volume. These pumps are used along with two microseparators to demonstrate two-stage countercurrent and cross-flow liquid-liquid extraction of N,N-dimethylformamide from dichloromethane to water starting with 4.4 mole percent

mixture. The in-line pumps also allowed recirculation with a constant flowrate that enabled long residence time reactions. As an example, peptide synthesis from amino acids, using the Merrifield technique is implemented. Specifically, the pentapeptide, Leuenkephalin is synthesized on different resins simultaneously as an example. A new design for the silicon microreactor for packed bed reactions is developed to enable larger catalyst loadings and offer manageable pressure drops across the packed bed even when the solid loading increased in volume during operation, as is the case with the peptide synthesis experiments. These microchips are also used to study "click chemistry" reactions to synthesize drug-candidate molecules. The packed bed microreactor experiments give higher conversions and better selectivities than batch experiments after the same amount of reaction time as the microreactor experiments provide increased relative catalyst concentration, and reduce side reactions that otherwise reduce selectivity.

As an example of multi-step synthesis involving reactions and separations, the synthesis of carbamates starting from azoyl chloride and sodium azide, using the Curtius rearrangement of isocyanates is performed. This example also demonstrates parallel synthesis of analogous carbamates by introducing branching in the synthesis sequence after the isocyanate production to form microreactor networks. The second reaction involved heat decomposition of the organic azide, and performs faster when catalyzed using solid acid zeolite catalyst in a packed bed microreactor. Continuous operation of the microdevice network for ~ 7-10 days at flowrates of 1-5 μl/min show no change in performance. The microreactor based synthesis is run at higher temperatures than conventional batch scale reactions due to the inherent safety in microreactor based production. The multiple-carbamate-synthesis microreactor network consists of five microreactors and two separators. This demonstration is the first multi-step organic synthesis involving reactions and separations, and showcased the major contributions from this thesis.

The development of micro-unit-operations in this thesis has advanced the microchemical field from single device based demonstrations to systems that can perform continuous-flow multi-step series and parallel chemical synthesis.

Thesis Advisor: Klavs F. Jensen
Title: Department Head, Chemical Engineering
    Warren K. Lewis Professor of Chemical Engineering
    Professor of Materials Science and Engineering

To my parents
Maya and Ramesh
with love

Acknowledgments

Klavs has been a wonderful advisor. I am thankful to him for providing constant encouragement, advice and mentorship, and for being supportive of my ideas. He fostered a great work atmosphere that is the foundation of this thesis. I am also thankful to Professors George Stephanopoulos and Martin Schmidt for their valuable suggestions during and outside committee meetings and for always finding time for discussions despite their busy schedules.

I could not have completed this thesis without Jason, Patrick, and Jon who worked with me on parts of this thesis. I am deeply indebted to Jason for showing me around in my early days at KFJ Group. Patrick's ability to understand the big picture and work independently helped me reach closure on my projects – I am grateful to him for working with me. I am thankful to Jon for the many rigorous and insightful discussions on work-related topics, and the light-hearted discussions on outside issues.

I am deeply thankful to Richard Cook from the Biopolymers Lab at the Center for Cancer Research for the long discussions on peptide synthesis and analysis. His commitment and love for work will always inspire me. Many thanks to Peter Morley of the MIT Central Machine Shop for design suggestions, staff at the Microsystems Technology Laboratories for holding my hand and making me comfortable in the cleanroom, staff at the Department of Chemistry Instrumentation Facilities for NMR help and analytical techniques discussions. I sincerely thank Joan, Alina, Mary & Suzanne for help with all scheduling and paperwork.

I am grateful to the many lab mates I have had over the last five years and who made my time at KFJ Group memorable. Jason, Saif, Jamil, Jane, Andrea, Kishori, Ed, Axel, Nick, Jon, Vicki, Kevin, Sam, Jake, Ryan, Joe Martinelli, and Yongbae – the list is long. Working with them has been a stimulating experience.

Special thanks to Saif for mentoring me early on in the group, Harpreet for providing sound advice on most matters and Jamil for being a sounding board for my ideas during the long lunches. The 10.65 TA experience was rewarding, thanks to a great working relationship with Jane, Arup and Klavs.

Life outside of the lab was welcoming. I am grateful to Kartik, Gunaranjan, Sugata, Joy, Debashis, Jagmeet, Bala, Anjali, Jayku, Amit, and Manish for always being there, for the home-like atmosphere. I will miss all the squash and tennis games with Gunaranjan and Jamil, and the skating and sailing times with many others.

I would also like to thank the many people I met during my stay in Cambridge, without whom, my memories are incomplete.

This thesis is dedicated to my family. My parents, Maya and Ramesh, and my sister, Kavita have been an unending source of motivation. I am grateful to them for everything - their teachings, sacrifices, love, and prayers.

Table of Contents

List of Figures

11

15

List of Tables

1 Introduction, Motivation and Objectives

1.1 Research and development in the chemistry laboratory

A typical, simple experiment in the chemistry laboratory involves adding two reagents in a glass vessel, and analyzing the mixture after some time to look for the distribution of desired and undesired products, and unreacted reagents. Often heating the mixture results in increased rate and may change product distribution, as does adding soluble (homogeneous) or insoluble (heterogeneous) catalysts. The organic and inorganic reactions are studied systematically in a chemistry laboratory with one of the following goals-

- **Understanding chemical mechanism**

    The analysis of products formed, and their distribution gives an insight to the mechanism of reactions, and helps design better reagents to achieve desired products. These studies help increase the fundamental understanding of interactions at the molecular level.

- **New product discovery**

    A strong driving force for chemistry research is to develop new materials or better, economical replacements for existing materials to enable new technologies. Plastics, synthetic drugs, are some from the many examples where new chemistry discovery ushered in a new era. New discovery is done by using fundamental chemistry knowledge and designing directed experiments, or more often by sifting through a library of promising candidates. Though most historical discoveries have been serendipitous, both above approaches aim to increase the chance of an accidental discovery. Screening of a large number of chemical compounds is often performed to look for suitability in an application, such as testing of a number of drug candidates in a pharmaceutical research department.

18

- **Parameter screening**

  Once a chemical reaction of interest is discovered, many reactions are performed at different conditions of temperature, concentration, stoichiometric ratios, solvents, and other related parameters, to find out the condition that best satisfies the objective, i.e. maximize product yield or minimize byproduct or some other similar objective function.

- **Kinetic studies**

  Related to parameter screening, kinetic studies are performed to understand the rate law – the speed of consumption of reagents, formation of products, and its dependence on variables such as pressure, temperature, and concentration. Kinetic information is used to design bigger reactors for large scale production of the chemical product of interest.

For all the reactions performed in any of the stages of research and development, it is of utmost importance to reliably obtain the information being sought, and have no artifacts as a result of the manner of performing these experiments. The apparatus and hardware used in studies is a mere facilitator, and should be such that it does not add additional phenomena so that the required data is either difficult or impossible to obtain. The ideal hardware is the one that is the most convenient to use, allows the researcher to obtain required data from the experiments, and adds no overlying phenomena of its own.

1.2 Chemical Synthesis – The Old Way

Chemical organic and inorganic synthesis has been performed for years in glass apparatus such as the round-bottom flask. Excellent chemical inertness and optical transparency have been their key operational advantages. While these glass systems have been the working horse of the chemistry laboratory for many years, increasing chemistry demands have exposed limitations in their usability. These limitations are –

- **Mass transfer limitations for fast reactions**

  Formation of chemical product involves the two steps of i) reagent mixing, followed by ii) chemical reaction. The rate of mixing is dependant on the scale of operation, reactor design and geometry, while rate of chemical reaction is a function of parameters (such as temperature, concentration ...) that are independent of scale of operation. When the reaction rate is faster or comparable to the rate of mixing, the measured kinetics is not the chemical reaction rate – it is the rate of mixing. Reactor scaleup based on such data often fails. In the lab, though magnetic or overhead stirrers are used to enhance mixing for a fast reaction, concentration gradients exist, and spatial inhomogeneities make it difficult to study fast reactions in traditional glassware.

- **Thermal management of energetic reactions**

  Energetic reactions release a large amount of energy in a very short time. Often in the form of heat, this high energy flux, if not managed properly, results in a runaway reaction. Typical examples of these include oxidation reactions, reactions involving highly reactive chemicals, such as fluorine or reactions involving unstable compounds, such as the high-nitrogen-containing organic compounds. Glass hardware has limited capacity for heat removal because of i) limited heat transfer area per unit volume, and ii) poor thermal conductivity of glass. Hence many interesting high-energy reactions cannot be studied in traditional hardware. Even for reactions that are performed in traditional glassware, but are highly exothermic or endothermic, temperature gradients exist due to the poor thermal characteristics of such hardware, making it difficult to have accurate kinetic data.

- **Batch operation resulting in prolonged times for parameter screening**

  Consider the case where an interesting chemistry has been discovered, and needs to be optimized to find the best operating i) temperature, ii) concentration, and iii) molar excess, for a given solvent, reaction time and catalyst amount. In the simplest method, using prior expertise, one will fix the parameter spans, and pick, say, four temperature

points, four concentrations, and four molar excesses to perform $4^3 = 64$ experiments. Using design of experiments to reduce this number and still capture the trends, say this number is brought down to 16. The batch of operation for most experiments means that after every experiment, the glass hardware needs to be cleaned and dried to perform the next experiment. This process is even more laborious if the chemistry is air or moisture sensitive. Depending on the nature of experiments, it may take up to a week to perform these sixteen experiments and analyze all results. It is possible to speed up the parameter optimization studies by performing experiments in parallel or using automated chemistry platforms. However, the increased experimentation speed comes at the expense of increased resources, and there is not much gain in efficiency, measured as the ratio of results obtained to the resources employed. In order to fundamentally increase the rate of chemistry research, a new model different from the glass apparatus based batch experimentation is needed.

- **Difficulty in performing high temperature and pressure experiments**

  Many organic reactions perform faster at higher temperatures. Increasing temperature to get improved rates works only till one reaches the boiling point of the solvent used for the synthesis. Assuming the reagents or products do not degrade at higher temperatures, one could achieve better rates at even higher temperatures, which can be achieved with the same solvent under pressure to elevate its boiling point. Unfortunately, most standard glassware are not designed to withstand high pressure, so the highest studied temperature is often close to the boiling point of solvent being used. One could use different, higher boiling solvents, but that is not always possible without expecting changes in the reaction itself. It is not a coincidence that most chemical reactions are reported at temperatures near the solvent boiling point. It is because refluxing – the most common way of performing reactions involves boiling the solvent and recycling condensed vapors to maintain isothermal operating conditions. The ability to probe at higher temperature may provide new insights. Most temperature optimization graphs could then be peaks, showing a best point, rather than monotonically increasing graphs that are common in chemistry literature.

In order to overcome the limitations of traditional glassware, new chemistry tools need to have fast mixing, high thermal conductivity, higher specific surface area, continuous mode of operation and ability to handle elevated pressures, without sacrificing the advantages of excellent chemical inertness and optical transparency.

1.3 Microreactors – The New Paradigm

Microreactors were developed in the 1990s[1-6] to address these increasing chemistry requirements. Although the first microreactors developed in the 1970s[7, 8] were developments from the MEMS field, there was a parallel evolution of miniaturized devices and systems for analysis that led to the development of micro-Total-Analysis-Systems (μTAS). Silicon-based microreactors of today are a confluence of the MEMS and μTAS efforts. A microreactor has feature sizes of the order of a few hundred micrometers – hence the name. When these devices are used to perform reactions, they are called microreactors; a general term to use is microdevices, or microchemical devices. Other examples of microdevices include microseparators, and micropumps. As shown in Figure 1.1, a microreactor[9] typically has dimensions of a few centimeters in length and breadth, and is fractions of millimeters in depth. The working volume is defined by long channels, which could be straight or winding, and vary from a few millimeters to several meters in length. The equivalent diameter of these channels is usually always in the order of a few micrometers. The feature sizes are decided by the intended application of the microdevice, and also by the material and method of fabrication.
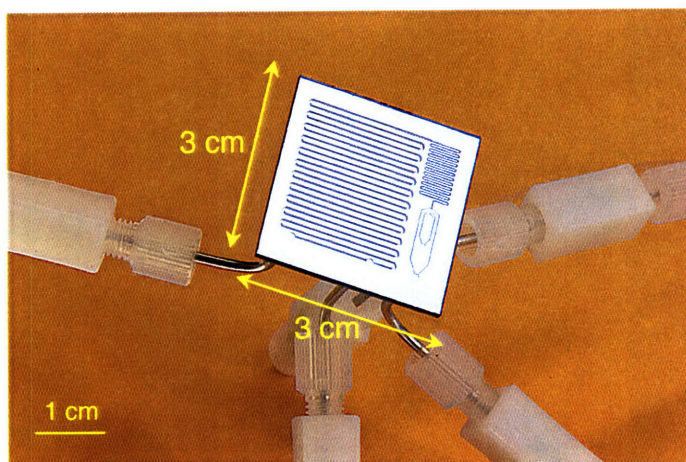
Figure 1.1 Example of a silicon-based microreactor

Microdevices can be made of glass[10, 11], silicon[12], metals[13], ceramics[14], soft polymers[15, 16] and hard plastics[17]. Methods to fabricate[18] these devices include cleanroom microfabrication, micromachining, molding, and stamping. Besides organic chemistry experiments, microdevices are also in use for biological experiments[19], nanoparticle synthesis[20, 21], and energy research[22]. Most devices developed for organic chemistry applications are fabricated from silicon, glass or metals so as to be chemically compatible with the harsh organic solvents often used in synthesis. Most of the work in this thesis uses microdevices fabricated from silicon and glass. Besides providing excellent chemical inertness, thermal conductivity and optical transparency, the silicon based microdevice fabrication uses standard lithography techniques and processes that have been optimized over the years for computer chip manufacturing in a cleanroom environment. The ability to microfabricate silicon devices allows for novel geometry reactors, such as ones with posts, or non-standard shapes. It provides a greater flexibility with reactor designs and functionalities not possible before. As a result, one could design specialized microdevices for specific chemistries. It is also possible to fabricate generic microdevices that find applications in most organic synthesis applications and could be used as the initial step while transitioning from traditional glassware to microdevices, before designing specific microdevices for the specific application.

- **Benefits of silicon-based microdevices over standard glassware[12, 23-25]**

Advantages due to small size-

i) **Improved rates of mixing, and better transport characteristics**

The small feature sizes and the ability to design reactors to limit the mixing distance by methods such as intertwining fluid streams[26-31] offers the much improved mixing rates, thus allowing the study of fast reactions. Higher areas per unit volume at smaller length scales provide correspondingly higher heat and mass transfer coefficients with permits reactions with high heat flux in microdevices.

ii) **Ability of perform high pressure reactions**

Silicon based microdevices are capable of withstanding high pressures, permitting reactions at temperatures beyond the boiling point of the solvents[32]. More than the

device mechanical strength, the connections and packaging method determine the pressure rating. Solder-based connections methods are used to package devices for high pressure operations[33].

iii) Safety of operation and Process Intensification

The small size of reactors permits safer operation of hazardous chemistries as the total amount of material involved is limited. The smaller size and lower thermal masses lead to faster time constants for control of parameters such as flowrate and temperature. Microchemical processes are inherently greener as they reduce chemical consumption and minimize waste generation, are safer to operate and amenable to automation. Microreactors are a thus a tool for process intensification[34], and a step in the right direction as a tool for chemical syntheses as they are operationally better and environment-friendly.

Advantages due to continuous mode of operation-

iv) Rapid profiling of parameter space

Continuous mode of operation permits a number of experiments to be performed in much shorter timespan. The increase in number of experiments is the result of elimination of manual handling, and apparatus preparation in between each experiment because of the ability to quickly change temperatures and concentrations in continuous flow systems. As an example, glycosylation studies were performed in a microreactor in one afternoon, the conventional equivalent of what would have taken about a week[9].

Advantages due to materials used-

v) Chemical compatibility

The chemical inertness of silicon-based devices is the same as that of glass – silicon has a thin native or intentionally grown silicon dioxide (silica) layer, which is the same material as glass. Additionally, the silicon based devices are capped with Pyrex affording visibility of the reaction channels – a feature liked by chemists used to traditional glass apparatus for chemical synthesis.

vii) Thermal conductivity

The high thermal conductivity[35] of silicon (150 $Wm^{-1}K^{-1}$) compared with regular glass (1 $Wm^{-1}K^{-1}$) permits faster supply or removal of heat for endothermic or exothermic reactions. Isothermal operation is also easier as a result preventing thermal gradients that mar kinetic studies.

Highlighting these advantages, a number of chemistry demonstrations in microdevices have been performed, and have helped increase their adoption in the chemistry community. Exothermic, hazardous and difficult reactions such as direct fluorination[36, 37], hydrogenation[38, 39], and ozonolysis[40] have been demonstrated. Many other organic chemical syntheses have been performed in continuous flow microreactors[41-45] utilizing one or more of the advantages mentioned above.

1.4 Thesis Motivation

While microreactors have been shown as a superior chemistry tool for many chemical syntheses than traditional glassware, most applications have remained restricted to single step demonstrations in microchips. Most chemical syntheses, however, involve multiple reaction steps, such as A→B→...→P, before the final product (P) is formed. Moreover, there are workup steps in-between successive reaction steps. Having seen the microreactor potential with individual demonstrations, there is an increasing interest in the chemical synthesis community to advance microchemical systems to higher level applications, such as optimization of multistep syntheses, parallel synthesis of related compounds, scaleup for microreactor based manufacturing of chemical compounds. Unfortunately, most of these applications require the use of microchemical systems for multistep syntheses, the methods for which do not exist.

When a multistep synthesis is performed in batches at the lab scale, the transfer of product after the first reaction, separation of unreacted reagents or byproducts, and addition of new reagents is done manually. On the other hand, when the same chemistry is performed industrially as a continuous flow operation, there is seamless flow of material between different unit operations such as mixing, reaction, heating, and separation. Pumps provide the energy for fluid flow after each unit operation. All unit

operations are standardized, and each operation such as a separation using distillation columns has been extensively studied and understood over many years. There are advanced control systems to maintain set-points and ensure reliable operation.

The strong desire to develop small-scale versions of these unit operations, to realize multistep syntheses in continuous flow microsystems cannot be met by simply scaling down the unit operations. Distillation, for example works on the differences between the boiling points of the different components of a mixture – the more volatile components enrich the vapor phase and flow upwards based on density differences. Small scale operations are fundamentally different, because the surface forces, such as interfacial tension, dominate body forces, such as gravity, i.e. the Bond number (Bo), the ratio of gravitational forces to interfacial forces is much less than 1. Consequently, scale down of distillation fails. Similar arguments apply to most unit operations. Pumping, for example is usually performed using centrifugal pumps on the large scale. The low flowrates and laminar flowrates at the small scale render centrifugal pumps unusable at the microscale.

Therefore, there is strong interest, and an unmet need for a microchemical system that enables multistep syntheses, thereby extending the advantages of microdevices to the entire synthesis train. Such systems would eliminate the manual process of workup and enable reactions with reagents having short lives, and save time otherwise lost between reagent transfers. Development of microchemical system for multistep chemistry is challenging because supporting microdevices such as microseparators and micropumps do not exist, and need to be developed, and combined with microreactors to form the microchemical system. This thesis aims to fill in this void by developing microscale versions of unit operations and using them to demonstrate functioning microchemical synthesis networks.

Previous attempts at extending microreactor uses to multistep chemistries have focused on specific chemistries. As a result, the systems developed have been specific to the chemistries tried, and not universally applicable. The total synthesis of ^{18}F-labeled fluorodeoxyglucose[46] in an integrated microfluidic chip built in poly(dimethylsiloxane) (PDMS) combined five sequential steps: [18]F ion concentration on a solid capture agent, water evaporation through PDMS, radiofluorination, solvent exchange by evaporation through PDMS and replacement, and hydrolytic deprotection in sequential submicroliter

batch quantities. PDMS devices however cannot be used for most organic chemical syntheses. Multistep syntheses of natural products were performed[44, 47], but the workup steps were manual, and off-line. These examples show that multistep syntheses are possible when reactions can be performed sequentially without major workup steps in-between. They also highlight the need for microseparators for more universal multistep chemistries.

Commercial microchemical systems such as the Cellular Process Chemistry Systems[48] (CPC), IMM Microreactors[49], Syrris[10], Micronit Microfluidics[11], Thalesnano[50] and Epigem[17] have been developed noting the demand of industrial and academic chemistry research groups adopting microreactors for chemical studies. These are commercial vendors for microchips in different materials such as glass (Syrris, Micronit), metals (IMM) and polymers (Epigem). They also make systems of microreactors attached together (CPC, IMM) or specialized systems (hydrogenation reactors, Thalesnano). These systems make performing reactions easier, and allow chemists to buy microreactors off the shelf, and focus on chemistry. Almost all these commercial ventures have root in academic groups, and their technologies are products from microreactor based demonstrations performed earlier in academia. (As an example, the hydrogenation reactors called H-Cube commercially available from Thalesnano were first demonstrated earlier in literature[38, 39]). As these systems are trains of reactors alone, they lack workup capabilities.

The real growth in multistep syntheses capabilities will be provided by development of unit operations that support microreactors. Kitamori et. al. have worked to develop micro-unit operations further and have shown two-phase contacting and extraction[51-53] across interfaces. This work illustrates advantages offered due to prevalence of surface forces over gravity to effect separation. However, the techniques work at only very low flowrates, good for the analytical applications they were developed for, but fall short for chemical synthesis. Strong interest in multistep syntheses in microchemical systems is not only in academia, but also in industry[54] for the same applications of research and developments discussed in 1.1. It is understood that current systems are not good enough as supporting components do not exist. There is thus a need to develop robust, reliable and scalable multistep syntheses microchemical systems.

1.5 Thesis Objectives and Layout

This thesis addressed the challenges to further advance the microreactor field to include multistep chemical syntheses. Specifically, the objectives of this thesis included development of microseparators and micropumps, and to use them together with microreactors to construct microreactor networks for parallel and series multistep reactions, and demonstrate the working systems by choosing interesting chemistry examples. Development of the microchemical system along with the fundamental understanding of the operation of its different components is the main technological leap enabled in this thesis.

Two-phase separation development using capillary forces and its application for liquid-liquid extraction is presented in chapter two. The development of a micropump using gas-pressure driven fluid-flow is discussed in chapter three. Multiple separators and micropumps are used together in chapter four to design, develop and demonstrate multistage liquid-liquid extraction. As the first example of multistep chemistry, chapter five discusses solid-phase peptide synthesis using micropump based recirculation techniques. The multistep serial and parallel synthesis of related carbamates involving three reactions and two separations is presented in chapter six. The seventh chapter ties together the accomplishments of this thesis, and details the future direction for microchemical systems research.

2 Two-Phase Separators and Liquid-Liquid Extraction

2.1 Introduction

Performing multistep chemical synthesis on the microscale requires development of reaction and separation techniques in microfluidic devices. Microreactors have been developed for a wide range of chemical applications[24, 45], but further development of continuous flow chemical separators is needed for implementing continuous, multistep microchemical synthesis.

Common separation processes, such as liquid-liquid extraction, are complicated by the need to continuously perform phase separation after mixing and contacting the phases. Traditional continuous phase separation is achieved using a settler tank where differences in density of the two fluid phases drive the separation. However, at the microscale, gravitational forces are small compared with surface forces, so it is difficult, if not impossible, to achieve complete phase separation using differences in density. Thus, alternative forces for driving phase separation must be considered. Surface tension effects are particularly attractive as they dominate gravity and viscous forces at the microscale (i.e., the Bond number (Bo) and the capillary number (Ca) are both $\ll 1$)[55]. Additional issues to address in designing and implementing a microextractor include materials compatibility with aqueous and organic solvents, good mixing for high mass transfer rates, and continuous phase separation.

Categorization of microfluidic extraction devices is typically based on the method of immiscible fluid contacting. Side-by-side immiscible fluids in co-current and counter-current flow arrangement offer the advantages of phase separation by laminar flow splitting and the potential for more than one equilibrium extraction stage, but often have relatively low interfacial surface area to microchannel volume ratios with corresponding modest separation capacity (throughput).[51, 56-61] Maintaining phase separation in these systems is usually achieved by using small interfacial areas to maintain sufficient capillary pressure to counter balance the imposed driving pressure or by modifying wetting characteristics to stabilize interfaces. However, chemically modified surfaces (e.g.

29

by attachment of hydrophobic silanes) can degrade over time either through limited solubility of the coating in the solvent flowing through the device or via susceptibility to chemical attack. For these reasons it is difficult to realize a practical counterflow extractor capable of more than one equilibrium stage. Therefore, it is desirable to develop a method of maintaining phase separation that incorporates microfabrication materials with very different surface properties, such as hydrophilic glass and silicon in combination with hydrophobic Teflon.

Segmented flow facilitates convective mass-transfer between the phases[55, 62-64] and thus enables high overall throughput relative to laminar co-current flow situations, which are typically limited by diffusion to the interfacial area. However, the two phases must ultimately be separated. There have been several approaches to phase separation in microfluidic devices.[61, 62, 65-70] Capillary forces have been demonstrated to be effective means for separating gas-liquid mixtures in microfluidic systems.[63, 71, 72] In these segmented flow applications, channels of 20 μm size were used to selectively separate one phase from the other. The interfacial forces in liquid-liquid systems are often low due to small interfacial tensions, and contact angles of the liquid-liquid-solid interface approach 90° rendering liquid-liquid phase separation with such channel sizes difficult.

In this chapter, liquid-liquid phase separation was realized by using a thin porous fluoropolymer membrane that selectively wets non-aqueous solvents, has average pore sizes in the 0.1-1 μm range (giving high capillary pressures), and has a high pore density giving high throughput. Pressure drops throughout the microfluidic network were modeled and operating regimes for the membrane phase separator were determined based on hydrodynamic pressure drop and capillary pressure forces. A microdevice with a PTFE membrane sandwiched between microchannels illustrates the capillary pressure-induced phase separation behaviour for a hexane-isopropanol-water system.

A silicon-based solvent extraction device that integrates mixing and phase separation processes was also demonstrated. An integrated design decreases the number of device-device fluid connections reducing dead volumes at the expense of increased microfabrication complexity. Chemical separations benefit from integration of mixing and separating as the same steps are used in most chemical extraction processes. Mass transfer rates are similar for small molecules and chemical compatibility is achieved by

using glass or silicon as the material of construction. The integrated devices were realized by using silicon micromachining and modeling served to establish operating limits. The device was capable of completely separating several organic-aqueous and fluorous-aqueous liquid-liquid systems, even with high fractions of partially miscible compounds. In each case, extraction was equivalent to one equilibrium extraction stage.

2.2 Separation principle

Consider a two-phase flow flowing in the microseparator shown schematically in Figure 2.1.
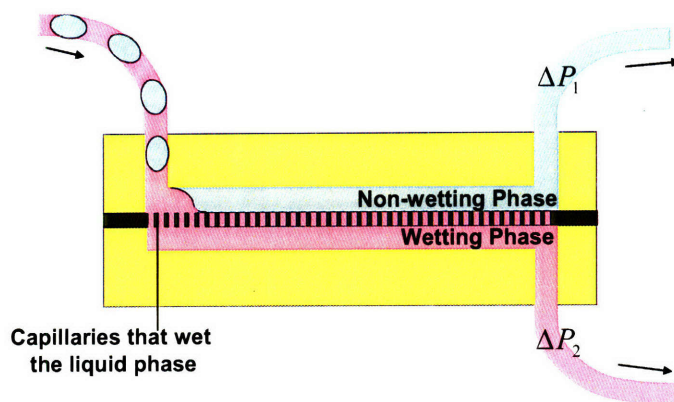
Figure 2.1 Schematic of two-phase liquid-liquid separator. The schematic shows a segmented flow of an aqueous solution (blue) dispersed in an organic phase (pink). The organic phase wets the hydrophobic membrane and is driven through the membrane pores by the imposed pressure difference leaving the aqueous solution behind in the top portion of the device.

As shown in the Figure 2.1, two channels are sandwiched together with capillaries in between them. The capillary material is such that it only wets one phase of the two-phase flow flowing into the microseparator device. The blue-colored phase is the non-wetting phase, while the pink-colored phase is the wetting phase. The backpressures, ΔP_1 and ΔP_2 due to pressure drop from the two outlets are given by the Hagen-Poiseuille equation for laminar flow-pressure relationship. It will be shown later (section 2.5.1) that the pressure-drop on the same side of the capillaries within the separator device, compared ΔP_1 and

31

ΔP_2 to can be ignored. Thus, the pressure difference existing across the capillaries is $(\Delta P_1 - \Delta P_2)$. The wetting phase forms an interface at the capillary inlets with the non-wetting fluid. The pressure required to force this wetting fluid down the capillaries by the non-wetting fluid is provided by the Young-Laplace equation, $\Delta P_c = \frac{2\gamma}{R}\cos\theta$. The pressure drop through the capillaries ($\Delta P_{mem\,flow}$) when the wetting phase flows across it is also given by the Hagen-Poiseuille equation.

The conditions for a working separator are-

1) The non-wetting phase does not cross the capillaries

To ensure none of the non-wetting phase crosses the membrane, the existing pressure difference across the capillaries ($\Delta P_1 - \Delta P_2$) should always be less than that required to flow across, ΔP_c

$$(\Delta P_1 - \Delta P_2) < \Delta P_c$$

2) All of wetting phase crosses the capillaries and flows out the bottom outlet.

To ensure none of the wetting phase goes out the top outlet, the hydraulic flow resistance on the non-wetting side must be much more than that on the wetting side.

Non wetting side flow resistance >> Wetting side flow resistance

For 1:1 volumetric flow, this condition becomes $\Delta P_1 >> \Delta P_{mem\,flow} + \Delta P_2$

For this special case of 1:1 volumetric flow, the two necessary conditions for separation can be combined as $\Delta P_c > (\Delta P_1 - \Delta P_2) >> \Delta P_{mem\,flow}$

These are the overall conditions necessary for complete separation of two-phase flow in capillary separators. These conditions will be analyzed in more detail in section 2.5.1

2.3 Experimental

Two devices were fabricated, one to explore the phase separation principle (Figure 2.2) and the other to examine the phase separation combined with mixing and extraction (Figure 2.3). The proof of principle device was fabricated in polycarbonate and the integrated extraction device was microfabricated in silicon.

2.3.1 Proof of Principle Polycarbonate Device for two-phase separation

Standard machining techniques were employed to fabricate 0.5 x 0.5 x 20 mm channels in two pieces of polycarbonate (Figure 2.2). Inlets and outlets were 0.5 mm holes drilled directly into the channels, and ¼"-28 screws with 1/16" Tefzel tubing (Upchurch Scientific; Oak Harbor, WA) were used for fluid connections. Tubing sizes ranged from 250-1000 μm ID and 10-30 mm long. Typically, 250 μm ID x 210 mm long tubing was used on the aqueous outlet, while 500 μm ID tubing x 210 mm long was used on the organic/fluorous side. A piece of Zefluor membrane (~7x30 mm from 47-mm disk and separated from the support, Pall Company; East Hills, NY) was placed between the two pieces to divide the channels, and compressed using 10 1/16" cap screws.
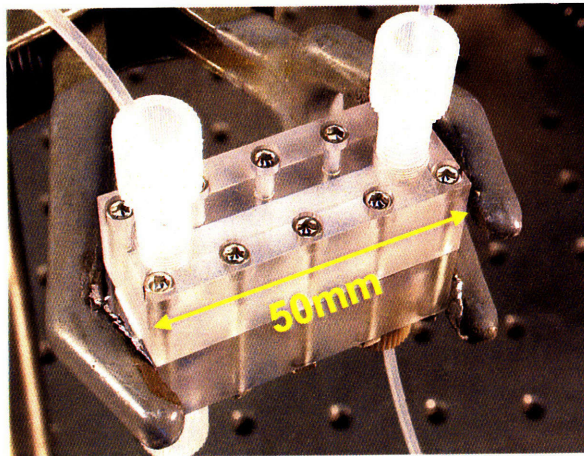
Figure 2.2 Photograph of the proof of principle membrane device fabricated in polycarbonate. The device dimensions are 10 mm width, 50 mm length and 20 mm height.

Flow rates of organic and aqueous solutions were varied between 10 and 2000 μl/min. Hamilton Gastight Syringes (Reno, NV) of 1, 5, and 10 mL volumes were used, and PTFE tubing was connected using luer fittings (Upchurch Scientific, now part of Idex Corp). Hexane (VWR Scientific; West Chester, PA), isopropanol (VWR Scientific), and DI water (from a Milli-Q water system, 18.2 MΩ; Billerica, MA) were delivered by syringe pump (PHD 2000, Harvard Apparatus; Holliston, Massachusetts), mixed and contacted using T-mixers (Upchurch Scientific), and fed to the phase separator.

2.3.2 Integrated Silicon Device for liquid-liquid extraction

A schematic of the device layout shows the mixing, contacting, and separation sections (Figure 2.3). Silicon microdevice processing consisted of micro-machining a silicon wafer using MEMS bulk fabrication techniques (Figure 2.4). Beginning with a 650-700 μm thick (100) double-side polished silicon wafer (Silicon Quest; Santa Clara, CA) coated with 500 nm low-stress nitride, the backside was spin-coated with positive photoresist, patterned, and developed to define the fluid ports and membrane trench. SF_6/O_2 plasma was used to etch the nitride layer, exposing the underlying silicon. Next, the wafer was etched in 25 wt% KOH at 85°C to a depth of 320-340 μm, depending on the wafer thickness.
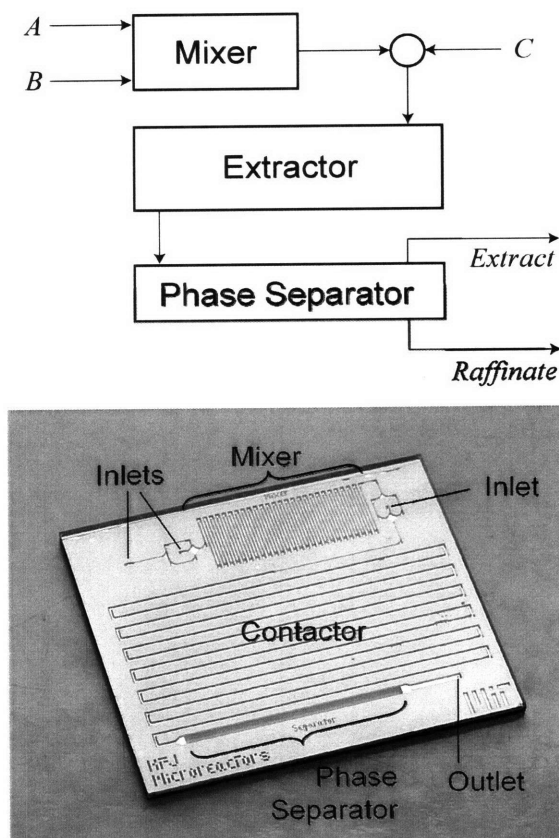
Figure 2.3 Schematic (top) and photograph (bottom) of the integrated extractor device. Fluids A&B are mixed; then contacted with an immiscible liquid C, where the partially miscible component A partitions between B&C. Finally, the two phases are separated by the membrane. The footprint of the device is 35×30×1.5 mm (W×L×H).

The wafer was cleaned with a piranha bath (3:1 concentrated sulfuric acid: 30% hydrogen peroxide), and the frontside was aligned to backside features and patterned using positive photoresist to define the main flow channels for the mixer, contactor, and membrane trench. The frontside silicon nitride layer was patterned and etched the same way as the backside, concurrently etching both sides of the wafer until the inlets met the flow channel, ~190 μm on both sides. The wafer was cleaned and 49% HF was used to etch the remaining nitride. Finally, a 762 μm thick Pyrex 7740 wafer (Bullen Ultrasonics; Eaton, OH) was anodically bonded to the frontside of the silicon device and individual devices (Figure 2.3) were obtained after the silicon wafer was cut using a diesaw. Using KOH etch processing to define flow channels can result in the over-etching of exposed convex silicon corners due to the significantly faster etch rate of the <411> crystal plane compared to the <100> (~1.5x).[73] Low-stress nitride as the KOH mask layer was used and small "tabs" were added at these exposed corners to significantly reduce the amount of overetching (Figure 2.5).[74]
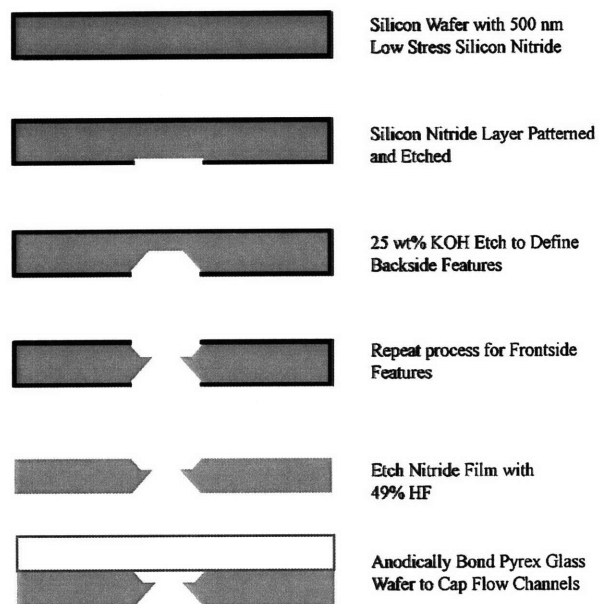
Figure 2.4 Silicon microfabrication process
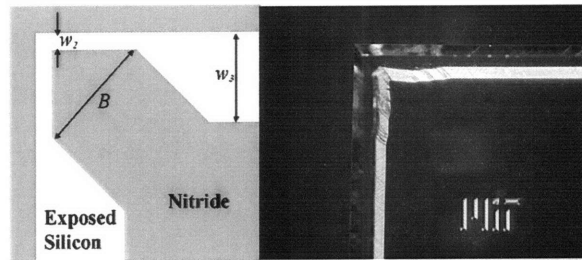
Figure 2.5 Photo mask structures (left) designed to compensate for the fast etching rate of the exposed convex corners during the KOH etch process. The resulting corners after KOH etching (right) show little edge erosion.

Table 2.1 Silicon Device Dimensions

Section	Depth (µm)	Width (µm) (at the top surface of the silicon wafer)	Length (µm)
Flow ports	500	750	Not applicable
Mixer	71	100	350
Contactor	156	300	400
Separator	648	1000	21

The size of the tabs was calculated using a correlation described elsewhere,[74] with a channel width (w_1) of 300 µm and a gap width (w_2) of 25 µm. As a rule of thumb, it was found that the method of using tabs to protect the convex corners allowed a maximum etch depth of ~0.6-0.7 times the channel width. Finally, a 150 mm Pyrex 7740 wafer (Bullen Ultrasonics) was anodically bonded to the device wafer and the stack was diced into individual devices measuring 35×30×1.5 mm. Each section of the device contains channels of different size and length (Table 2.1).

2.4 Liquid-liquid extraction experiments

Fluids were delivered using Harvard Apparatus syringe pumps. DI water (Milli-Q) and N,N-dimethylformamide (DMF) (Sigma-Aldrich; Milwaukee, WI) were loaded into plastic syringes (B&D Scientific; Franklin Lakes, NJ), and the organic solvents

dichloromethane (DCM) and diethyl ether (Sigma-Aldrich) were loaded into a removable needle Hamilton Gastight syringe. Typical flowrates of the aqueous and organic phases were 25 µL/min each, and DMF flowrates were varied from 0-2.5 µL/min.

2.4.1 Packaging

A custom microfluidic chuck was machined from glass-filled PTFE and polycarbonate (McMaster-Carr; Atlanta, GA). PTFE O-rings measuring 3/16" OD (PTFE AS568A-003, McMaster-Carr) were used to seal the fluidic connections and the 0.5 µm pore PTFE membrane (Pall) was cut to ~ 8×25 mm from a 47-mm disc and compressed between the trenches on the chuck and silicon device. Fluid connections on luer-type syringes were made using luer fittings (Upchurch Scientific, now Idex Corp), while Valco fill ports (VISF-2; Houston, TX) were used on the Hamilton Gastight syringe. 1/16" OD PTFE tubing with 0.01"-0.02" ID and ¼"-28 screw fittings were used to connect to the fluid chuck in all cases (Figure 2.6).
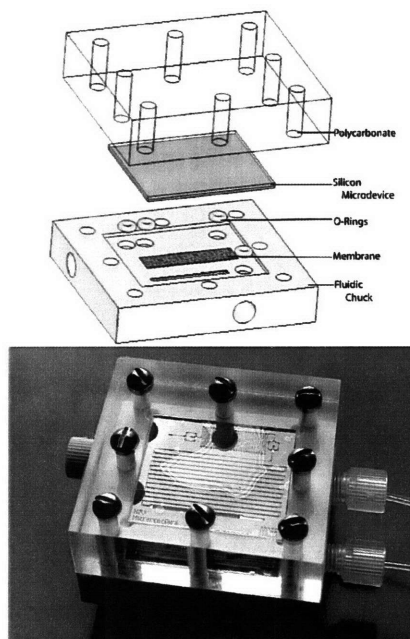
Figure 2.6 Exploded schematic view of the microfluidic device and packaging (top), and final packaged silicon device (bottom). The membrane and silicon microdevice are sealed by compression using Teflon o-rings with the fluid chuck and polycarbonate top plate. 1/16" PTFE tubing and fittings are screwed into to the chuck.

2.4.2 Analytical

For phase separation-only experiments, visual inspection of the outlet fractions was used to confirm no immiscible phase passed to the wrong outlet. The use of red and blue dyed aqueous pH 4 and 10 buffers (VWR Scientific) made this straightforward. Videos were also obtained for qualitative analysis using a COHU 2222-1000 color CCD camera (COHU; Poway, CA) and a Leica stereo-microscope MZ12 (Leica Microsystems Inc.; Bannockburn, IL).

For extraction analyses, HPLC (Waters; Milford, MA) with a reverse phase C-18 column and 0.1 M aqueous monobasic phosphate buffer at 1 mL/min for the aqueous extract was used. A calibration curve of the concentration vs. absorbance at 220 nm was prepared for known concentrations of extractant (DMF, VWR Scientific) in de-ionized water to quantify results. 25-100 μl of each sample was diluted in 900 μl of water and run 3 times. Variation in area counts between runs was less than 3% and typically less than 1%. The measured concentrations were then scaled by the dilution factor to give the concentration of the sample.

2.5 Results and Discussion

2.5.1 Liquid-Liquid Phase Separation Using Capillary Forces

The immiscible liquids are delivered to the membrane separator where selective wetting and capillary pressure are used to induce and maintain separation of the two phases. A sufficient difference in the surface wetting by the two immiscible phases is required to drive the phase separation. For example, no suitable materials were identified for separating organic (hexane) and fluorous (perfluorohexane, Lancaster Synthesis, Inc.; Pelham, NH) phases, but either of those phases could be separated from water. Materials studied included PTFE (Pall), cellulose (filter paper, VWR), and ethyl acetate (Sigma Aldrich). The aqueous phase, which does not wet the PTFE membrane, passes across the membrane surface to outlet 1 while the organic/fluorous phase wets and flows through the pores of the membrane to outlet 2 (Figure 2.1). The pressure drop due to laminar flow is given by the Hagen-Poiseuille equation.

$$\Delta P = \frac{8\mu QL}{\pi R^4} \quad (1)$$

The pressure drop from the aqueous phase outlet 1 to the point of collection of the separated aqueous phase is ΔP_1. Denoting Q_{tot} as the total flowrate of the two phase fluid flow, Q_1 is the aqueous phase flowrate and Q_2 is the organic phase flowrate, R_1 and L_1 are the outlet tubing radius and length, respectively. There are two extreme cases based on the duration of segments relative to the length of the membrane separator: (i) small alternating aqueous and organic segments, and (ii) large aqueous segments followed by large organic ones. In the first case, the flowrate through the outlet 1 will be Q_1 as all the organic phase that comes with the aqueous phase goes through the membrane and out from outlet 2. In the second situation, when the aqueous phase is longer than the separator region, there is no flow through the membrane when the aqueous segment is in the separator and the flowrate through the outlet 1 will then be Q_{tot}. Actual operation falls between the two cases, but flow through outlet 1 can be approximated as Q_{tot} to obtain a worst case design criterion. ΔP_1 is then given as:

$$\Delta P_1 = \frac{8\mu_1 Q_{tot} L_1}{\pi R_1^4} \quad (2)$$

An order of magnitude analysis shows that the pressure drop due to flow in the channel on the aqueous side in the separator device ($\Delta P_{aq,mem}$) is very small compared to ΔP_1:

$$\frac{\Delta P_{aq,mem}}{\Delta P_1} = \frac{\dfrac{8\mu_1 Q_1 L_{sep}}{\pi R_{sep}^4}}{\dfrac{8\mu_1 Q_1 L_1}{\pi R_1^4}} = \frac{L_{sep}}{L_1}\left(\frac{R_1}{R_{sep}}\right)^4 \sim \frac{21\,mm}{210\,mm}\left(\frac{0.25\,mm}{0.66\,mm}\right)^4 \sim 0.002 \quad (3)$$

Consequently, $\Delta P_{aq,mem}$ needs not be included in further analysis and the pressure at any point on the aqueous side of the membrane is approximately ΔP_1. The pressure drop through the membrane (ΔP_m) and organic outlet tubing (ΔP_2) are also described by the Hagen-Poiseuille equation. By a similar order of magnitude estimate (3), the pressure at any point on the organic side of the membrane is approximately ΔP_2. The pressure drops through outlets 1 and the sum of the membrane and outlet 2 must equal since the two fluid streams exit at the same ambient pressure. The total flowrate must also be conserved.

39

$$\Delta P_1 = \Delta P_m + \Delta P_2 \tag{4}$$

$$Q_{tot} = Q_1 + Q_2 \tag{5}$$

$$\frac{8\mu_1 Q_{tot}}{\pi R_1^4} L_1 = \frac{8\mu_2 Q_2}{\pi n R^4} L_m + \frac{8\mu_2 Q_2}{\pi R_2^4} L_2 \tag{6}$$

The fluid viscosity is μ, L is length of the flow path, and n is the number of capillaries through which fluid is flowing. The membrane has a high pore density ($\sim 10^8$ pores/cm^2), reducing hydrodynamic resistance of the wetting phase by distributing the flow. The number of active capillaries (n) was typically much less than the actual number of capillaries present (~ 1-10%), but this provides an upper limit for operation. If cylinders are used to represent the membrane pores, the capillary pressure (ΔPc) is:

$$\Delta P_c = \frac{2\gamma}{R} \cos\theta \tag{7}$$

where γ is the interfacial tension, R the pore size, and θ the wetting angle. Typical pore sizes in the membrane were ~ 0.5 μm according to the manufacturer.

The minimum pressure needed to overcome the capillary pressure difference and force the aqueous phase through the membrane is ΔPc, whereas the real pressure difference between the two sides of the membrane is $\Delta P_1 - \Delta P_2$. As the capillary pressure difference prevents the non-wetting phase from penetrating the porous membrane surface, the condition for the aqueous phase to not cross the membrane is

$$\Delta P_c > \Delta P_1 - \Delta P_2 \tag{8}$$

Using Equations (4) and (7), this condition can also be written as

$$\Delta P_c > \Delta P_m$$
$$\gamma \cos\theta > \frac{4\mu_2 Q_2}{n\pi R^3} L_m \tag{9}$$

The Hagen-Poiseuille equation in terms of fluidic resistance (k) can be written as

$$Q = \frac{\Delta P}{k}$$
$$k = \frac{8\mu L}{\pi R^4} \tag{10}$$

The condition where the organic/fluorous phase does not flow through outlet 1 is now established next. As the organic/fluorous phase wets the membrane, it can flow out

through any outlet, and the only way to prevent it from flowing out through outlet 1 is to provide a much larger fluidic resistance for flow through the undesired outlet. Thus, $k_1 \gg k_2$ as given in equation (11).

$$\frac{8\mu_2 L_1}{\pi R_1^4} \gg \frac{8\mu_2 L_m}{\pi n R^4} + \frac{8\mu_2 L_2}{\pi R_2^4}$$

$$\frac{L_1}{R_1^4} \gg \frac{L_m}{n R^4} + \frac{L_2}{R_2^4}$$

(11)

The two conditions must be satisfied for successful operation of the device, specifically:

(i) The pressure difference between the aqueous and organic sides of the membrane should be less that the capillary pressure difference, and

(ii) The combined organic side fluidic resistance should be much lower than the aqueous side fluidic resistance.
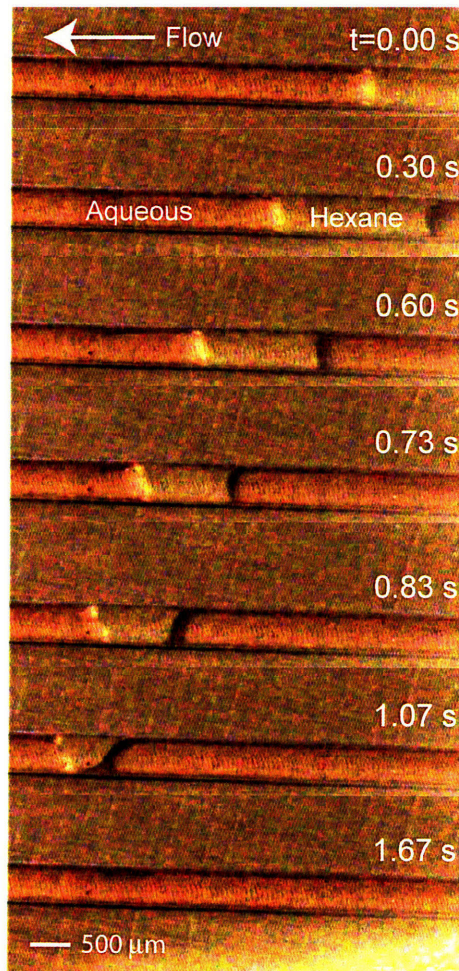
Figure 2.7 A series of images looking down onto fluids flowing atop the membrane. The images were captured from video of co-flowing immiscible aqueous (red) and hexane (clear) phases passing over the PTFE membrane. The hexane passes through the membrane and "disappears" from view. The total flowrate was 100 μl/min.

In a typical liquid-liquid phase separation, the interfacial tension term ($\gamma\cos\theta$) was estimated to be ~0.005 Nm^{-1} and an average pore size (R) to be 0.5 μm, giving a capillary pressure (ΔPc) of ~20 kPa. If the aqueous outlet tubing is 210 mm long with a 250 μm ID, the flowrate (Q_{tot}) can be ~100 μL/min ($\Delta P_1 \sim 3.65$ kPa). For the second (wetting phase) outlet, the tubing diameter and length are typically 500 μm and 210 mm, giving a pressure drop (ΔP_2) of 0.23 kPa. Using Equation (4) yields ΔP_m as 3.42 kPa. Using equal aqueous and organic volumetric flowrates and solving for n using this value of ΔP_m gives $n \sim 10^6$ pores. The separation membrane exposed to flow was 1 mm wide and 21 mm long (Table 1), having a pore density of ~ 10^8 pores/cm^2. Therefore, ~5 % of the total available pores were typically active for separation leaving room for additional separation capacity.

For each immiscible liquid-liquid system studied, the wetting fluid phase (e.g. organic, fluorous) was observed to pass through the membrane, while the aqueous phase did not enter the membrane and flowed out a second outlet (Figure 2.1). As an example, Figure 2.7 illustrates a series of images looking down onto fluids flowing atop the membrane. Hexane (clear phase) passes through the membrane and "disappears" from view. The supporting electronic file shows a movie of the liquid-liquid phase separation.

2.5.2 Effect of Reduced Interfacial Tension

The influence of lowering the interfacial tension on separation capacity was investigated experimentally with the polycarbonate device. The volumetric flow ratio of hexane and water was kept at 1:1, while isopropanol (IPA) was added to hexane using a T-mixer (Upchurch) to lower the interfacial tension. The droplet sizes ranged from relatively large (~5 μL) to small (~1 nL). It was not attempted to tightly control the segment sizes in order to mirror typical extraction conditions expected in routine

microchemical applications. Moreover, the variation introduced by the different segment lengths will reduce as $\frac{1}{\sqrt{N}}$ with increasing number of segments (N) passing through the device. The maximum operating flowrate decreased significantly with increasing IPA vol%, though the polycarbonate device was still capable of separating in excess of 100 μL/min of total fluid flow at 17 vol% IPA (Figure 2.8). At higher concentrations of IPA, the interfacial tension decreases to a value at which point the Equation (9) is no longer valid and complete phase separation is no longer possible.
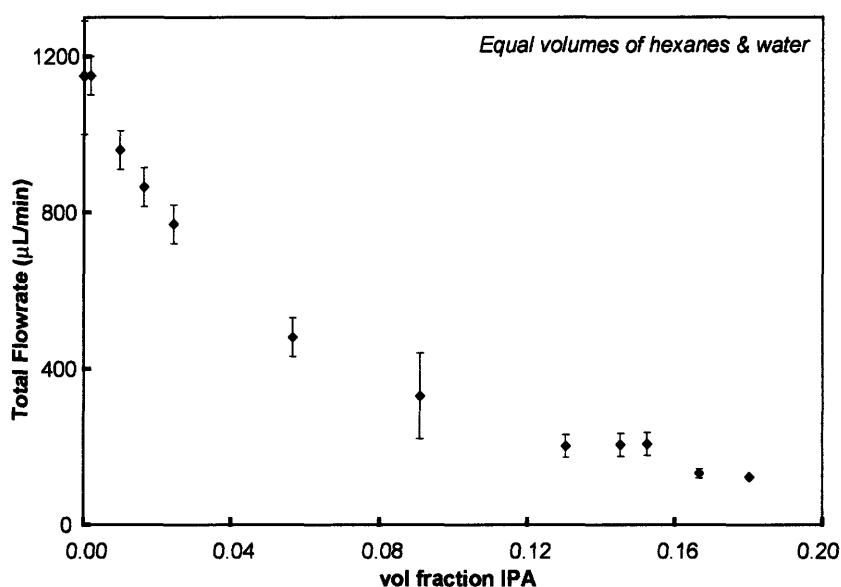
Figure 2.8 The effect of lowering the interfacial tension on phase separation performance was studied by adding IPA to a flow of hexane/water. The maximum operating flowrate decreased significantly with increasing IPA concentration.

2.5.3 Integrated Liquid-Liquid Extraction Device

In the design for the integrated liquid-liquid extraction device fabricated in silicon, characteristic times for mixing, contacting, and phase separation were estimated to aid in characterizing device performance. Mixing of miscible components is sometimes necessary in solvent extraction processes. In a solvent switch process, for example, a reagent and its initial solvent are mixed with a new miscible solvent before the initial solvent can be extracted. The mixer design was based on diffusive mixing of co-flowing

43

streams, with flow splitting and lamination used to reduce the diffusive path length by half.[31] The KOH-etched channel in this section was 340 mm long and 100 µm at the top, or ~ 50 µm at the channel centre. Using typical liquid diffusivities (~10^{-9} m^2/s), the mixing time was estimated as ~0.6 seconds and the maximum operating flowrate as ~120 µL/min.

Liquid-liquid mass transfer is accomplished with segmented flow of immiscible aqueous and organic/fluorous phases. The mass transfer coefficient for the Taylor flow of segments in capillaries is used, based on penetration theory[75]. Only the species flux at the end (cap) of the segment is considered as the most conservative estimate for this design:

$$k_L a = \frac{8\sqrt{2}}{\pi(L_1 + L_2)} \sqrt{\frac{DU}{d_{hyd}}}$$ (12)

The hydraulic radius (d_{hyd}) is used to simplify the analysis. The shape of the channel is trapezoidal with all sides between 100-300 µm, suggesting that this characteristic dimension will be sufficient as a first-order approximation.

$$d_{hyd} = \frac{4A}{P} = 4\frac{\left(H/_2 (w_1 + w_2)\right)}{w_1 + w_2 + 2s}$$ (13)
$$s = \sqrt{H^2 + 0.25(w_1 - w_2)^2}$$

The internal recirculation of the segment affects the mass transfer rate because of surface renewal. For our system, characteristic model parameters[76] gave a recirculation mass transfer coefficients ($k_L a$) of 0.26 s^{-1}. A conservative estimate of the time to reach equilibrium is ~20s using the characteristic parameters. Therefore, the maximum expected operating flowrate for this system before mass-transfer effects are observed is ~50 µl/min. The conservative design estimate implies that equilibrium is reached in the system at flowrates lower than this value.

2.5.4 Solvent Extraction

Large amounts of equilibrium data have been compiled for partially miscible systems and help simplify solvent selection for extraction.[77] As a model system, extraction of N,N-dimethylformamide (DMF) from an organic phase into water was chosen.

Dichloromethane (DCM) and diethyl ether (DEE) were each used as the non-polar organic solvent and the DMF fraction in the organic stream was varied from 1-20 mol%. The partition coefficient did not change significantly over this concentration range, as indicated by a linear plot of aqueous extract DMF mol fraction vs. the initial organic DMF mol fraction (Figure 2.9).

The concentration of DMF was measured in the aqueous extract stream and a mass balance was performed to calculate the extraction yield. For a system with a constant partition coefficient, the extraction yield is constant. The extraction yield values obtained from the microfluidic device agree well with the equilibrium data obtained from shake-flask experiments for these two cases. Hence, longer extraction times will not improve the yield. The DCM/DMF/water values also agreed well with those reported in the literature.[78] Thus, each device is capable of a single equilibrium extraction stage.
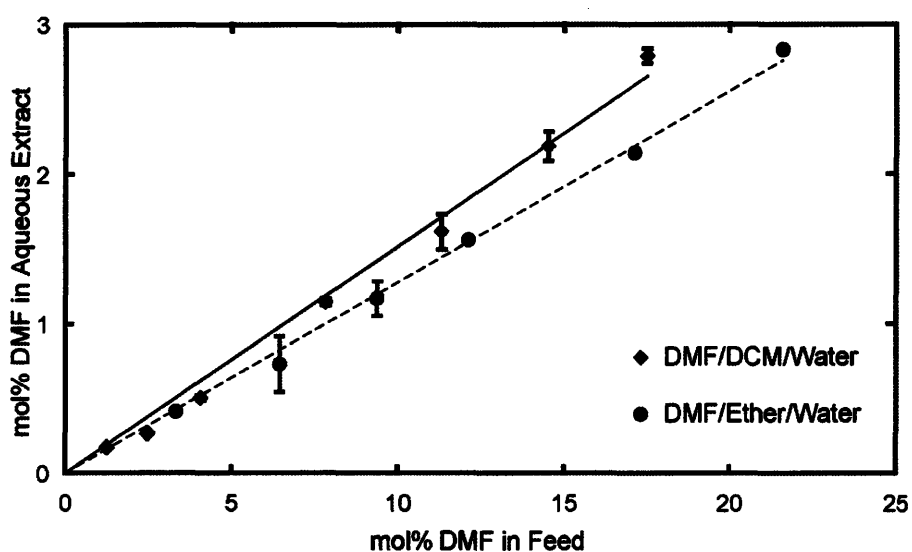
Figure 2.9 The partition coefficients of DMF in the DCM/water and DEE/water systems are nearly constant at low to moderate DMF concentration as evidenced by the linear increase in aqueous extract concentration vs. the feed concentration.

Using multiple extractor units in series would improve extraction of the partially miscible component.[79] Assuming constant single-stage extraction yield, a process with a single stage yield of 60% will therefore remove ~94% of the undesired species in 3 stages.

2.6 Conclusions

The reported extraction devices represent a step towards developing continuous microchemical separations for multistep synthesis processing. Surface forces provide continuous separation of immiscible liquids in microfluidic devices when they are balanced appropriately by fluid flow pressure drops; specifically, the capillary pressure difference must be much greater than the pressure used to drive the fluid flow through the device, and the pressure drop for the two fluid outlets must be adjusted so that the membrane non-wetting phase experiences a larger pressure drop than the membrane wetting phase. A thin, porous, PTFE membrane enables quantitative phase separation by being hydrophobic and having high density of micron sized pores. The use of a hydrophobic membrane circumvents surface modifications of the device and has the additional benefit that the membrane can be replaced if it becomes plugged by impurities. As a demonstration, a membrane device was capable of complete phase separation of aqueous/organic and aqueous/fluorous systems, even with high fractions of partially miscible components significantly lowering the capillary pressure.

Phase separation was implemented with mixing and liquid-liquid contacting to create an integrated microfluidic liquid-liquid extraction unit operation. The device was manufactured using silicon micromachining and packaged with the membrane using compression sealing. In this device, solvent extraction of DMF from DCM and diethyl ether to an aqueous phase was performed and found to be equivalent to one equilibrium stage. Because of the devices' robustness, chemical compatibility, and ease of use, this technique can be used with a wider range of chemistries and operating conditions. If the pressure drops are controlled according to the design guidelines, multistage extraction can be performed using multiple devices in series. Thus, it should be possible to conduct continuous processing and achieve the same extraction yield as multiple shake-flask extractions performed during traditional chemical workup.

3 In-line Pumps for Microchemical Systems

3.1 Introduction and Motivation

As discussed in chapter 1, several promising devices have been developed previously for applications in chemistry and biology. Further development of lab-on-a-chip applications involves connecting these individual microfluidic devices to form a microchemical system, capable of performing many more steps of an organic synthesis than currently possible. Current synthesis steps involve use of a syringe pump upstream of all devices. The syringe pump operates by displacing a fluid in a syringe through controlled piston movement to deliver a desired fluid flow rate. This works well as long as the number of devices connected downstream of the syringe pump is less, about five at the most. As the number of devices connected increases, the syringe pump starts reaching its limit to provide energy to overcome the increasing pressure drop through multiple devices. Specialized, high pressure syringe pumps exist, for such applications (such as those by Teledyne Technologies, Inc.), but their high cost makes it prohibitive to have multiple such pumps in a typical laboratory. Many times, use of such high pressure pumps is further complicated by the existence of capillary separators in the microreactor network. As discussed in chapter 2, these separators have pressure constraints and they do not work properly if the imposed pressure exceeds design limits. Many microfluidic pumping devices have been developed[80-82], such as those by Quake, but they all provide non-constant flow, and use soft polymers incompatible with most organic solvents. They also provide very low flowrates (order of several nanoliters per minute), so are inadequate for the chemical synthesis applications.

As the number of devices starts increasing, the current method of having one pump at the start does not work as a result of pressure constraints on each individual device (such as a separator) and limits on pumping capacity of existing syringe pumps. These problems are further accentuated when the microreactor network is used for small-scale chemical synthesis, and involves reactions having slow reaction rates. Flowrates of the order of a few milliliters per minute (for small-scale synthesis) coupled with the longer residence time (due to slow reaction rates) results in significant pressure drop. Thus, there

is a need for micro-versions of in-line pumping devices, similar to the feed charge pumps in the conventional chemical industry before each unit operation. It would help maintain the pressure at all points in the system below a critical pressure (P_C), beyond which, individual devices start failing (Figure 3.1). Such pumps need to be compatible with most chemicals and provide steady flow with a wide range of operation.
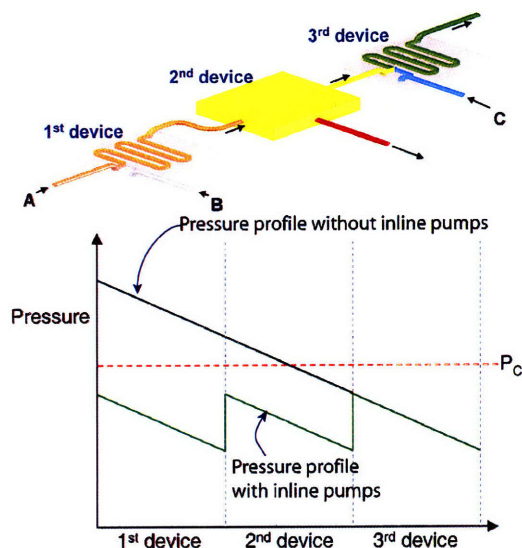
Figure 3.1 Pressure profiles in a three-unit system with and without in-line pumps

In-line pumps increase the pressure energy of a fluid stream in-between two unit operations (Figure 3.1). In conventional chemical manufacturing, centrifugal pumps perform this function. However, for microchemical continuous multistep synthesis, centrifugal pumps cannot provide the low flowrates (order of µl/min) necessary. Peristaltic pumps have often been used in this flow regime in medical applications. However, they have two shortcomings that render them unsuitable for organic synthesis – Firstly; peristaltic pumps provide pulsating flow. This non-constancy of flow alters the residence time of reactions, and also changes the pressures in the system affecting device performance, such as separation operation. Secondly, peristaltic pumps need flexible, compressible material for peristaltic action. It is difficult to find mechanically stable, chemically compatible material for the harsh chemical solvents often used in synthesis and separation steps. The micropumps developed by Quake also cannot be used for the same reasons.

In this work, pneumatic pressure is used to pump liquid. Pressure driven flow techniques have existed before[83] to flow liquid out from liquid reservoirs upstream of all devices to replace syringe pumps, thus providing much constant flow than syringe pumps. Use of pressure driven flow to enable in-line pumps is discussed in this chapter. The pressure driven flow work required further design and development to function as in-line pumps. In this work, chemically compatible, mechanically and functionally robust in-line pumps capable of providing a wide range of substantially constant flowrates are designed, developed and demonstrated.

3.2 Pressure driven flow

A pressure driven flow setup consists of a small enclosure (such as a microchip with a cavity, or a glass vial) with connections as shown in Figure 3.2. The gas inlet is connected to a source such as a gas cylinder, and is at a constant high pressure P_1. R_1 and R_2 represent the resistance to flow in the respective sections of the gas line. When the valve is open, the head space in the enclosure attains pressure P_2 given by $P_2 = P_1\left(\dfrac{R_2}{R_1 + R_2}\right)$. This relationship is derived in Appendix A. As the pressurizing of the enclosure is a first order charging equation, the time it takes to reach 99.3% of steady state is $5\tau_1$ ($\tau_1 = \dfrac{V}{RT}\dfrac{R_1 R_2}{R_1 + R_2}$). The time it takes to decay back to the ambient atmospheric pressure from the steady state pressure P_2 after the high pressure gas inlet is closed, is $5\tau_2$ ($\tau_2 = \dfrac{V}{RT}R_2$)($V$ is the headspace volume, R the Universal Gas constant and T represents the temperature of operation).

49
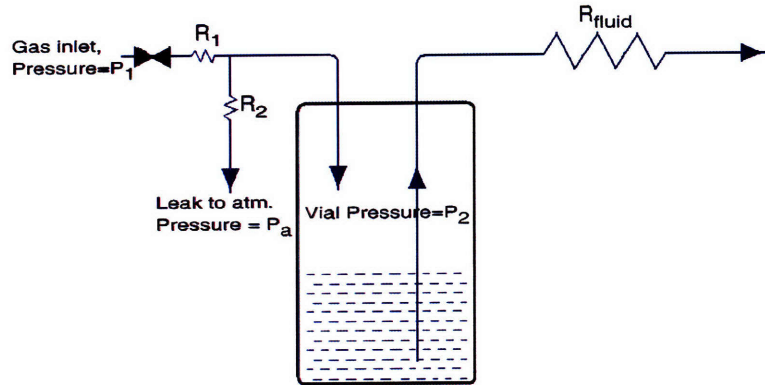
Figure 3.2 Schematic of pressure driven flow. A constant high pressure source (such as a helium gas cylinder) is connected to the head-space of the enclosure, with a leakage line to the atmosphere. R_1, R_2 and R_{fluid} represent flow resistances.

By varying parameters such as diameter and length of the flow path, the fluid-flow resistances R_1 and R_2 can be tuned, to give charging and discharging times varying from sub-second values to several seconds. When tuned to charge or discharge in less than a second, the system performs like a switch, with the on/off valve at the gas inlet serving as the changing knob. When the valve is open, the pressure in the enclosure is high and there is fluid flow out of the enclosure; and when the valve is close, the pressure is low and there is no fluid flow. This is depicted graphically in Figure 3.3.

(a)   (b)
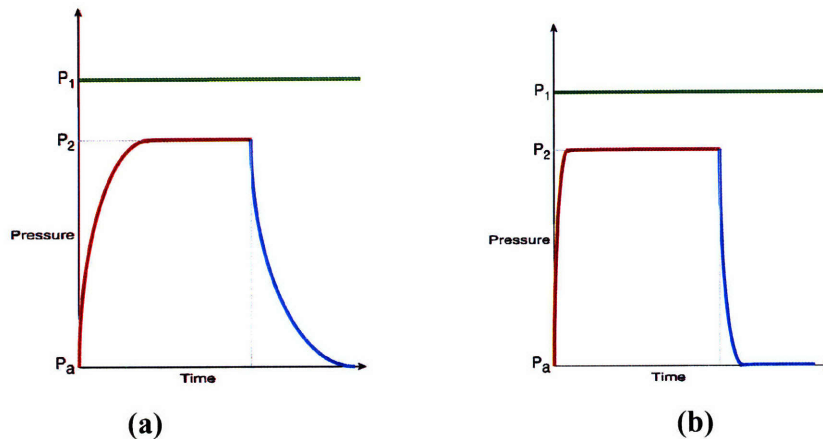
Figure 3.3 Figures (a) and (b) represent switch operation of two systems with high and low time constants, respectively.

3.3 In-line pump design

The purpose of an in-line pump is to increase the pressure in-between in a train of microfluidic devices as shown in Figure 3.4.
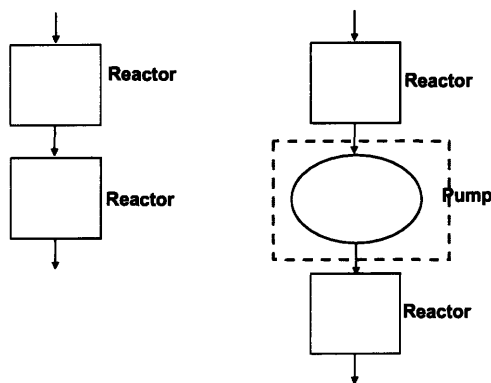
Figure 3.4 Schematic showing an in-line pump in a train of micro-unit operations.

A design for such a pump is shown in Figure 3.5. A high pressure gas source (P_0) connects two enclosures with each enclosure having an on/off valve, V and fluidic resistances R_1 and R_2. While the pump is in operation, the two valves, V_1 and V_2 are always in toggled states with respect to each other, i.e. when V_1 is on, V_2 is off, and *vice versa*. When Valve V_1 is open, the pressure in corresponding enclosure is P*

$$\left(P^* = P_0 \left(\frac{R_2}{R_1 + R_2} \right) \right)$$ and when V_1 is close, the pressure is P_a. Thus, at any time of

operation, one of the two enclosures has pressure P* and the other is at ambient atmospheric pressure, P_a. The solid arrows shown in the flow lines are one-way valves that allow flow only in the indicated direction.
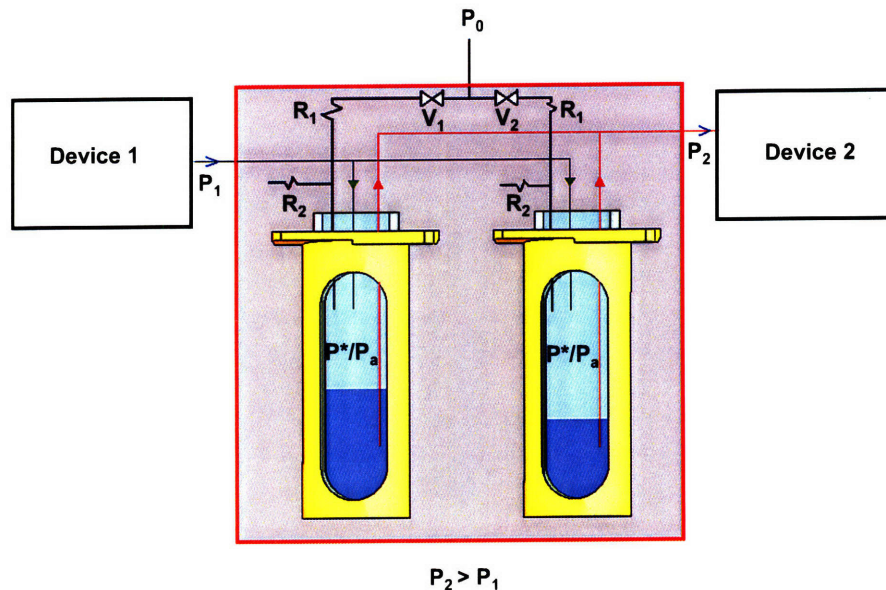
Figure 3.5 Design of an in-line pump. The solid arrows represent one-way valves. The two valves, V_1 and V_2 are always in opposite states, i.e. when V_1 is on, V_2 is off, and vice versa. When V_1 is open, the pressure in corresponding enclosure is P* and when it is close, the pressure is P_a. The fluid pressure after device 1 is P_1 and before device 2 is P_2. The pumping action of the in-line pump results in $P_2 > P_1$

During the operation of the pump, consider the case when V_1 is on, and V_2 is off. In such a case, The pressure in the left enclosure is P* and the right enclosure is P_a. Flow from the upstream device coming at pressure P_1 goes into the right enclosure having low pressure P_a. At the same time, flow from the left enclosure at pressure P* flows into the downstream device, with pressure P_2. When the right enclosure is close to reaching its capacity or if the left enclosure gets depleted of the fluid, the valve states are toggled, so that flow downstream now occurs through the right enclosure. As the switch action almost instantly changes the pressure in the enclosure from one state to the other (when time constants are small, corresponding to Figure 3.3(b)), the downstream devices do not see the switching of enclosures.

In the normal mode of operation, the resistances for fluid flow in both the gas lines leading to the two enclosures are kept identical to achieve the same pressure P* in each enclosure when the corresponding valve is on. However, novel schemes can be developed

by deliberately keeping them different. Resulting oscillating pressure profiles can find interesting applications.

3.4 In-line Pump

Based on the design in Figure 3.5, there is no constraint on the size of the enclosure. Two different enclosure volumes were considered – 10 ml and 40 µl.

i)   10 ml scale

The 10 ml scale was attained using 3 dram (12 ml) shell vials from VWR International. A manifold (Figure 3.6) was machined from aluminum and anodized to house either one or four such glass vials, and provide pressure-tight seal using o-rings and standard ¼-28 screwed fluidic connections to the sealed enclosure. The design was made to enable quick attachment and release of the glass vial to enable fast change of reagents.
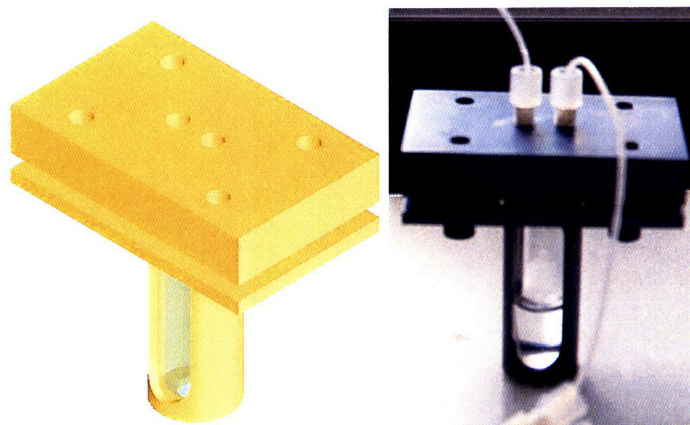
Figure 3.6 Schematic and photograph of the manifolds used for pressure driven flow. Design details are discussed in Appendix D

ii)   40 µl scale

The 40 µl scale enclosures were microchips (Figure 3.7) microfabricated from 1 mm thick silicon wafer and capped with Pyrex wafer to form a 42 µl cavity in the device. The fabrication details are discussed in the Appendix C. The design of the in-line pump using the microchips is shown in Figure 3.8
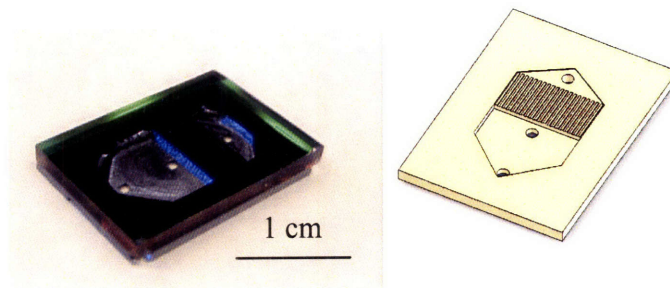
Figure 3.7 Photograph and schematic of microchip. Design details provided in Appendix C.
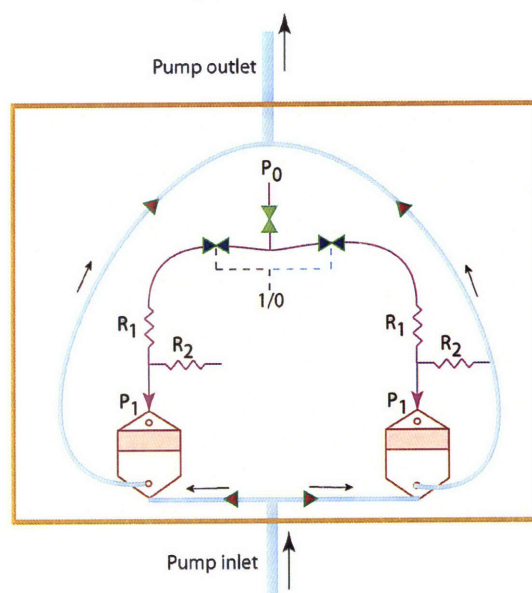
Figure 3.8 Design of in-line pump with microchips. The solid red arrows are one-way check valves.

A helium gas cylinder was used as the high pressure source to drive the in-line pump operation as helium has the least solubility in liquids at standard conditions of all common gases. The helium cylinder at constant high pressure was connected to a 3-way on-off solenoid valve (model # LHDA0523212H from The Lee Company), shown in Figure 3.9. It had a common inlet and two outlets – one was Normally Open (NO), while the other was Normally Closed (NC). The NO and NC states toggled on application of a 5 V voltage to the valve. The helium gas inlet to the common port could then be made to flow out the NO or NC ports upon application of low (0 V) or high (5 V) signals. Automated switching was used to toggle the high pressure source between two

enclosures. A square wave signal generator (model # DS335 from Stanford Research Systems) was used to toggle the enclosures at a set frequency that could be varied from 10^{-6} Hz to 3 MHz. The Lee 3-way valves had a response time of 2 millisecond. Practically, the switching frequencies were made to vary such the switching times were 3 seconds at the fastest and 10 minutes at the slowest. At 100 µl/min flowrate, 5 µl liquid flows out in 3 seconds – the lower bound when the chip of 40 µl volume keeps an average of 20 µl fluid in it on an average. This half filled strategy keeps the microchip most away from running dry or flooding. The longer switching times were used for the larger scale enclosure.
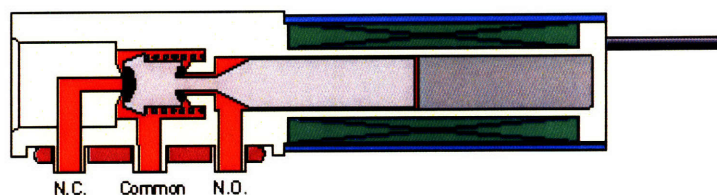
Figure 3.9 Schematic of the 3-way on-off valves (from The Lee Company)

The one-way valves used were part # CV3330 from Upchurch Scientific (now part of Idex Corp). They have a 1 psi cracking pressure to start flowing in the direction of flow, and can withstand up to 2000 psi pressure in the opposite direction of flow without leaking. The variability in the rated 1 psi cracking pressure was substantial, and it altered the downstream resistance seen by the two enclosures of the pump, leading to different flowrates out of the two enclosures during their corresponding half of the pumping cycle. Hence, a modified design shown in Figure 3.10 was used that eliminated the need to use check valves, and used the three-way valves instead. In the figure, green color on the valve represents open position, and red color represents closed position. For example, when the left chip is pressurized, it pumps liquid out whereas the right microchip is at low pressure and takes the incoming flow. The gas side switching was performed using the Lee valves, but they were found to i) heat up in long-term use and ii) be chemically incompatible with organic solvents, particularly dichloromethane and N,N-dimethylformamide. The first issue is manageable, but the incompatibility caused the inner gasket material to swell up blocking flow out of the valve. Chemically compatible valves were bought from Burkert Fluid Control Systems (part # 0127). These 3-way rocker solenoid valves were made from more chemically resistant polyvinylidene

fluoride. As they were more expensive than the Lee valves, they were only used on the fluid side (two such valves per pump) when the fluid was incompatible with Lee valve seals, and the Lee valves were always used on the gas side.

The presence of bubbles in the lines changes the flow resistance, causing unequal flow out of the two enclosures. To prevent bubble formation, the pure liquid samples used for experiments were degassed by placing under vacuum for about 30 minutes.
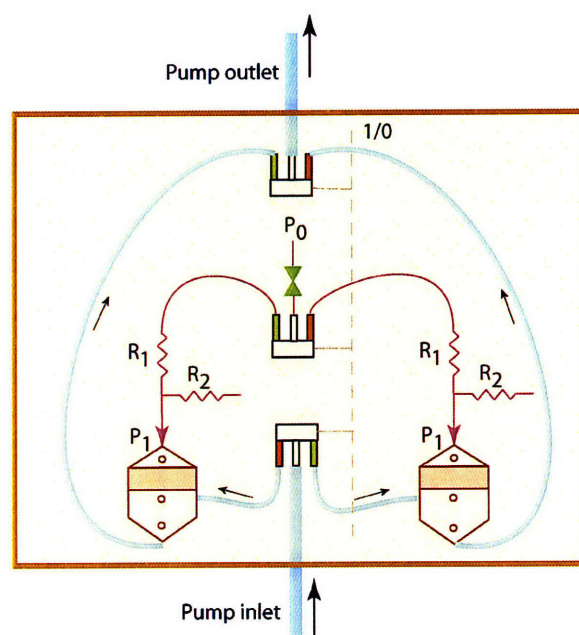
Figure 3.10 In-line pump with check valves replaced with 3-way on-off valves

3.5 Experiments

The demonstration of the in-line pump design was performed using the experimental setup showed in Figure 3.11
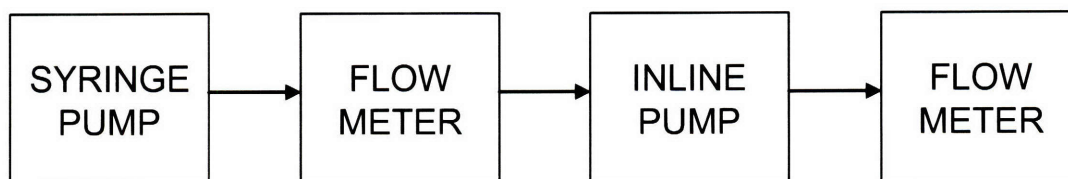
Figure 3.11 Experimental setup for in-line pump studies

The details of the in-line pump were described in 3.4. The syringe pump used for the study was bought from Harvard Apparatus (model # PHD2000). The flow rate was measured using flow sensors form Sensirion (model # SLG1430) that worked on the principles of flow anemometry. The flowmeter measured flow from 1-40 µl/min with a resolution dependant on the sampling rate. At 12.5 Hz sampling rate, the resolution of measured flow was 1.2%, with a response time of 20 millisecond. A commercial flowmeter for microfluidic applications enabled measurement of flow profiles after a syringe pump and the developed in-line pump.

Syringe pumps are known to provide oscillatory flow as a result of the screw rotary motion causing the syringe piston to move forward. The Sensirion flowmeters helped measured the variance of flow, and compare it with the in-line pumps. The availability of a direct flowmeter was a useful analytical tool as most other approaches use alternatives such as pressure measurements or dye injections and image wavy patterns. Experiments were performed at different flowrates, sampling rates, syringe sizes, and switching frequency.

3.6 Results and Discussions

In the experimental setup described in Figure 3.11, a set value of flowrate was keyed in the syringe pump, and the gas inlet pressure to the in-line pump was adjusted to provide outlet flow at the same flowrate so that there was no accumulation or depletion in the pump. Milli-Q water (Millipore) was used as the working fluid for these experiments. The flow profiles from the syringe pumps and the in-line pumps when the flowrate was set to 20 ml/min, in-line pump switching at 0.02 Hz and data sampling at 1.56 Hz are shown at different timespans in Figure 3.12. The pressure provided to the inlet pump was 2.5 psi.
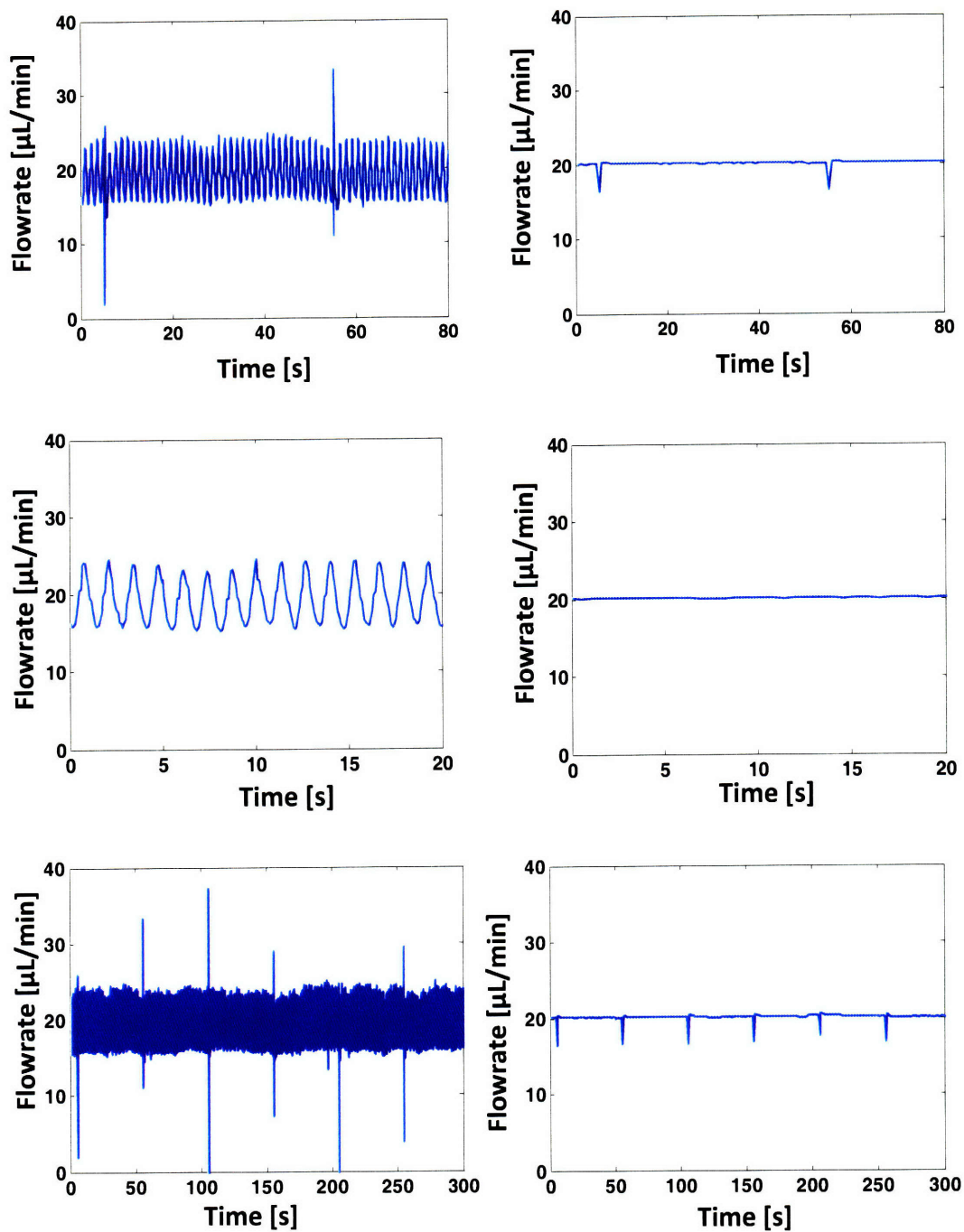
Figure 3.12 Flow profile from a syringe pump (left) and in-line pump (right) for set flowrate of 20 μl/min at different timespans, from 20 seconds to 300 seconds. In-line pump switching at 0.02 Hz, and data sampling was at 1.56 Hz.

The blips seen in the in-line pump flow profile represent the switching between enclosures. As each enclosure starts flow from a no-flow state, these blips result, but by

making the time constants of the system smaller, it is possible to reduce their effect on the flow constancy. The oscillations seen in the syringe pump agree with most experimental observations and previous studies[84]. Both the syringe pumps, and in-line pressure driven pumps were studied for their flow profiles at different operating parameters and these results are discussed next.

3.6.1 Comparison of flow profiles

Comparison of flow profiles of the two pumps shown in Figure 3.12 was done numerically by using the mean and standard deviation of the measured data. Scaled error was defined as the ratio of standard deviation to the mean. As seen from Table 3.1, the scaled error in pressure driven in-line pump is less than half of the error in syringe pumps, supporting the more constant flow seen visually in Figure 3.12. The use of standard deviation was a harsher tool to study pressure driven flow constancy as the differences get squared, magnifying the effect of the blips in constant flow, while the syringe pump oscillations are regular around a mean value.

Table 3.1 Comparison of flow profiles shown in Figure 3.12. Syringe used was 10 ml Hamilton Gastight. Flowrate sampling was at 1.56 Hz, switching at 0.02 Hz.

Syringe Pumps			Pressure Driven In-line Pumps		
Mean flowrate (μ)	Standard deviation (σ)	Scaled error (μ/σ)	Mean flowrate (μ)	Standard deviation (σ)	Scaled error (μ/σ)
19.3048	0.8348	0.04324	20.1366	0.4088	0.02030

3.6.2 Flow profile from In-line Pumps

i) Effect of sampling rate

The flowmeter from Sensirion came with software that could sample data at rates of 1.56, 6.5, 12.5, 25, 50, and 100 Hz. Higher sampling rates gave lower resolution. The effect of sampling rate was studied for a pumping rate of 20.5 μl/min, and switching of enclosures at 0.1 Hz, all the above sampling rates were used. Figure 3.13 shows the same flow out from the pressure driven pump measured at sampling rates of 25, 1.56 and 6.25

Hz. As expected, rapid sampling shows deeper blips. The flow from each enclosure theoretically starts from zero – fast enough sampling observes that. The width of each blip is the same, however, irrespective of the sampling rate, as that is determined by the time constant of charging, which does not change with sampling rate. The time constants can be made smaller, (discussed in Appendix A) for reduced blip widths. Another way to completely eliminate the blips is to use a third enclosure as buffer volume – more on this approach is discussed in the chapter on recirculation.
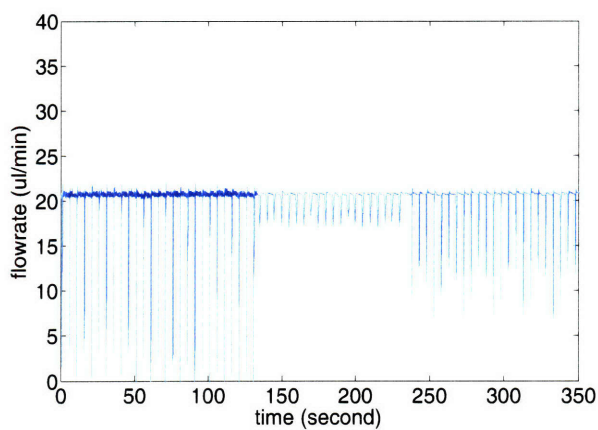
Figure 3.13 Flow profile from in-line pump at sampling rates of 25, 1.56 and 6.25 Hz

ii) Effect of switching frequency

Switching frequencies of 0.01, 0.05 and 0.1 Hz were used, corresponding to switching times from 50 to 5 seconds, respectively. A square wave to switch has one half high and the other half low signal, so a 0.1 Hz corresponding to 10 second wave was on for 5 seconds and off for the other 5 seconds. Figure 3.14 shows the flow profile with switching every 50 seconds. As the switching affects the otherwise constant flow, the ideal switching time is as high as permissible by the flowrate and scale of operation. At 20 μl/min flowrate, 1.7 μl liquid flows out in 5 seconds – sufficient drainage rate for a chip of 40 μl volume, where the average fill in the chip is maintained at 20 μl fluid on an average, keeping the microchip most away from running dry or flooding. While switching every 50 seconds, 17 μl liquid would flow out risking drying or flooding. Such operations therefore require tighter control systems to monitor liquid level that could be developed in future, or use the larger scale enclosures for operation, as is the case for the flow profile shown in Figure 3.14. Faster than necessary switching may be required when

very good mixing between the two enclosures is required, for example if the upstream device delivers fluid that changes with time due to some reaction, so large accumulations become undesirable. In such cases, the pump is started with very small initial fluid, and switching is performed at higher rates to maintain low dead volume and prevent fluid from ageing in the pump.
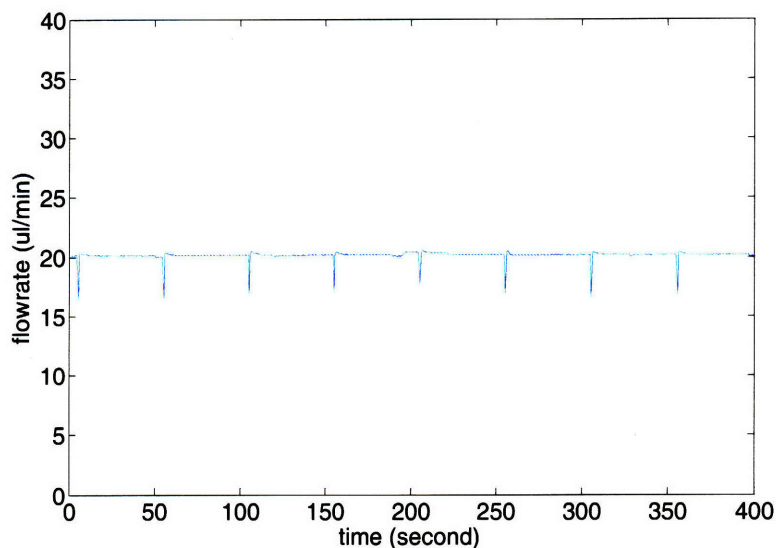
Figure 3.14 Flow profile from in-line pump at 0.01 Hz switching rate.

3.6.3 Flow profile from Syringe Pumps

Flows out of syringe pumps show oscillations because the screw over which the bulkhead pushing the syringe piston moves has a finite pitch, so the rotary action of the motor causing the flow becomes digitized to deliver an average overall desired flowrate. Syringe pump flows can be much smoother if finer pitch designs were used, but such pumps are expensive, and using multiple such pumps in a laboratory setup is not feasible.

i) Effect of different syringe sizes (or flowrates)

A syringe pump calculates the linear shaft speed needed for a desired volumetric flowrate by dividing the volumetric flowrate by the cross-sectional area of the syringe. The area of a syringe varies with the syringe capacity. Thus, increasing volumetric flowrate affects the linear shaft speed in the same way as reducing syringe size. The flow profiles from a syringe pump were observed at different shaft speeds by operating at

volumetric flowrates from 5 to 20 μl/min, and using 1, 10, and 25 ml Hamilton Gastight syringes. Sampling rates of 1.56 Hz, 12.5 Hz and 50 Hz were used. Table 3.2 summarizes the results for sampling rate of 1.56 Hz, while graphs in Figure 3.15 show the trends.

Table 3.2 Effect of syringe size on the flow oscillation from syringe pumps at different flowrates. The flowrate measurements were sampled at 1.56 Hz.

Flowrate (μl/min)	Mean (μ)	Standard Deviation (σ)	Scaled error (μ/σ)
1 ml syringe, diameter = 4.61mm			
1	1.0143	0.1473	0.145223
5	5.0440	0.1016	0.020143
10	9.9647	0.1752	0.017582
20	19.0916	0.2746	0.014383
30	27.9191	0.4035	0.014452
10 ml syringe, diameter = 14.57 mm			
1	1.1120	0.1739	0.156385
5	5.2349	0.5781	0.110432
10	9.9346	0.7367	0.074155
20	19.3048	0.8348	0.043243
30	28.2825	0.7686	0.027176
25 ml syringe, diameter = 23.00 mm			
1	1.1289	0.1863	0.165028
5	5.2927	0.5063	0.095660
10	9.9769	0.7400	0.074171
20	19.4898	1.0786	0.055342
30	28.0496	1.3277	0.047334
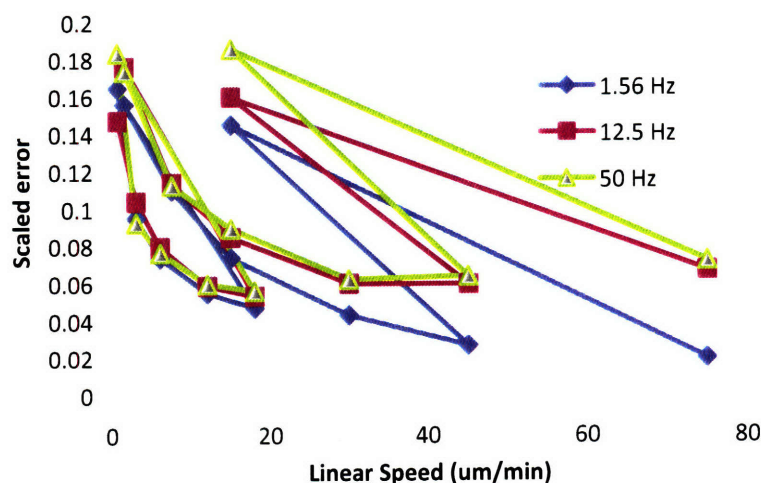
Figure 3.15 Effect of syringe size on the flow oscillation from syringe pumps at different flowrates. The linear speed of the shaft is determined from the flowrates and the syringe size. The three distinct curves seen represent syringe sizes of 1, 10 and 25 ml going from left to right, respectively.

Figure 3.15(b) is a close up of Figure 3.15(a) displaying full scale. The three distinct curves seen represent syringe sizes of 1, 10 and 25 ml going from left to right, respectively. As expected, increasing flowrates for any one syringe reduce the extent of oscillations measured by the scaled error. For any flowrate, lower size syringe gives fewer oscillations than higher size syringes. However, the relationship between error and linear shaft speed is not universal – for the same shaft speed, lower syringe sizes provide fewer oscillations. Thus, to avoid fluctuations in flow, use of lowest syringe size is best. Unfortunately, lower size also means lower capacity and puts a constraint on how long an experiment can be run.

ii) Effect of sampling rate

The effect of varying sampling rates on the flow profiles were studied at 1.56, 12.5, and 50 Hz sampling rates, and are shown in Figure 3.16 and Figure 3.17. As the syringe pump flow profiles oscillate around a mean value, changing sampling rates has a less dramatic effect than on pressure driven pumps. High rates of sampling measure the noise

along with the oscillations, while the lower rates tend to capture just the oscillations as long as the sampling rates are higher than oscillation frequency. The observations are consistent with the Nyquist-Shannon sampling theorem. As the lower sampling rates are less likely to capture the extremes of oscillation, the lower sampling rates show smaller scaled errors than for higher sampling rates as seen in Figure 3.17. The effect of different syringe sizes and flowrates follows the trend discussed earlier.
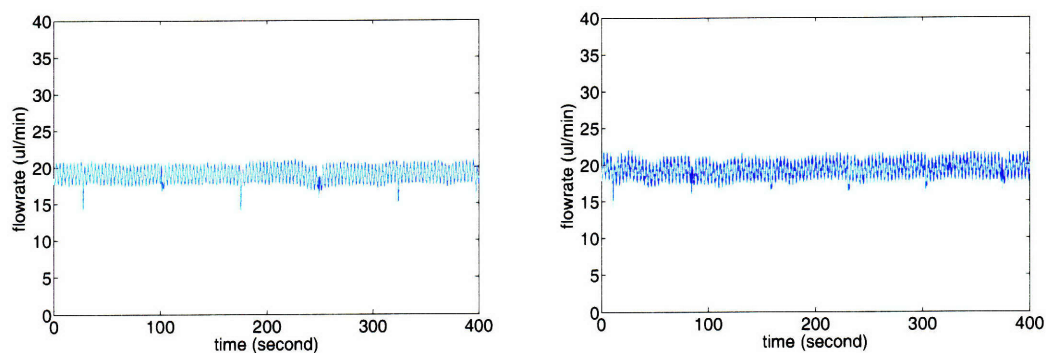
Figure 3.16 Syringe pump flow profile measured at 12.5 Hz (left) and 50 Hz (right). Flow is at 20 μl/min and is from a 25 ml syringe
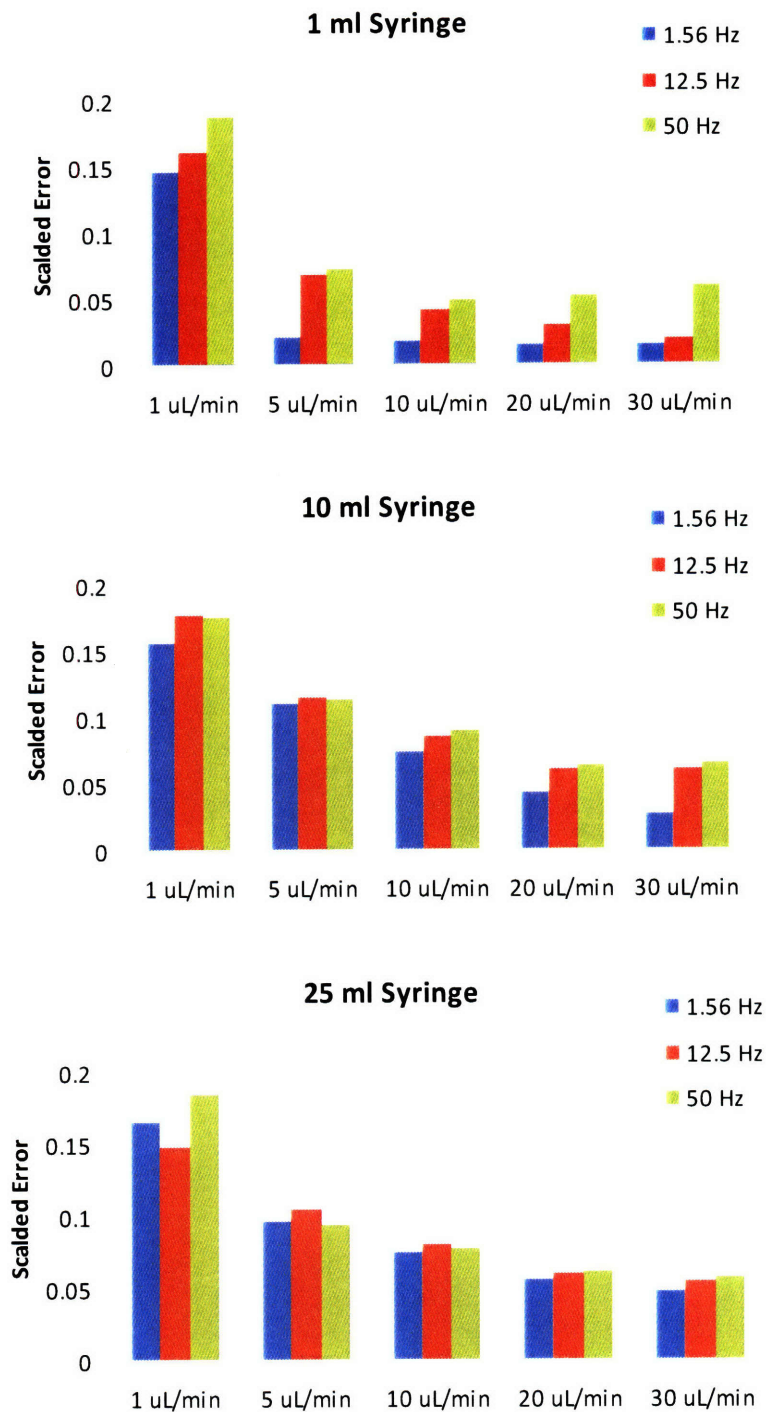
Figure 3.17 Effect of sampling rate on the extent of oscillation in the flow profiles from syringe pumps. The x-axis denotes the set point flowrates. The experiment was performed at 1.56, 12.5 and 50 Hz sampling rates for 1 ml, 10 ml and 25 ml capacity Hamilton Gastight syringes and Harvard Apparatus PHD 2000 syringe pump.

3.7 Microfluidic transistors

3.7.1 Real-time on-off flowrate control

Extending the discussion started in section 3.2, it is possible to add a feedback control system to measure the downstream flowrate, and change the pressure to get desired flowrates. The control diagram is shown in Figure 3.18. Pressure sensors or flowmeters were used to measure downstream pressure and the values were fed to a controller that sent out a binary signal to either open or close the valve. A binary output was used because proportional valves for the small scale did not exist. An on-off valve (Lee Company, part # LHDA0523212H) was used instead. The on-off control algorithm opened the valve if the measured flowrate was less than the set point, and closed if the measured flowrate was more. If pressure sensors were used to measure the downstream flowrate, the set point was a desired pressure drop corresponding to the desired flowrate using the Hagen-Poiseuille equation.

A challenge using such an on-off control is handling the oscillations as a result of the overshoot during the delay in signal measurement, transmission, processing or control action. The amplitude of oscillations can be dampened, and flow constancy can be achieved by either

1)   Having fast on/off cycles

2)   Having large resistances so that charging/discharging was slow

3)   Using Model Predictive Control

The first option was limited by hardware as the sampling rate is limited, so the second alternative was used, and steady controlled flow at different flowrate set points (in µl/min) was attained as shown in Figure 3.19. The system time constants were made large enough that the oscillations seen had amplitude equal to the resolution (0.228 µl/min for this example, 40 µV[85] at 1 V operation in general) of the Analog to Digital converter (FP-AI-110 and cFP-AI-110 from National Instruments) used for sampling pressure drop values. The use of Model Predictive Control was considered beyond the main focus of this thesis, but is certainly an attractive approach for future studies.
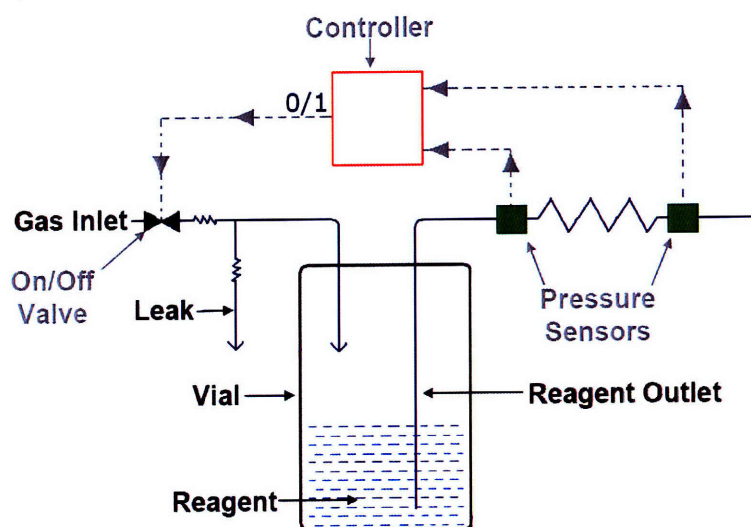
Figure 3.18 Schematic of Pressure Driven Flow with Closed-Loop Real-time Control
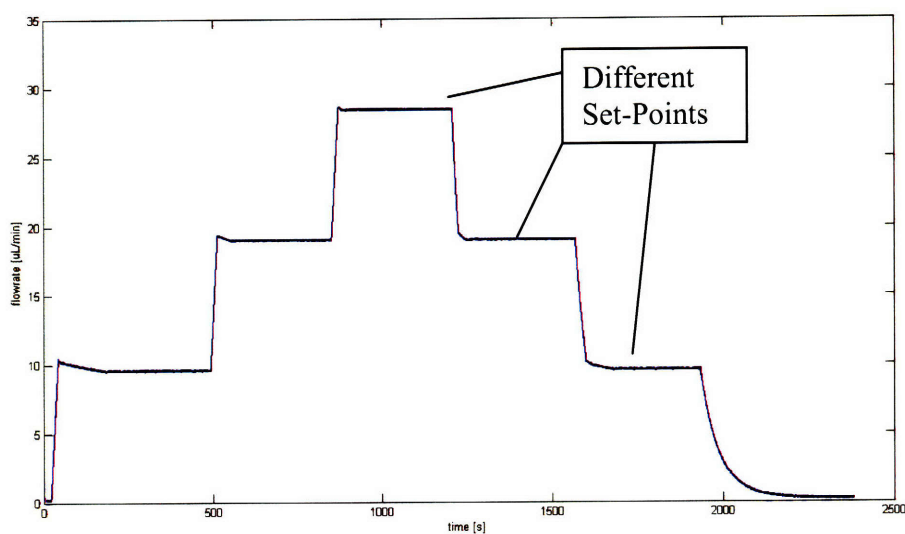
Figure 3.19 Flow profile with on-off control

Microfluidic analogs of digital electronic circuit components such as microfluidic large scale integration[86], coding/decoding of information in microfluidic droplets[87, 88], and microfluidic bubble logic[89] have recently been developed that provide the lab-on-a-chip community with innovative tools to apply in the quest of development of complete, universal lab-on-a-chip systems. The in-line pumps developed in this chapter are

microfluidic analogs of the digital transistor, the invention of which accelerated the growth of the computer industry at breakneck speed.

Addition of a control system to the in-line pump as shown in Figure 3.20 ensures a set point of either constant output pressure (P_2 = constant) or desired output flowrate. It can also be run to provide a constant gain (Gain = β = P_2/P_1). Such a configuration may find application in cases when the change in pressure drop over time during operation requires dynamic adjustment of the pressures to maintain constant desired flowrates. Specific chemical examples include increase in pressure drop across a catalyst bed due to deactivation or particle breakup, or increase in pressure drop due to solids formation, clogging, or swelling of organic support resin as in solid phase peptide synthesis.
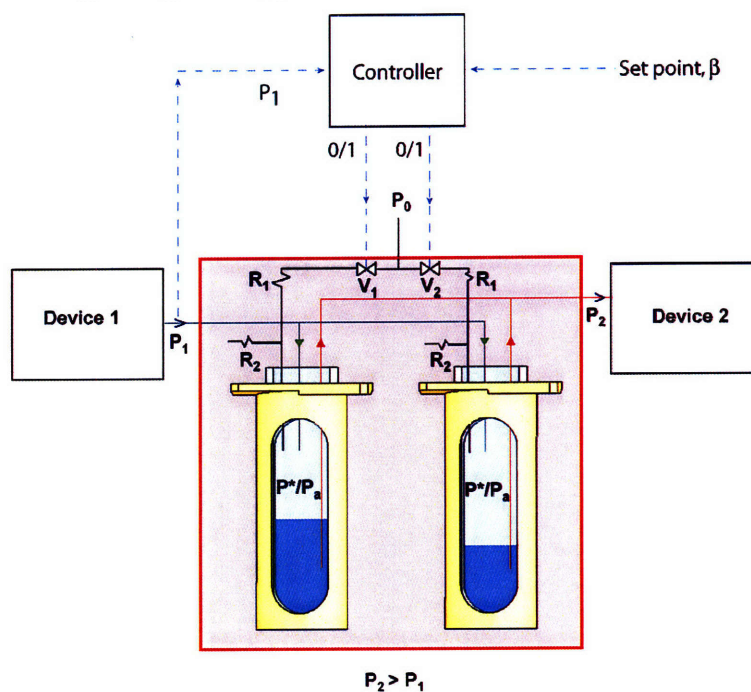
Figure 3.20 Design of In-line Pumps as Microfluidic Transistors

Table 3.3 and Figure 3.21 consider a simple case when the flowrate is maintain constant despite increasing flow resistance.

Table 3.3 Simulation of increasing flow resistance (could be due to catalyst coking, fines generation or support swelling). The flow resistance is assumed to increase 5% per hour. The pressures are assumed to increase without any time lag to maintain constant flowrate.

| Time | Resistance | P1 | P2 | (P1-P2) | Flowrate |
Hours	psi/(ul/min)	psi	psi	psi	ul/min
0	0.20	7.00	2	5.00	25
1	0.21	7.25	2	5.25	25
2	0.22	7.51	2	5.51	25
3	0.23	7.79	2	5.79	25
4	0.24	8.08	2	6.08	25
5	0.26	8.38	2	6.38	25
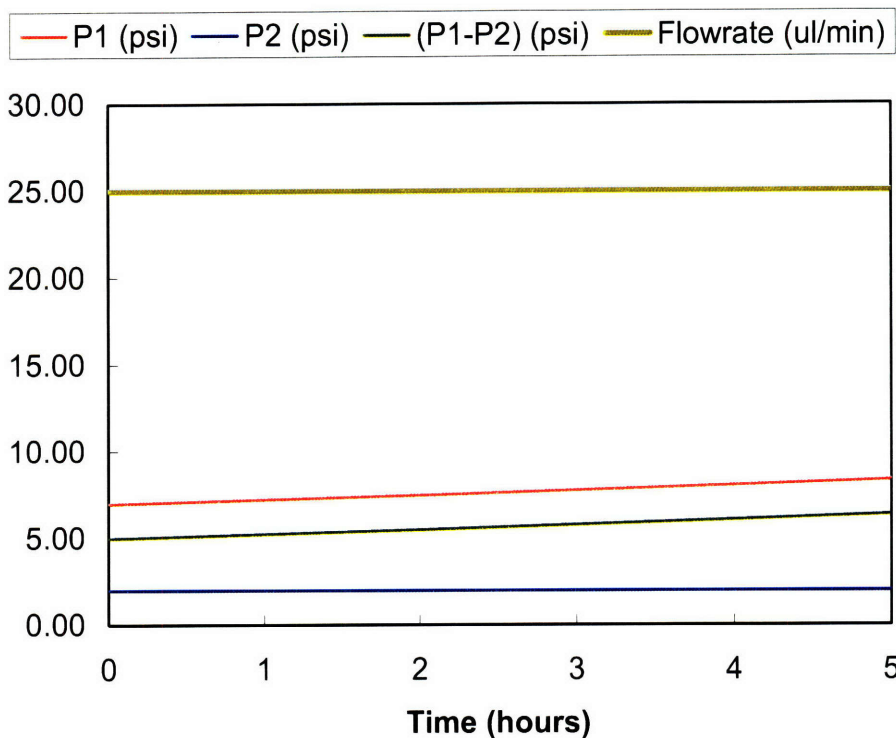
Figure 3.21 Simulation of changing pressures with varying resistance to maintain constant flowrate. The flow resistance is assumed to increase 5% per hour

3.8 Advantages of pressure driven in-line pumps

The pumps developed in this chapter find their use as

i) In-line pumps in-between devices, used to increase the flow pressure in-line of a microfluidic network – the equivalent of which currently do not exist.

ii) Replace syringe pumps altogether as the primary drivers for flow upstream of all devices, as pressure driven in-line pumps offer more constant flowrates.

3.8.1 Operational advantages

1) Quick response times

In-line pumps are instant on (have short transients, less than one second), unlike syringe pumps that take from 5-10 minutes to adjust to new conditions, thus allowing quick stopping of flow for techniques such as stop-flow lithography (SFL)[90]. So far, such techniques have been used alone, but the development of in-line pumps enables SFL to be used along with chemical syntheses opening new, interesting possibilities.

2) Constant flow

As seen in section 3.6, in-line pumps provide substantially constant flowrates compared to syringe pumps or systems with cyclical pumping such as peristaltic pumps. Moreover, the time constants for the systems can be tuned to always provide with a level of constant flow better than the demands of the system.

3) Different flowrates through different devices, and decoupling

The in-line pumps act as buffers, and have capacity to accumulate volume, thus permitting different flowrates upstream and downstream of the device. This ability is unique as all current applications use the same flowrate over the entire system.

4) Decoupling of systems upstream and downstream of the in-line pump

In-line Pumps also help to decouple devices and stop the propagation of disturbances through the microsystem. This can be seen from the noisy input and rectified output from the experimental setup in Figure 3.11 and the flow profile results in Figure 3.12. This keeps the multiple devices decoupled and prevents disturbances in one device from propagating onto other devices. Therefore, these in-line pumps help in broadening the operable range of a microsystem by allowing independent operation upstream and downstream of these pumps.

5) Infinite reservoir

When used as upstream starting pump, the volume of fluid flowed can be replaced by an additional checked line for feed inlet. Thus, the pressure driven pumps can be used for very large times without the need to stop the running system. This feature is of value in applications such as microreactor networks for chemical synthesis or in multistep extractions, where a substantial amount of initial feed is used to prime and get the system to steady state – all of this is lost if the systems has to be stopped to refill the feed lines. One could argue that very large syringes could be started with, in syringe pumps – but as it was seen, larger syringes lead to increased fluctuations in the flowrates.

6) Large range of flowrates

The microchip is known to withstand high pressures (15 atm.)[33]. The glass-vial system was pressure tested under water to 15 atm. Liquefaction of ammonia was performed in the glass-vial system successfully at room temperature. Thus, the pressure driven flow can generate flows at pressures varying from a few psi to several atmospheres. The flowrates depend on the flow resistance, and there is no constraint in attaining flows from as low as 1 ul/min to several ml/min. However, as in-line pumps for flowrates greater than 1 ml/min exist (for example, from Burkert Fluid Control Systems), the real utility of these pressure driven in-line pumps is in the low flowrate regime.

3.8.2 Mechanical advantages

1) No moving parts

Unlike syringe pumps or systems with multiple microfabricated valves, the pressure driven pumps have no constantly moving parts. As a result, these pumps do not change their performance over time, and hence are more reliable. The valves used are external and can be easily replaced.

2) Simple setup

The simple setup costs far less compared to equivalent syringe pumps, and it is easy to scale these pumps to have many independent units running from the same single high pressure source.

3.8.3 Scale advantages

The in-line pumps were demonstrated in two size ranges – 10 ml and 40 µl. Having demonstrated these extremes of capacity scales, it is possible to demonstrate at any in-between size range. The choice of the in-line pump volume depends on the intended application.

i) Advantages of the 10 ml scale in-line pump

The large volume allows for longer operation at different inlet and outlet flowrates utilizing the large buffer volume in the system. This is useful for subsequent chemical reactions having different reaction time or flowrate requirements. The large volume also means the enclosures are less likely to get flooded or run dry, so the switching between enclosures can be performed less often provided fewer blips in the constant flow rate.

ii) Advantages of the 40 µl scale in-line pump

In applications that require the system volume to be minimized, the 40 µl in-line pumps are the preferred choice. The small volume allows quick startup of the system as less volume needs to be filled up before downstream devices become operational. The ability to microfabricate these pumps allow them to be mass produced, and presents the possibility of integrating multiple operations on a single microchip.

3.9 Conclusion

The use of pressure to control fluid path in the manner described here is an advancement in microfluidic flow technology. These schemes can provide substantially constant flowrate while recirculating a body of liquid or when used as an intermediate pump. The intermediate pump can also be used as a gas-liquid separator. Current syringe pumps are constrained in that they provide the same fluid flowrate through all the connected devices. On the other hand, by means of the temporary holdup inherent in the design, our design allows having different and independent flowrates through the different devices connected in series.

Pressure driven flow techniques were used in this chapter to develop and demonstrate pumps that can be used to replace current syringe pumps and be used as an in-line pump. The developed pumps are superior in performance to existing alternatives and have

capabilities such as maintaining different flowrates upstream and downstream of the pump that do not exist in current pumps. Development of robust in-line pumps in this chapter, and along with separators developed in chapter 2, enables microdevice networks for chemical syntheses applications as shown in further chapters. It is expected these pumps will become an integral component for all future microsystems. Microfluidics has often been likened to the circulatory system in humans – both have similar length scales of operation. In that case, the pump developed in this chapter is the equivalent of the heart – both pump fluid by imposing pressure.

4 Multistep Liquid-Liquid extraction in Microsystems

4.1 Introduction

The need for multistep synthesis in microchemical systems was discussed in detail in chapter 1. Continuous separation is the key in enabling continuous multistep synthesis. Consider as an example a simple organic transformation beginning with an alcohol, converted to organic halide in the first step, and used for further synthesis steps downstream. The first step is shown in Figure 4.1. In a continuous synthesis operation, it becomes important to maintain the purity of each reactant; else the impurity buildup after each step reduces the yield of the final product. In batch scale operation, a workup step usually follows the reaction to purify the product. As shown in the figure, a similar workup operation after each reaction is also needed on the continuous scale to maintain reagent purity. Continuous separation is thus, an essential element of multistep continuous synthesis. While many different chemical reactors for microsystems have been developed, few continuous separation techniques exist. The difficulties for continuous separation in microsystems were discussed in detail in chapter 2. While one stage liquid-liquid extraction was demonstrated in chapter 2, complete transfer of a chemical component from one phase into another requires multiple stages to deliver extraction beyond the single stage equilibrium values.
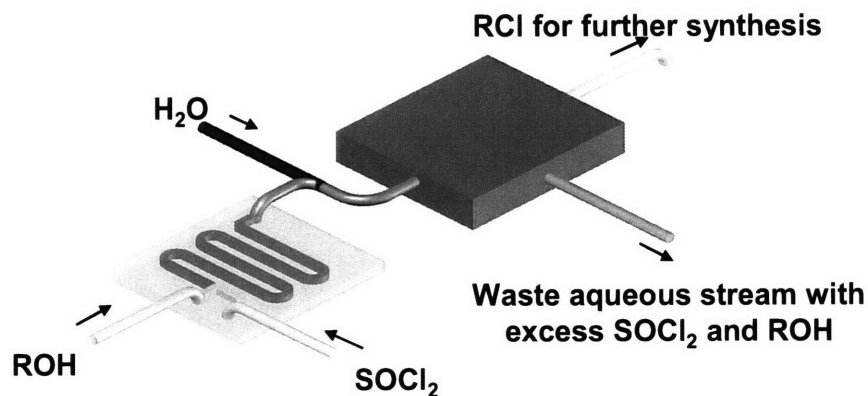
Figure 4.1 Example of a continuous reaction and workup operation for multistep synthesis

The most common separation operations on the batch scale and large scale continuous manufacturing are distillation and crystallization. Miniaturizing these operations for the microscale is still a challenge. Previous demonstrations[91, 92] of liquid-liquid extraction have presented it as a promising separation technique for continuous microscale operations. Kitamori and others have used surface modification of glass using organic silanes to alter its wetting characteristics[53, 57, 58, 61], along with two-phase contacting across the phase boundary to perform extraction. While these represent one of the first demonstrations of continuous workup, they have issues that render them not very scalable. The surface treatment tends to wear over time, rendering the devices functional only over short periods of time, making it a challenge to incorporate these devices in long-term continuous flow, multistep synthesis schemes. The throughput from these devices is another concern – they can be run at the most at ~ 1 μl/min. Higher flowrates result in interface instability and device failure. An ideal continuous workup device downstream of the microreactor should be chemically compatible with most reagents and have a wide and robust operable range. The two-phase separators developed in chapter 2 provide exactly those features. In chapter 2, these separators were used for single stage extraction. As the workup step often requires extraction beyond equilibrium values, there is a need to perform multiple staged extractions to deliver near complete separation. In this chapter, the separators developed in chapter 2 are combined with the in-line pumps developed in chapter 3 to develop a system capable of performing multistep extractions. The developed system was used to demonstrate two-stage extraction of the model system studied in chapter 2.

4.2 Multistep liquid-liquid extraction

Figure 4.2(a) shows a schematic of two separators connected in counter-current extraction mode of operation for the extraction of N,N-dimethylformamide (DMF) from dichloromethane (DCM) into water. This model system was chosen because DMF and DCM are common solvents; DMF also represents any generic small organic molecule that may be of interest for separations in multistep reaction-separation systems. The countercurrent mode of operation always maintains a driving force for extraction, resulting in enhanced separations. Fresh feed of DCM (with DMF) contacts water coming

from the second separator. The two phase segmented flow is provided enough residence time to attain equilibrium in the tubing that serves as inlet to the first separator. The lean DCM phase exits the separator and contacts fresh water inlet resulting in the second stage of extraction followed by separation. Lean DCM flows out the outlet of the second separator while water with DMF flows out the outlet of the first separator.
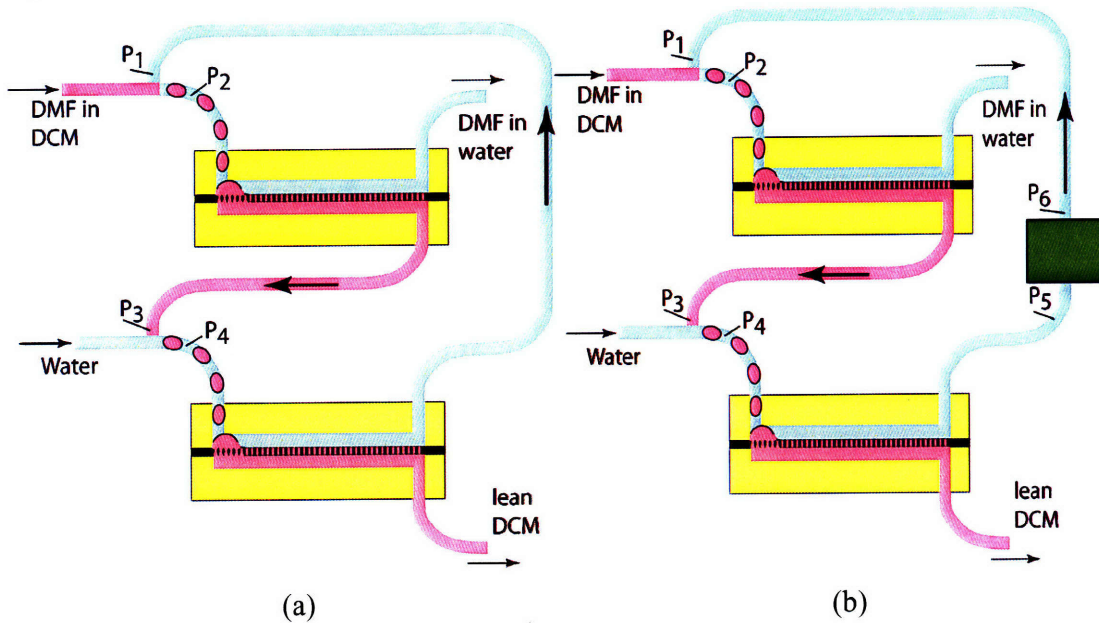
Figure 4.2 Countercurrent extraction arrangement with two stages (a) without in-line pump (b) with in-line pump.

In order to maintain the indicated flow directions, a positive pressure gradient is needed in the direction of flow. Thus, for the aqueous outlet from the bottom separator to form two phase flow with the organic feed, a necessary condition is

$$P_1 > P_2 \qquad (1)$$

Similarly, for the two-phase flow to flow into the separator, and organic flow to flow out of the organic outlet, the necessary condition is

$$P_2 > P_3 \qquad (2)$$

The necessary condition for the organic outlet from the top separator to form two-phase flow with the fresh aqueous feed is

$$P_3 > P_4 \qquad (3)$$

These three conditions, taken together, imply

$$P_1 > P_4 \qquad (4)$$

A necessary condition for the aqueous flow from the outlet of the second separator to the inlet of the first separator is

$$P_4 > P_1 \qquad\qquad (5)$$

This condition is the exact opposite of the one in (4). Hence, as shown in Figure 4.2(a), the flow direction forms a loop in a gridlock with no flow at steady state. This gridlock can be broken by the introduction of an in-line pump as shown in Figure 4.2(b). The pressure gradients in the modified system are given by-

$$P_1 > P_2$$

$$P_2 > P_3$$

$$P_3 > P_4 \qquad\qquad (6)$$

$$P_4 > P_5$$

$$P_6 > P_5$$

$$P_6 > P_1$$

These conditions are consistent, and result in flow in the intended direction, thus proving an in-line pump is necessary for countercurrent multistage extraction in a modular system using independent separators as shown in Figure 4.2. The experiments on multistage extraction discussed in this chapter were performed using the in-line pumps developed in chapter 3.

4.3 Countercurrent and cross-flow extraction

Figure 4.3 shows a schematic of the two-stage countercurrent extraction setup with the in-line pump. The in-line pump design presents the option to perform the multistage extraction as either a countercurrent or a cross-current extraction. Say, the right enclosure is primed with the same fresh aqueous feed that is also the inlet to the second separator. If there is no switching of enclosures, all flow out of the pump is from the right enclosure, while all flow in is in the left enclosure. This state of operation is possible only as long as either the left enclosure floods or the right enclosure runs dry. For a 20 μl/min flowrate, the length of time the pumps can be run without switching is 2 minutes for the 40 μl enclosure, and 500 minutes (8 hours, 20 minutes) for the 10 ml enclosure. In this manner of operation, the aqueous stream in both separators is fresh feed providing the maximum

driving force for extraction. This manner of operation is cross-flow extraction, and schematically shown in Figure 4.4(a). Cross-flow extraction is used when the extractant (water in this case) is plentiful, and the main aim is to remove as much solute as possible. When operated with switching of the enclosures such that the net flow in is the same as the net flow out, the in-line pump can be used indefinitely. In this mode, the aqueous outlet from the bottom separator flows through the pump and contacts the fresh organic feed, resulting in counter-current mode of operation. The startup of this setup, like any other continuous operation startup needs priming, and takes at least four volume sweeps before reaching steady state. Once the concentration of the sample in the pump enclosures becomes the same as that of the aqueous outlet from the bottom separator, the mode of operation is countercurrent, and independent of the switching frequency.
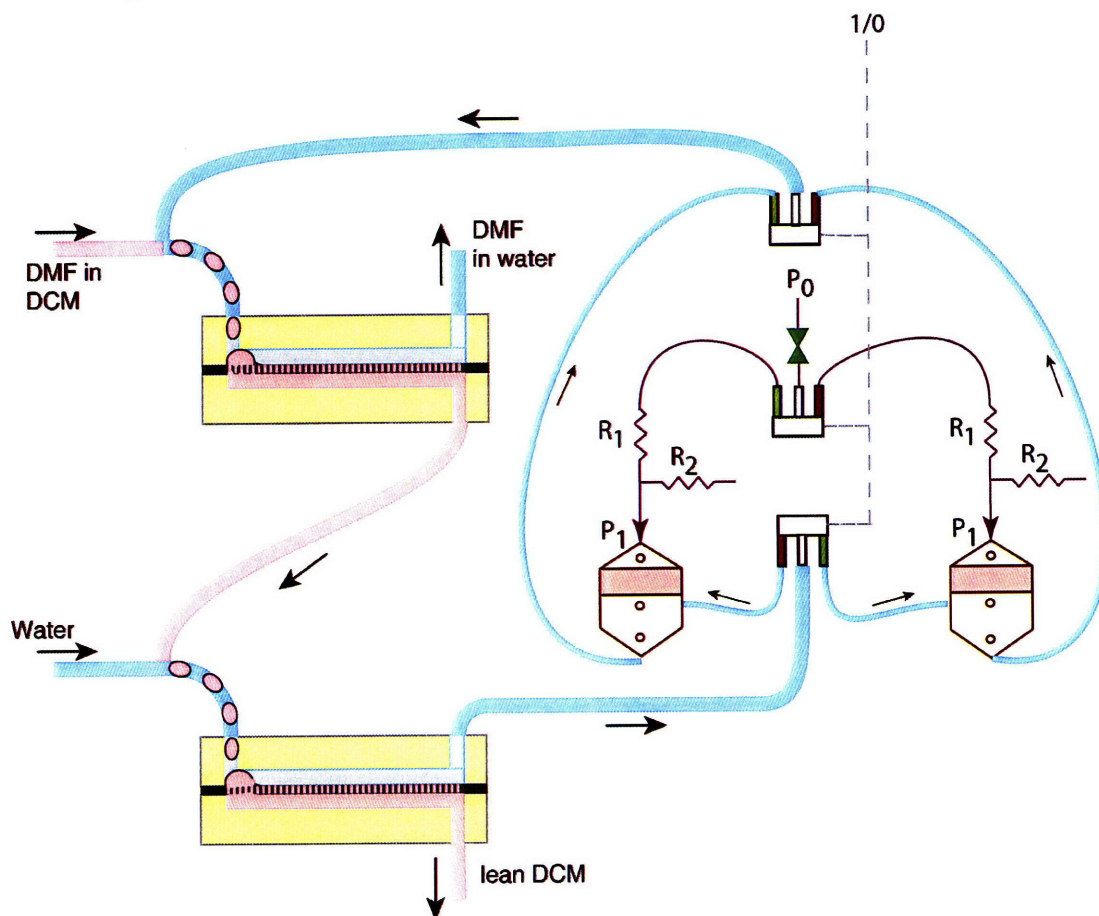
Figure 4.3 Schematic of the two-stage multistage extraction

4.3.1 Governing equations for Cross-flow extraction

Let y represent the mole fraction of solute in the extracting phase (aqueous), and x represent the mole fraction in the extracted phase (organic). F_D and F_S are the molar flowrates in the organic and aqueous phase, as shown in Figure 4.4(a). For each stage, the molar flowrates are known, as are the inlet concentrations. The two outlet concentrations are the two unknowns. The equilibrium relationship ($y=Kx$ – it is assumed linear for simplicity, could be non-linear as well) and mass balance are used to estimate the two outlet concentrations. Thus, for two stage cross-flow extraction, the equations are-

$$y_1 = Kx_1$$

$$F_D x_0 + F_S y_{1,in} = F_D x_1 + F_S y_1$$

$$y_2 = Kx_2$$

$$F_D x_1 + F_S y_{2,in} = F_D x_2 + F_S y_2$$

These equations can be solved analytically to yield the theoretical outlet concentrations after each stage. They can also be solved graphically using the McCabe-Thiele method as shown in Figure 4.4(b). The operating line has slope, $-F_D/F_S$. Knowing $y_{i,\ in}$, and x_0, the outlet concentrations after each stage are estimated[93].

(a)
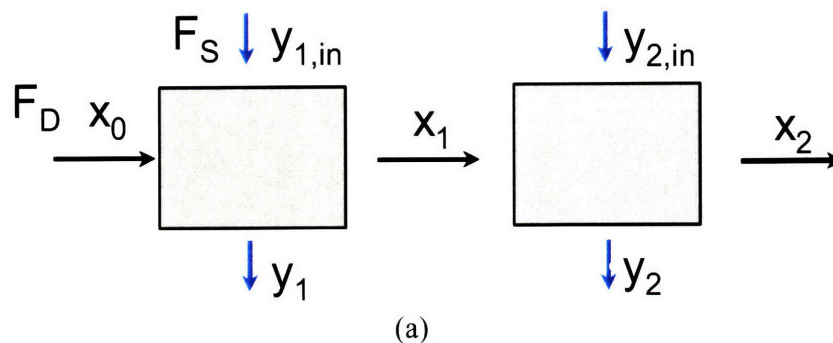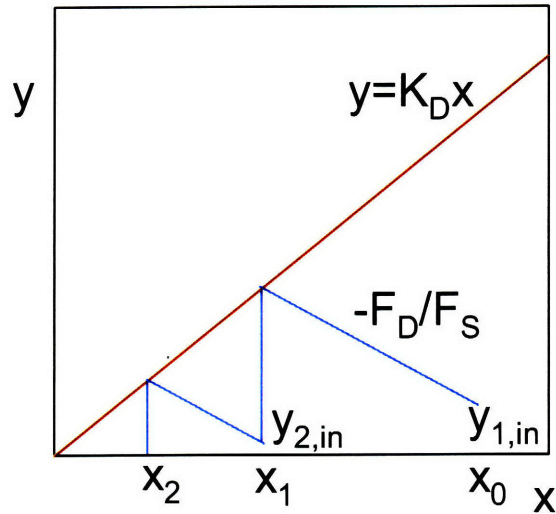
(b)

Figure 4.4 (a) Schematic and (b) graphical representation for two stage cross-current extraction.

4.3.2 Governing equations for Countercurrent extraction

The schematic of two-stage countercurrent extraction is shown in Figure 4.5(a). The equilibrium relationship and mass balance for each stage are used to estimate the unknown concentrations. For two stage countercurrent extraction, the equations are-

$$y_1 = Kx_1$$

$$F_D x_0 + F_S y_2 = F_D x_1 + F_S y_1$$

$$y_2 = Kx_2$$

$$F_D x_1 + F_S y_3 = F_D x_2 + F_S y_2$$

These equations are solved analytically to yield the theoretical outlet concentrations after each stage. To solve graphically using the McCabe-Thiele method as shown in Figure 4.5(b), the operating line has slope, F_D/F_S. These methods assume negligible solubility of the immiscible phases in each another. When the mutual solubilities are non-negligible, the ternary diagram with tie lines is used to estimate the concentrations of the outlet streams.
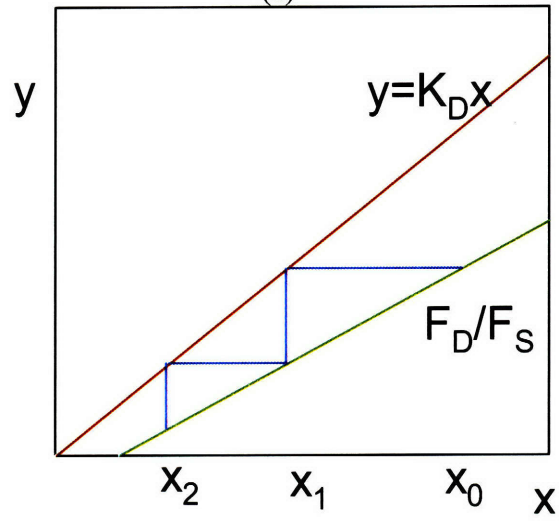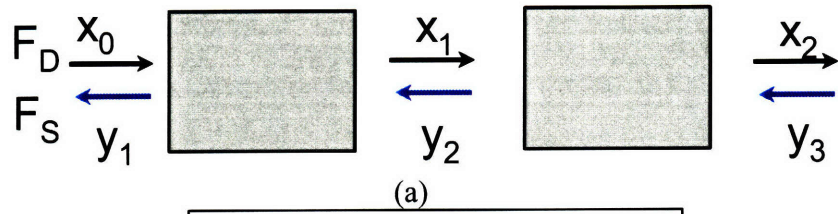
Figure 4.5 (a) Schematic and (b) graphical representation for two stage cross-current extraction.

4.4 Experimental

The multistage extraction setup used two two-phase separators described in chapter 2 and the in-line pump described in chapter 3, with the extraction schematic as shown in Figure 4.3. The flowrates were varied from 1-30 μl/min. The startup of the extraction required priming all the separators and pumps with liquids that would be running in the respective sections of the setup at steady state. Thus, the organic outlet of the separator was filled with the organic phase, and the aqueous outlet with the aqueous phase. Initial tests were performed using syringe pumps, but all experiments for countercurrent extraction were performed using pressure driven flow, as the syringe pump oscillations caused irregular two-phase flow, and introduced disturbances to the flow constancy and pressure distribution. The residence time for two-phase contacting that resulted in extraction varied from 10 to 15 minutes. The overall system volume, including all devices, tubing and attachments, was about 1-2 ml. At a flowrate of 20 μl/min, for a system volume of 2 ml, four complete volume sweeps required about 6 hours. For all experiments, data was collected after 6 hours to ensure collected data was from the steady state operation. Data gathered up to one hour after the initial 6-hour period showed no significant or systemic differences confirming the 6-hour wait was long enough to let the concentrations reach steady state of operation. The concentrations varied initially because of mixing with the primed fluid already in the lines. Fluidic priming was necessary to maintain the pressure differences required for the separators to work. If the separators fail, they do not self correct, but the system keeps shifting away from the desired state of operation. Consider, for example, if the lines have air to start with initially, the aqueous side outlet would offer significantly less backpressure because of the lower gas viscosity, causing the organic phase to flow out the aqueous side. With the system time constant being of the order of hours, any corrective action taken does not take effect immediately. Air bubbles, if present in fittings/tubing during startup offer similar destabilizing effect on the system. Therefore, all liquid phases were degassed before experiments and the whole system was primed to ensure trapped gas bubbles were minimized. Figure 4.6 shows the actual experimental setup with an in-line pump on both, organic and aqueous lines. Providing in-line pumps on both lines makes the system more robust and easier to

control, as the pump decouples the system into two independent sections and prevents propagation of disturbances downstream. Providing these pumps also keeps the system scalable to multiple stages of extraction, well beyond two or three.
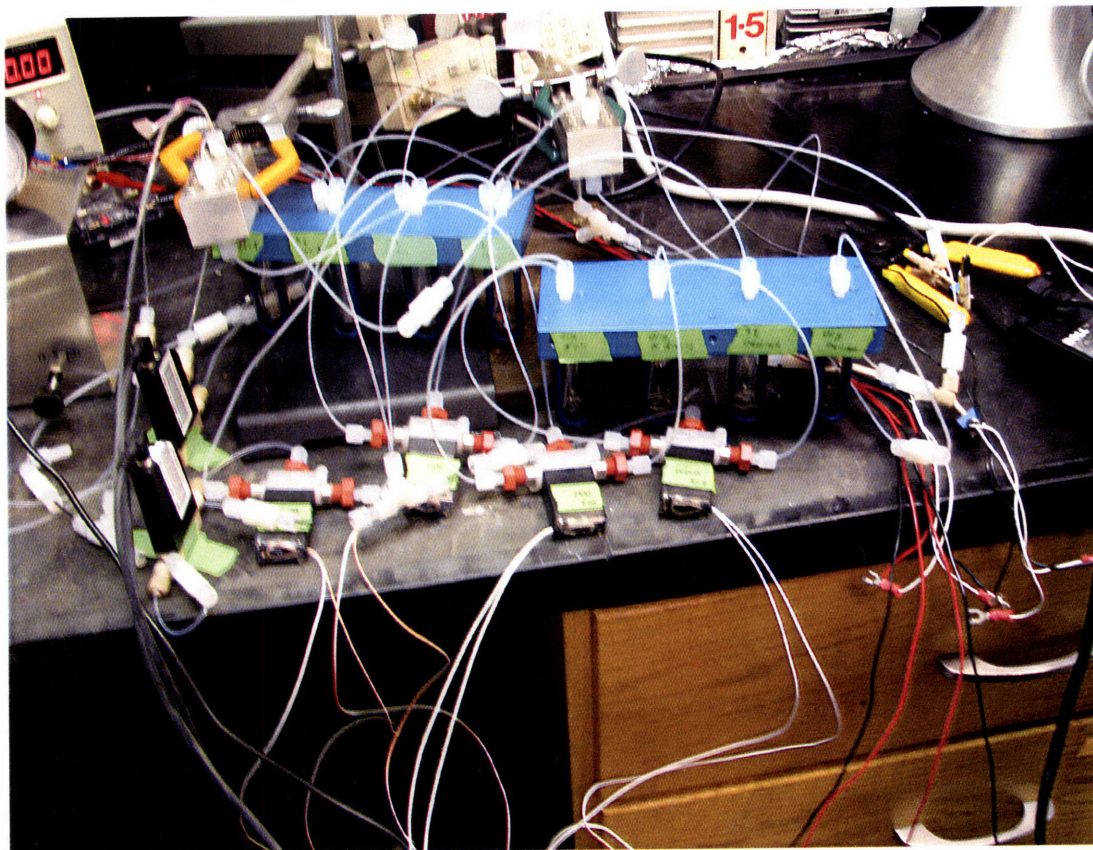
Figure 4.6 Photograph of the multistage extraction setup. The two separators were machined from stainless steel with a fluoropolymer membrane sandwiched between the two flow channels. In this experiment, in-line pumps were used on both, organic and aqueous lines. Two in-line pumps used four enclosures. Two additional enclosures were used to flow in the aqueous and organic feeds using gas pressure, while two more enclosures were used to collect the aqueous and organic outlet streams. Two Burkert three way rocker type solenoid valves and one Lee three-way solenoid were used per pump. The Burkert valves were used on the liquid lines as they are chemically compatible with most organic solvents. The Lee valve was used on the gas-side to control the switching between enclosures. A function generator was used to switch the states of the Lee valve. Details of the individual components are provided in Appendices D and E

As seen from the figure, there are three distinct parts that make the system - Electrical, Fluidic and Pneumatic. While all liquid flow takes place in the fluidic lines, the pneumatic lines are used to provide pressure, and the electrical lines are used to power the valves, and flowmeters.

When the syringe pump was being used, at very low flowrates (1-5 μl/min), periodic flow oscillations from one-phase to two-phase flow were observed. Referring to Figure 4.3, the oscillations were seen in the two-phase region where the fresh organic feed from the syringe met the aqueous flow from the pump. As the two immiscible phases met, and formed two-phase flow, the pressure drop in the two-phase region increased because a two-phase flow offers higher pressure drop than either single phase[103]. The important feature of this system was that the in-line pump flowed at constant delivery pressure, whereas the syringe pump works by volume displacement, hence provides constant flowrate, adjusting for required pressure to deliver the flowrate. So as the two-phase flow was formed, the pressure drop increased with each new droplet addition until the pressure drop became so high that the aqueous side stopped flowing being unable to provide increased pressure. A single phase organic flow was observed after about 20 drops of two-phase flow were formed. As the two-phase flow reached the separator and got separated, the pressure drop reduced, starting the aqueous flow, and resuming the two-phase flow pattern. This oscillation between two-phase and single-phase flow was a result of comparable surface forces (that determine two-phase pressure drop) with the pressures existing in the system due to flow (a result of the flowrate set point), along with the uniqueness in the system in that of the two flow drivers, one was constant volume, the other at constant pressure. It is difficult to predict the pressure drop in two-phase flows as it depends on a number of factors – flow regime, wetting characteristics, impurities. Previous work[94-99] on simple model systems showed the complexity and uncertainty in multiphase microfluidic modeling. Attempts to numerically model the oscillations to compare with the experimental observation along the lines of previous work was found to depend on a number of assumptions, and resulted in being too involving. It is possible, however, to construct simpler systems to study just the flow oscillations if the aim is to glean more insight about two-phase flow behavior at the microfluidic scales. For

multistage extraction experiments, the system was made immune to disturbances, and physics of multiple forces by i) replacing syringe pumps by pressure driven flow, thus removing flow disturbance source ii) providing in-line pumps in both, organic and aqueous lines iii) collecting outlet streams under pressure that could be tuned as an additional handle to control the pressure gradients along the system. Removal of the syringe pumps got rid of the single and two-phase oscillations and provided steady, regular two-phase flow.

Experiments using the microdevice (discussed in detail in chapters 3 and 8) as enclosures for the pump over long times showed that an active level control system was needed to prevent the small enclosures from flooding or running dry. Any small error in measuring flowrate adds up over time resulting in actual volume in the enclosure being different from the one measured using integrated flowrate values over time. There are also other disturbances such as tiny air bubbles that introduce challenges in operating small enclosures for prolonged time periods. Use of the larger enclosures provided enough time for accumulation or depletion without any enclosure running dry or flooding. The larger capacity also allows a large run time after steady state is achieved. The large scale system can be reliably run for multiple days without any decline in performance. Extraction using large enclosures uses long switching times, has longer startup times because of greater volume, and is suitable for use in cross flow and countercurrent extraction modes, while the microchips use short switching times, have shorter startup times and can be used countercurrent extraction, but not for cross-current as a result of the lower volumes.

4.5 Results

The results after extraction of DMF from DCM into water after two stages of operation are shown in, and depicted graphically in Figure 4.7. The results confirm two-stage countercurrent extraction, as the amounts extracted are very close to the two-stage theoretical expectation. In most experiments, the extracted amounts were slightly less than 100% of theoretical, while one reading was over 100%. These differences are a

result of the small errors in estimating flowrate for the organic phase by measuring volume in a given amount of time. As the flowrate was needed to be kept constant, the volumes were measured in short time intervals resulting in the small uncertainty in flowrate.

Table 4.1 Multistage extraction results

COUNTERCURRENT EXTRACTION						
	Phase	Flowrate (μl/min)	Concentration in feed (mole percent)	Concentration at the outlet (mole percent)		Total extraction as a percentage of theoretical expectation[a]
				Experimental	Theoretical	
Run-1	Organic	13.87	5.6845	0.6546	0.6043	99.01
	Aqueous	25.22	0.0000	No Data	0.7940	
Run-2	Organic	24.90	4.4299	0.3465	0.6199	107.17
	Aqueous	37.35	0.0000	0.7369	0.7998	
Run-3	Organic	13.35	3.9976	1.0034	0.9544	98.39
	Aqueous	13.35	0.0000	0.6790	0.8687	

CROSS-FLOW EXTRACTION						
	Phase	Flowrate (μl/min)	Concentration in feed (mole percent)	Concentration at the outlet (mole percent)		Total extraction as a percentage of theoretical expectation
				Experimental	Theoretical	
Stage-1	Organic	5.00	4.4350	2.3620	2.8048	96.91
	Aqueous	3.06	0.4261	0.9070	1.0871	
Stage-2	Organic	5.00	2.3620	1.0540	0.9460	
	Aqueous	5.00	0.0000	0.3641	0.3667	

[a] Total extraction as a percentage of theoretical expectation $= \dfrac{\text{total change in organic concentration}}{\text{expected theoretical change in organic concentration}}$

Run-1

DMF mole fraction in water

DMF mole fraction in DCM

Run-2

DMF mole fraction in water

DMF mole fraction in DCM
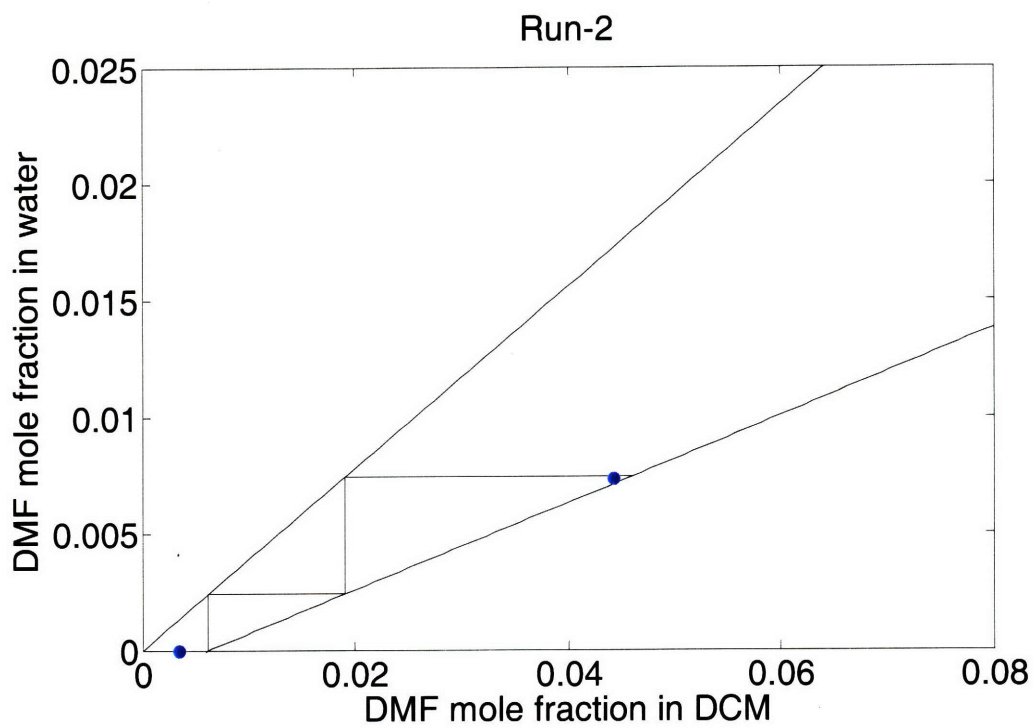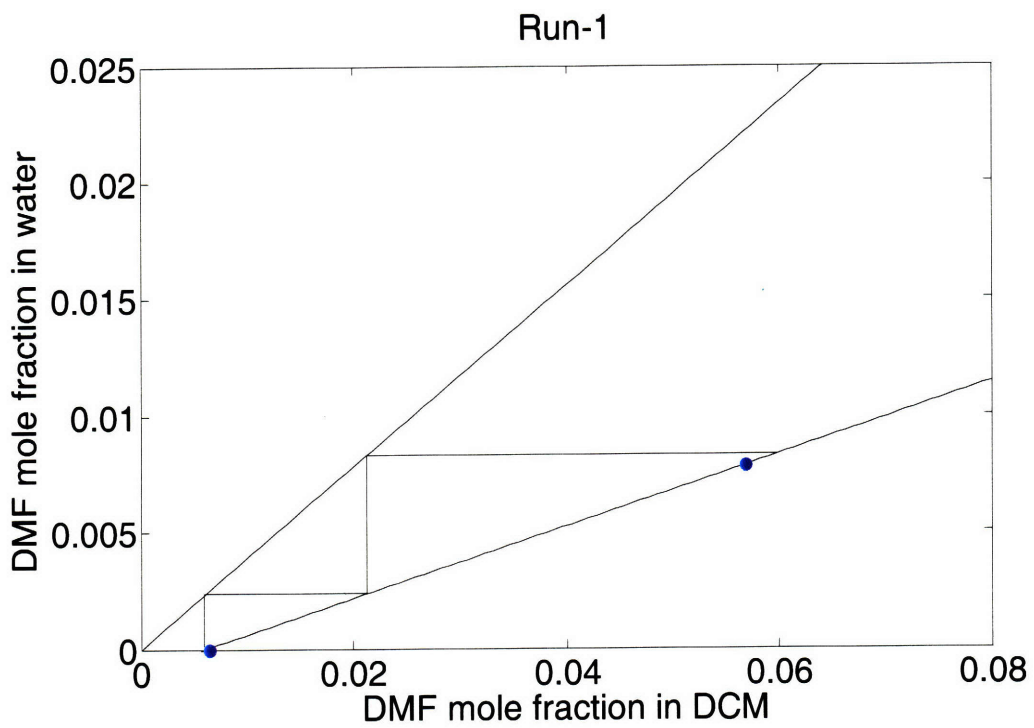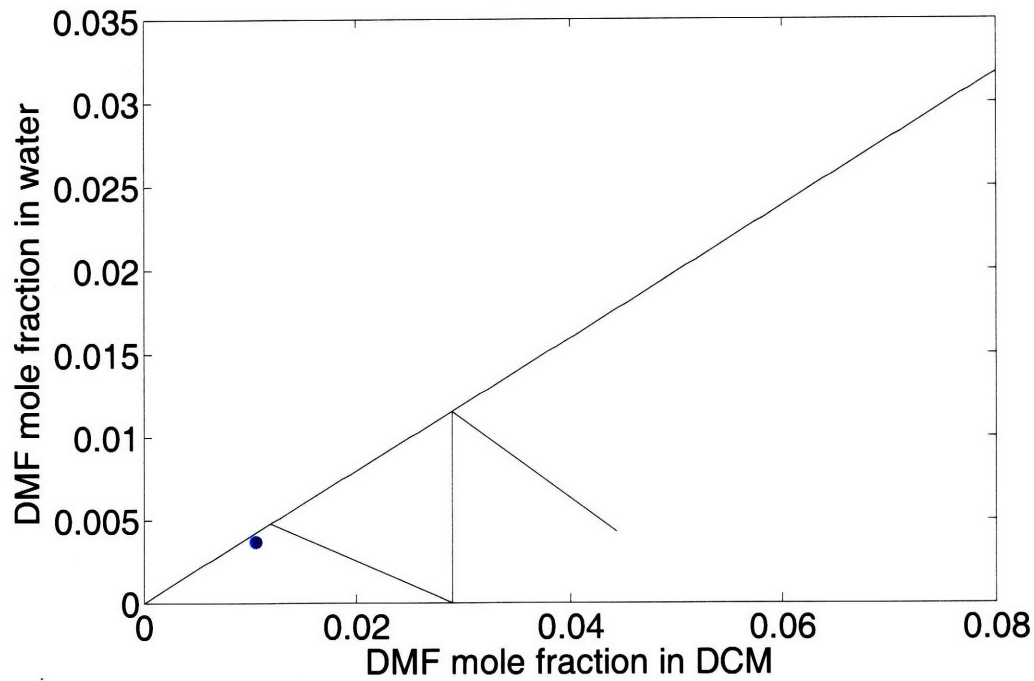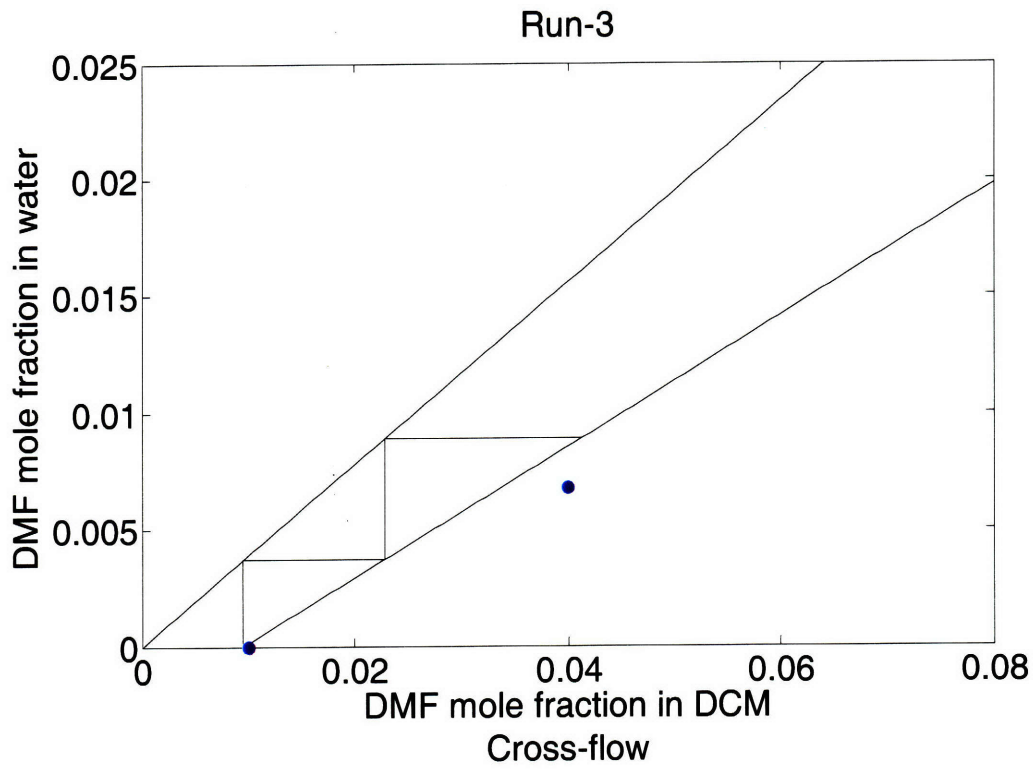
Figure 4.7 The results from multistage extraction shown on a McCabe-Thiele diagram. The theoretical stages are marked off, while the blue dots represent final experimental concentrations.

4.6 Discussion and Conclusions

The extraction result is scalable to many more stages when an in-line pump is used after each stage for both the phases. It is the microscale equivalent of the feed-charge pump common before each unit operation at large scale continuous operations. As with all continuous operations, the startup takes time, but the system is robust in operation once steady state is reached. The system can be easily integrated with reactions upstream or downstream – not possible if syringe pumps were used. Initial materials issues were solved by using chemically compatible three-way valves from Burkert Fluid Control Systems. Interesting systems engineering challenges were met with and the observed phenomena could be studied further. Further development of the system could involve adding automated control systems and level monitoring for the flowrates, and new generation chip design that integrates most of the tubing, valves, and enclosure volume to provide a more elegant multi-stage system.

The system demonstrated for multistage extraction is much more robust than previous work as it provides a larger operation regime, and the ability to add multiple stages. The level of electrical and fluidic connections is relatively simple compared to the work of Quake[100] that interfaces gas lines with fluidics and electrical connections. The multiple stages were enabled by the inline pump, and resulted in extraction beyond the single-stage equilibrium. The system provides the opportunity to transfer a solute almost entirely from one phase to another opening the door for multi-step chemical reactions involving different solvents.

5 Recirculation in Microchemical Systems

5.1 Introduction

As seen in chapter one, a number of chemistry examples have been performed in microreactors. These examples have helped to demonstrate the numerous advantages microreactors offer over conventional synthesis methods. One common thing that stands out among all examples is the time scale of chemical reactions – all are relatively fast reactions that vary from a few milliseconds up to 30 minutes residence time in the microreactor for appreciable conversions. Going over the advantages of microsystems, it becomes obvious that fast reactions gain the most from a change in experimental apparatus from conventional glassware to microreactors - hence, the preponderance of fast reactions in microsystems! However, there are other reasons why mainly fast reactions have been used in microsystems-

i) Fabrication ease

The simplest microreactor is a straight channel about a few centimeters in length providing enough residence time for appreciable conversion for only the fast reactions. Advanced designs with turns in channels for larger residence times, and modifications over straight channel configuration to maintain good mixing are needed to provide larger volume microreactors. Designing such microdevices requires knowledge of the fabrication processes. When designs start getting advanced, they also start becoming specialized for certain types of chemical applications. Most microreactor users are chemists who prefer having generic microdevices for a wide range of applications. As a result, most microreactors found in literature are relatively simple designs running fast chemical reactions.

ii) Pressure drop

The simplest manner of increasing residence time for a given flowrate in microdevices is to have longer channels. However, this approach leads to increased pressure drop. As pressure drop scales as the fourth power of the channel diameter, microdevices already present increased pressure drop, which becomes difficult to manage with longer channels. These issues become a significant challenge while handling packed

bed reactions – where catalysts or solid support materials are loaded in the channel with the void fraction providing the flow path. As a result of the difficulty of managing large pressure drop in microsystems, most examples found in literature deal with simpler configurations that provide lesser residence time appropriate for fast reactions.

As the microsystems community moves forward from single demonstrations to multiple unit systems, the effort is to miniaturize all reaction systems – whether or not they have fast reactions. There is a strong effort in industry to move to continuous manufacturing at all scales of operation. When production requirements are small in continuous systems, as is the case at the research level, the system is inherently a microreactor. The continuous microreactor systems present easier and faster scaleup for large scale production along with other cost savings, such as possibilities to perform processes very differently.

Thus, there is a need for microsystems that can handle reactions with large residence times, but few such systems exist. In this chapter a system capable of performing long residence time reactions is presented. The developed microchemical system recirculates flow to increase the residence time, permitting slower reactions to be studied in microreactors without much increase in flow pressure drop. Flow recirculation was performed by pumping the microdevice outlet stream back in the inlet of the microdevice, thus increasing the residence time. Microscale fluid recirculation has been performed earlier, and was used to concentrate a solid phase capture agent by circulating a solution round in a loop. Microscale valves, fabricated using soft-polymer lithography were used to enable the recirculation by Quake[111]. As discussed in chapter 3, this manner of pumping fluid is not applicable for general chemical synthesis for the reasons of chemical incompatibility of soft polymers with most organic solvents, the narrow range of flowrates achievable, and lack of constancy of flow. The method presented in this chapter uses the pump developed in chapter 3 and overcomes all these disadvantages.

5.1.1 Batch versus Continuous

A truly continuous system is shown in Figure 5.1. A simple approach to increase residence time is shown in Figure 5.2, where multiple units are added to increase residence time. The approach used in this chapter is more like Figure 5.3, where the

outlet is pumped back as the inlet to increase residence time. Depending upon the concentration and reaction types, there are four distinct possibilities-

1) Reaction only in chip

2) Reaction everywhere

3) $C_{out,n-1} = C_{in,n}$

4) $C_{out,n-1} \neq C_{in,n}$

When the reaction takes place only in the chip, and $C_{out,n-1} = C_{in,n}$, systems shown in Figure 5.2 and Figure 5.3 are identical after four passes of the reactor. The system in Figure 5.3 is still a batch system as there is no overall inlet and outlet, but the reaction chip operates in a continuous flow manner. It is possible to make the system continuous by adding an inlet and an outlet stream to the system shown in Figure 5.2, in which case the recirculation would provide recycle, and based on recirculating and outlet flowrates, different recycle ratios could be achieved. No recycle would mean a plug flow operation while very high recycle ratios would imply a CSTR-type operation.
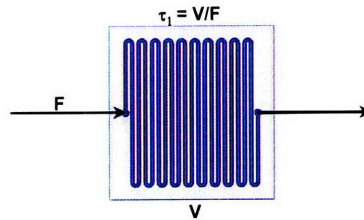
Figure 5.1 Generic microreactor
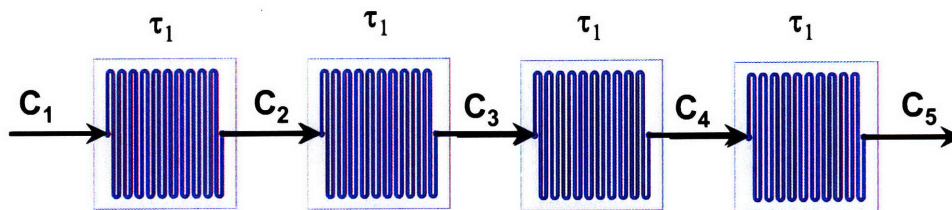
Figure 5.2 Increased residence time by addition of microreactor units
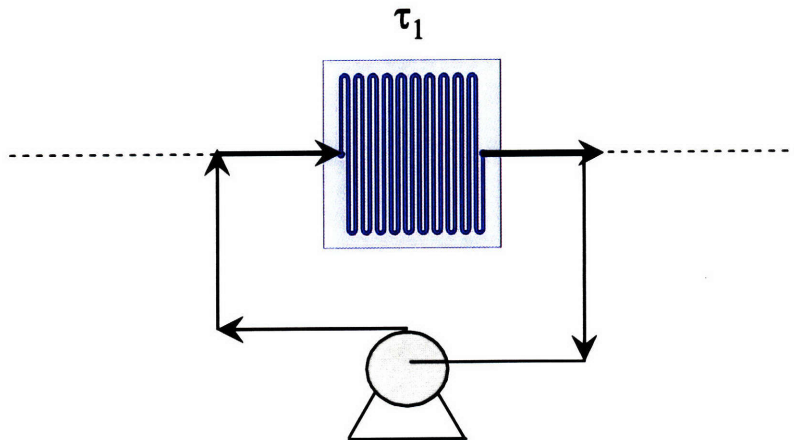
Figure 5.3 Recirculation using pump

5.2 Recirculation Setup

5.2.1 Description

The inline pumping technique used gas pressure from a high pressure gas source and involved no moving parts. The pressurizing principles are the same that were developed in chapter 3. The flow recirculation system involved three enclosures – E1, E2 and E3 connected in cyclic fashion to form the recirculation loop, with the microdevice between E1 and E2, which were kept at constant pressures, P_1 and P_2, respectively, in order to maintain constant pressure drop, hence a constant flowrate across the microdevice. Pressure in E3 was varied periodically using a square-wave profile with the higher pressure as P_3 and lower as P_a (atmospheric ambient pressure), such that $P_3>P_1>P_2>P_a$, to enable the flow recirculation. When the valve is closed, liquid from E1 flows to E2 through the microdevice at a constant flowrate, and then from E2 to E3. When the valve is open, liquid flows from E3 to E1, completing the loop. The frequency of valve opening and closing depends on the flow resistances between E2 and E3, and E3 and E1. Usually, these resistances are kept same, in which case, the valve is open half the time and closed the other half. The flowrate though the microfluidic device remains constant as the pressure drop (P_1-P_2) is held constant. If the flow resistance in the device changes with time (as when the microdevice is a packed bed catalytic reactor), flow sensors can be attached and feedback control as described in chapter 3, can be used to maintain constant flowrate by accordingly adjusting the enclosure pressures. This method of recirculation

94

uses either silicon microdevices as enclosures or glass vials as discussed in chapter 3 – both materials excellent in their chemical compatibility with most reagents. The flowrate in this system remains very constant as shown in the next section, and by varying the pressures P_1 and P_2, a large range of constant flowrates are achievable in the loop. Similar to the demonstration of the inline pump in chapter 3, the recirculation experiments were performed using enclosures of two scales – i) 10 ml scale, and ii) 40 µl scale. Microdevices described in chapter 3 were used as enclosures for (ii), while shell glass vials with pressurized manifold were used for (i).

$\Delta P = P_1 - P_2 = \text{constant}$

$P_3 > P_1 > P_2 > P_a$
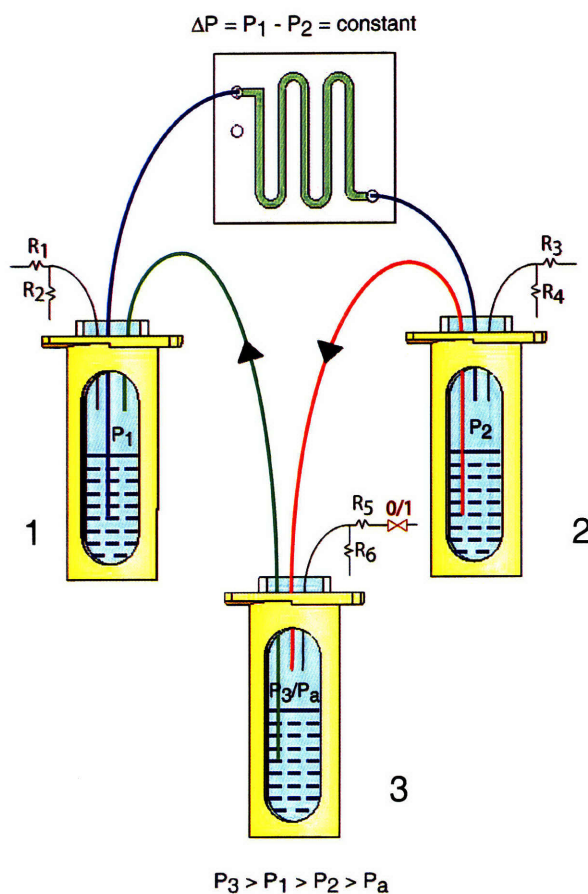
Figure 5.4 Design of the constant recirculating flow system. The solid arrows represent one-way valves. P_1 and P_2 are the steady state pressures achieved in corresponding enclosures using the system described in chapter 3. The on-off valve on the third enclosure is periodically switched, and the pressure inside the enclosure is P_3 when the valve is open and P_a when it is closed. When the active valve is open,

fluid flows from the third enclosure to the first and from the first to the second, through the microfluidic device, following the pressure gradient $P_3 > P_1 > P_2$. When the active valve is closed, fluid flows from the first enclosure to the second through the microdevice and from the second to the third, following the pressure gradient $P_1 > P_2 > P_a$.

5.2.2 Governing equations

Let V_1, V_2 and V_3 represent the volumes of the liquid-free space in enclosures 1, 2 and 3 respectively. Let R_D, R_α and R_β represent the fluid flow resistance between enclosures 1 and 2 through the device, between enclosures 3 and 1, and between enclosures 2 and 3 respectively. R_1, R_2, R_3, R_4, R_5 and R_6 are gas-side flow resistances as shown in Figure 5.4. P_0^i (for i=1-3) represents the constant high pressure for the three enclosures. There are six variables – the three pressures in the enclosures and the three flowrates; and there are six equations that determine these values as a function of time in the two cases – when the valve is open, and when it is closed.

The flowrate out of enclosure 1 ($\frac{dV_1}{dt}$) is the difference between flow out ($\frac{P_1 - P_2}{R_D}$) and flow in ($\frac{P_3 - P_1}{R_\alpha}$). The pressure, P_1 in the enclosure is given by the solution of a mole balance differential equation on the gas side explained in section 3.10 of chapter 3. Using these balances, the governing equations are-

When valve open, (P_3 is high, $P_3 > P_1 > P_2$)

$$\frac{dV_1}{dt} = \frac{P_1 - P_2}{R_D} - \frac{P_3 - P_1}{R_\alpha}$$

$$\frac{dV_2}{dt} = -\frac{P_1 - P_2}{R_D}$$

$$\frac{dV_3}{dt} = \frac{P_3 - P_1}{R_\alpha}$$

$$\frac{1}{RT}\frac{d(P_1 V_1)}{dt} = \frac{P_0^1 - P_1}{R_1} - \frac{P_1 - P_a}{R_2}$$

$$\frac{1}{RT}\frac{d(P_2 V_2)}{dt} = \frac{P_0^2 - P_2}{R_3} - \frac{P_2 - P_a}{R_4}$$

$$\frac{1}{RT}\frac{d(P_3 V_3)}{dt} = \frac{P_0^3 - P_3}{R_5} - \frac{P_3 - P_a}{R_6}$$

When valve closed, (P_3 is low (=P_a), $P_1 > P_2 > P_3$)

$$\frac{dV_1}{dt} = \frac{P_1 - P_2}{R_D}$$

$$\frac{dV_2}{dt} = -\frac{P_1 - P_2}{R_D} + \frac{P_2 - P_3}{R_\beta}$$

$$\frac{dV_3}{dt} = -\frac{P_2 - P_3}{R_\beta}$$

$$\frac{1}{RT}\frac{d(P_1 V_1)}{dt} = \frac{P_0^1 - P_1}{R_1} - \frac{P_1 - P_a}{R_2}$$

$$\frac{1}{RT}\frac{d(P_2 V_2)}{dt} = \frac{P_0^2 - P_2}{R_3} - \frac{P_2 - P_a}{R_4}$$

$$\frac{1}{RT}\frac{d(P_3 V_3)}{dt} = -\frac{P_3 - P_a}{R_6}$$

$$R_D = \frac{8\mu LM}{\pi r^4 \rho}\frac{Pa.s.m.kg/mol}{m^4 kg/m^3} = \frac{8\mu LM}{\pi r^4 \rho}\frac{Pa}{mol/s}$$

As shown in chapter 3, pressure driven flow provides constant and steady flow after the pressure in the enclosure is fully developed. In the recirculation setup, as enclosures 1 and 2 are kept at constant pressure, the flowrate through the microdevice remains constant. The only time when this constancy is affected is when the valve on the gas side on enclosure 3 is toggled leading to a change in governing equations. The equations above were used to simulate the change in constancy. Figure 5.5 shows that substantial

constancy of flow can be achieved when the gas side resistance is made small enough that the time scale for pressures to adjust to changed conditions is much smaller than the time-scale for flowrates to readjust.
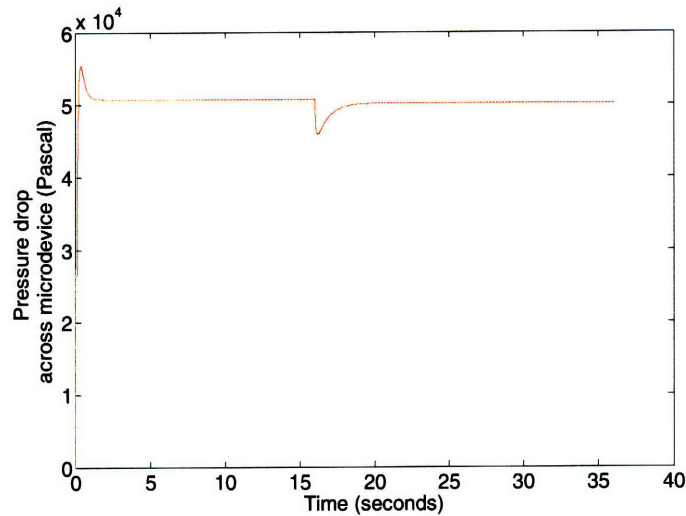
(a)
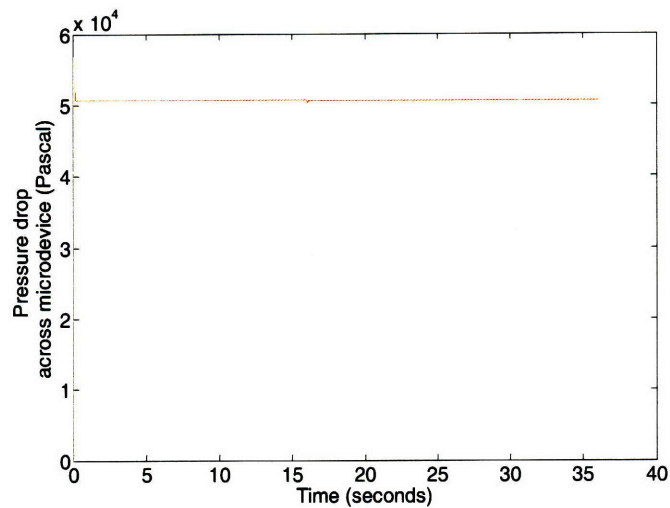
(b)

Figure 5.5 Constancy of flow as a function of leak resistance on the gas line. The difference between the two graphs is that R_1 through R_6 are lower by a factor of 16 in (b) compared to (a). Tubing used to provide the resistance was 500 micrometer diameter instead of 1 millimeter diameter in (a) leading to a sixteen-fold reduction in resistance. The governing equations discussed in 5.2.2 were used in a MATLAB program to generate these graphs. The MATLAB program is presented in the Appendix B

5.2.3 Constancy of flow

The constancy of flow was experimentally observed in the setup shown schematically in Figure 5.6. These figures will be explained in more detail in the section on peptide synthesis; for this section only the fluidic design is relevant. High pressure gas source from P_A and P_B resulted in pressures P_1, P_2 and P_3 in the three enclosures. The flowrate through the two microdevices was measured by adding an inline Sensirion flowmeter (not shown in the setup). The tubing lengths and diameters used were calculated to provide specific resistance values so that the model discussed in 5.2.2 could be verified. The detailed design calculations along with the lengths, diameters, and physical constants are presented in the Appendix B. The observed flowrate is shown in Figure 5.7. Two things stand out from this graph – the flowrate is very constant, and the constant value is very close to the designed value of ~ 8.5 μl/min. These confirm the model used to design the flow recirculation, and show that very constant flow can be obtained.
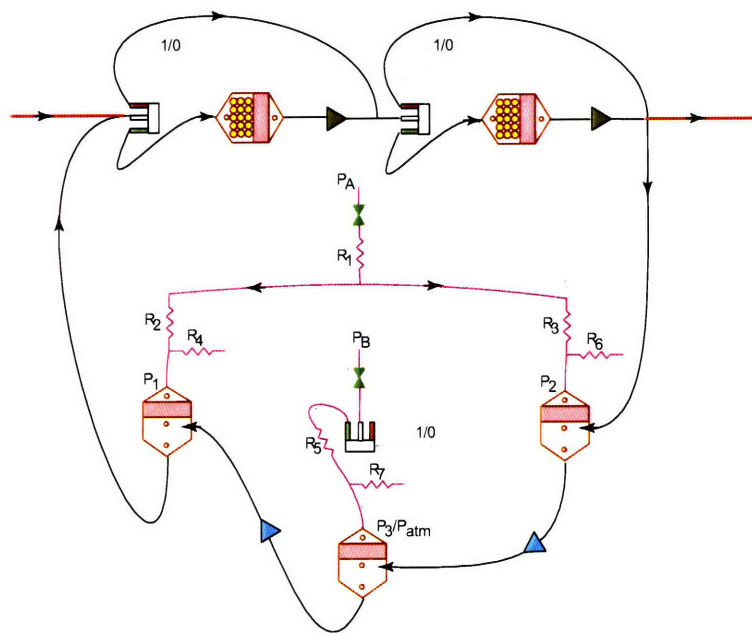
Figure 5.6 Schematic of flow recirculation set-up
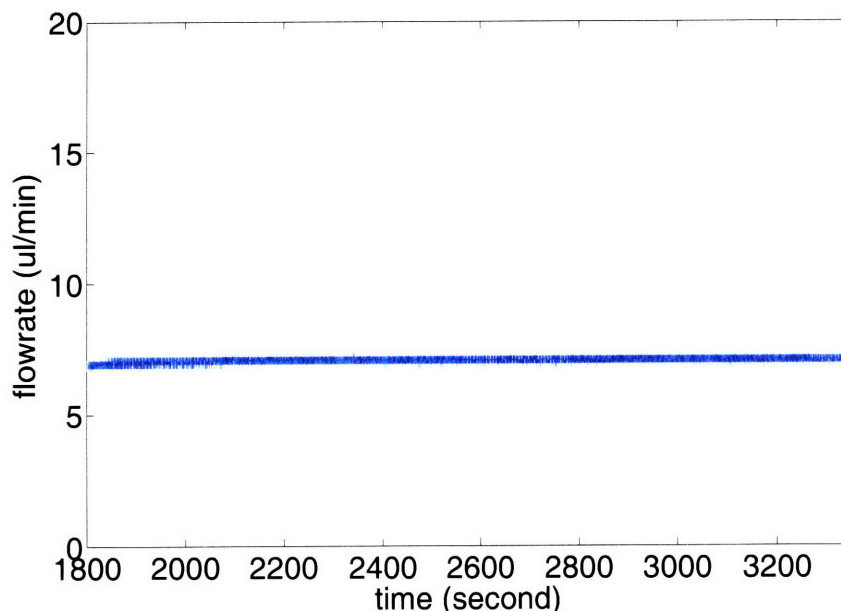
Figure 5.7 Study of flow constancy for the recirculation system shown in Figure 5.6

5.3 Chip design and fabrication

The recirculation system developed earlier in this chapter is a tool to provide longer residence times and hence, the ability to study slower reactions. It also has the ability to provide large pressures to overcome high pressure drops in the system. Packed-bed reactions in a microreactor tend to fall in this category – they are slow and packed bed reactions tend to offer increased pressure drop. The synthesis of peptides using the solid phase Merrifield techniques are an example of such reactions – the reaction times vary from 50 to 60 minutes, and the solid support increases in volume during reaction, up to double the initial volume or more depending on the size and type of peptide being grown. Preliminary test experiments for peptide synthesis were performed using standard tubes with a frit and ferrule at the outlet to prevent solid support from flowing. These tests showed the increase in solid support volume happens along all directions leading to partial blocking of the tube and presenting very high pressure drops. Therefore, use of microchips used for previous demonstrations of packed bed reactions such as hydrogenation was ruled out. The increase in solid support volume is a result of i) swelling of the organic matrix of the solid support ii) physical growth of the peptide chain length on the bead. Attempts were made to use inorganic silica beads

functionalized with organic linkers to act as peptide synthesis supports. However, silica functionalization led to poor surface coverage uniformity – only small islands on the bead surface got functionalized, which was inadequate for peptide growth as with increasing chain length, steric issues emerge. In addition, silica bead use only could solve half the volume increase challenge – the increase due to peptide growth would have still existed. Therefore, new silicon-based microchips were fabricated that permit volume change of the packed solid phase and were used for the peptide synthesis using flow recirculation. As shown in Figure 5.8, there is a large cavity of 650 μm depth with a shallow 50μm deep bank of 50 μm wide capillaries at one end. The outlet was on the other side of the bank of capillaries. The small feature size at the outlet served as a filter to prevent beads, usually 100 μm in diameter from flowing out. The large cavity allowed for increase in volume when packed partially.
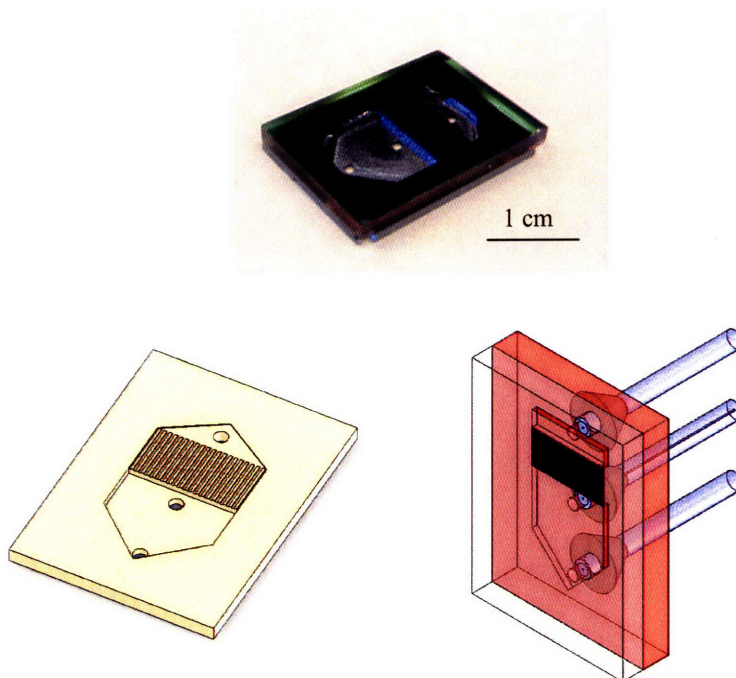
Figure 5.8 Photograph and schematic of microchip and packaged microdevice. Design details are provided in the AppendixC.

Having developed a recirculation system that provided constant flowrate, and microdevices capable of handling solid phases with variable volume, two different model

heterogeneous systems were demonstrated – one used solid phase to grow product, other used the solids phase as catalyst.

5.4 Peptide Synthesis

5.4.1 Packed bed protein synthesis

Peptides are important biological polymeric compounds that have amino acids as their basic building blocks. Their immense importance in biological research imparts significant value to their synthetic production techniques. So important; that Robert Bruce Merrifield was awarded the Nobel Prize in Chemistry in 1984 for the invention of solid phase peptide synthesis techniques. Today, most peptide synthesis is performed commercially in Applied Biosystems' Peptide Synthesizer machines that improve upon the process invented by Merrifield. Most previous effort towards peptide synthesis in microreactors has been by the research groups of Watts[101, 102], and that of Gulari[103-106]. The Watts' approach uses homogeneous solution phase chemistry to couple individual amino acids to form peptides. While this has been one of the first attempts at peptide synthesis in microreactors, peptide lengths attainable are limited, and the yield drops with increasing size. In general, all challenges with general homogeneous phase peptide synthesis apply to their work. The approach of Gulari has been to use functionalize silicon surfaces with bridging groups and use non-conventional methods such as optical activation to perform peptide coupling reactions. While these are promising approaches, they further the 96-well batch synthesis methods, and fail to capitalize on the continuous synthesis advantages that the commercial Applied Biosystems synthesizers utilize.

In this approach, the recirculation setup was used to achieve continuous flow peptide synthesis on a packed bed of polymeric matrix inside microchips along the lines of modified Merrifield synthesis methods. The recirculation was demonstrated at two scales of enclosures – 40 microliter and 10 milliliter to achieve flowrates up from 1 µl/min to several ml/min. The chemistry involved successive steps of deprotection of amino acid on the matrix, activation and addition of new amino acid, and washing to grow the peptide chain, followed by cleavage of the final peptide from the resin. The typical coupling times (30-50 minutes) were more than what most microdevices provide, hence the recirculation system was used to increase the residence time. The large volume

microdevices allowed for manageable pressure drop even with supports that swell during synthesis. The system design allowed for multiple different peptide syntheses simultaneously, and the small scale of operation permitted synthesis of very small amounts of peptides – sizes comparable to what most experiments require.

5.4.2 Peptide synthesis –Process Chemistry

In its simplest form, peptide synthesis of size n requires $n-1$ coupling reaction steps. Say A, B, C…represent amino acids, then formation of the peptide A-B-B-C-B, involves reacting A with B to form A-B, separating excess A and B from A-B, and then reacting the separated A-B with the next amino acid, B to form A-B-B…and so on. If the separation efficiency at any step is not 100%, the impurities build up in the system leading to a progressively decreasing yield of desired products. Furthermore, the reactants need to be protected at all but one reactive group in the amino acid to prevent self -couplings, and multiple couplings. The method just described is the homogeneous phase synthesis, and does not work well for long peptide chains due to exponentially diminishing yields. The method invented by Merrifield used a solid phase to immobilize the first amino acid. The use of heterogeneous synthesis greatly improved yields and allowed synthesis of many long chain, and biologically relevant peptides. The initial method used Boc chemistry or (t-Boc for (t)ert-(B)ut(o)xy(c)arbonyl) for protection of the amino group. Present day methods use Fmoc (9H-(f)luoren-9-yl(m)eth(o)xy(c)arbonyl) The supports are generally made of polystyrene resin. The general heterogeneous synthesis procedure is described in Figure 5.9.

Leuenkephalin, a type of endorphin has the structure Leu-Phe-Gly-Gly-Tyr. This peptide was synthesized using the system showed in Figure 5.11, where there were two chips in the synthesis line used two different types of beads, having different loadings of the first amino acid- Leucine. The system is scalable to many chips in line, and can be used to synthesize different peptides at the same time by using jumpers to skip a chip while circulating an amino acid not in sequence.

5.4.3 Experimental

Leu-Enkephalin has the sequence NH_2-Tyrosine-Glycine-Glycine-Proline-Leucine-COOH. The recipe used for its synthesis started with commercial Fmoc protected resin

with the starting amino acid, leucine preloaded. The supports used were Applied Biosystems' HMP polystyrene resin (Fmoc-L-Leucine-HMP Resin # 401424) having Leucine loading of 0.52 mmol/gm, and Novabioschem's TGA tentagel resin (Fmoc-Leu-NovaSyn® TGA Cat.# 04-12-266), having a loading of 0.24 mmol/gm. Approximately 1-2 mg beads were loaded in the microdevice and were swelled by flowing DMF for 1 hour. The Fmoc protecting group on Leucine was removed by circulating 20% piperidine in DMF for 5 min, followed by washing with DMF for another 5 minutes. 5 ml HBTU/HOBt (0.5 M in DMF) (HBTU = 2-(1H-Benzotriazole-1-yl)-1,1,3,3–tetramethyluronium hexafluorophosphate, HOBt = Hydroxybenzotriazole) were mixed with 5 ml Proline (0.2 M in DMF) along with 700 microliter DIEA (N,N-Diisopropylethylamine), and this mixture was circulated for 20 minutes over the beads for the amino acid coupling reaction. This was followed by washing with DMF for 5 minutes, and repeating the steps of deprotection, washing, coupling and washing till all the amino acids were attached to form the desired peptide. Finally, 20% piperidine in DMF was circulated for 5 minutes for deprotection of the Tyrosine and the beads were washed with DMF. The support beads with the peptide were removed by flowing dichloromethane in the reverse direction and treated with trifluoroacetic acid (TFA) for complete removal of the peptide from the resin. The peptide was analyzed using Matrix Assisted Laser Desorption Ionization (MALDI).

The analysis parameters are provided in detail in the Appendix B. After synthesis, the resin was cleaved and analyzed at the MIT biopolymer lab. As shown in Figure 5.11, two microdevices were used in the synthesis train simultaneously. They had different starting resins, Applied Biosystems' HMP polystyrene resin (Fmoc-L-Leucine-HMP Resin # 401424) having Leucine loading of 0.52 mmol/gm, and Novabioschem's TGA tentagel resin (Fmoc-Leu-NovaSyn® TGA Cat.# 04-12-266), having a loading of 0.24 mmol/gm.

Basic Steps in Solid Phase Peptide Synthesis Using Fmoc-Chemistry
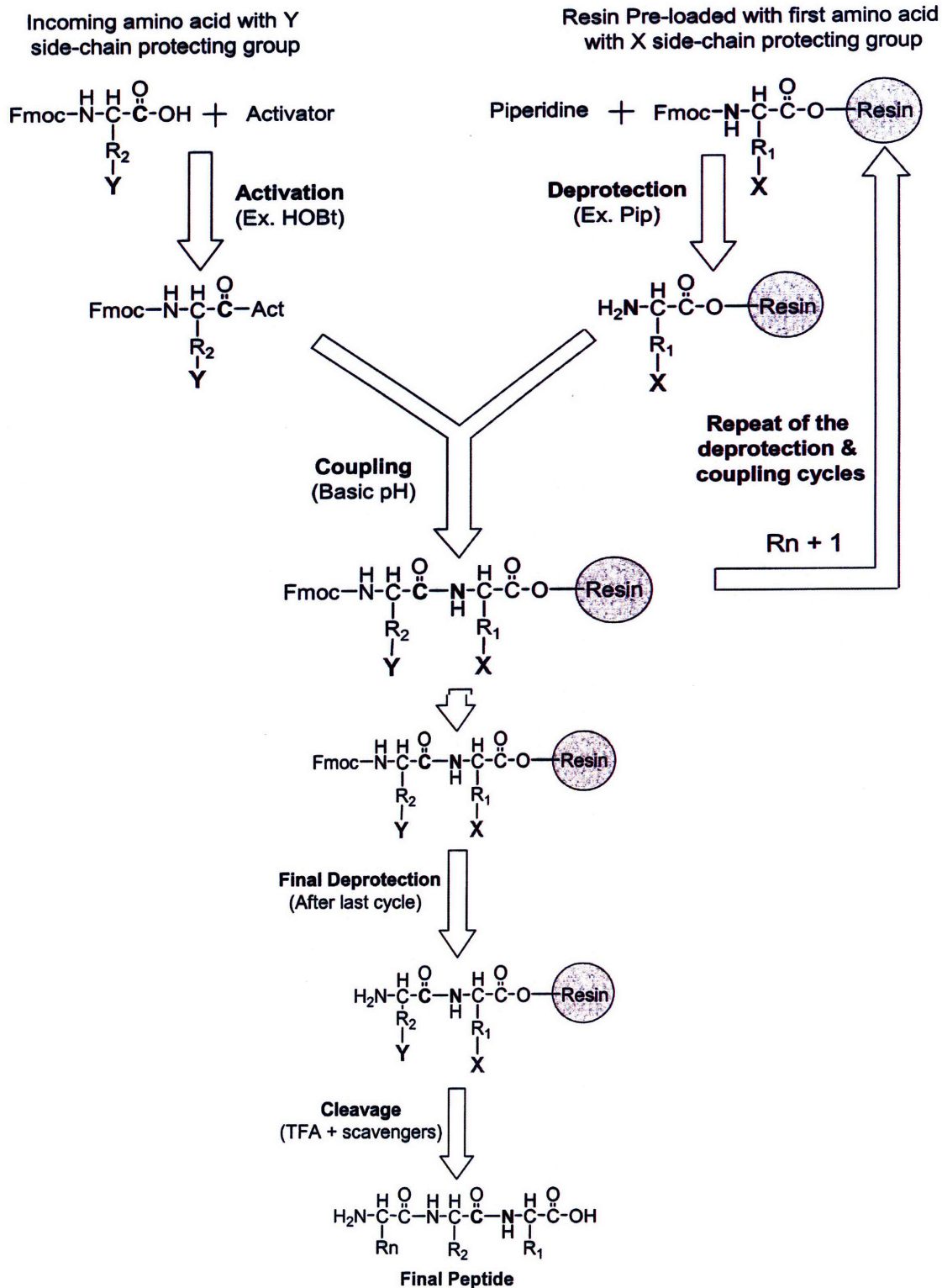
Figure 5.9 Generalized heterogeneous peptide synthesis procedure
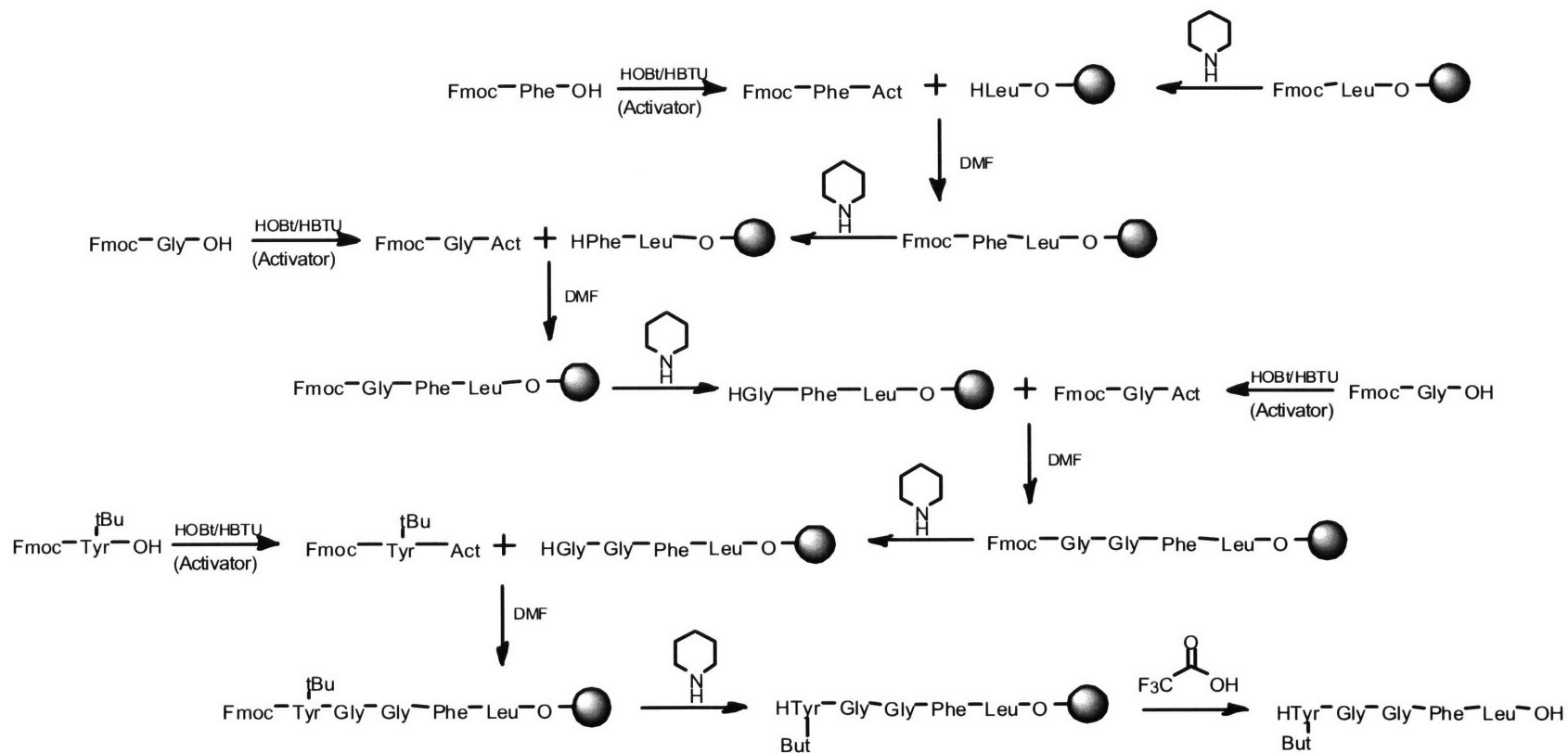
Figure 5.10 Reaction steps for the synthesis of the pentapeptide Leu-Phe-Gly-Gly-Tyr (Leuenkephalin, an endorphin sequence) using the Merrifield Solid Phase Synthesis scheme.
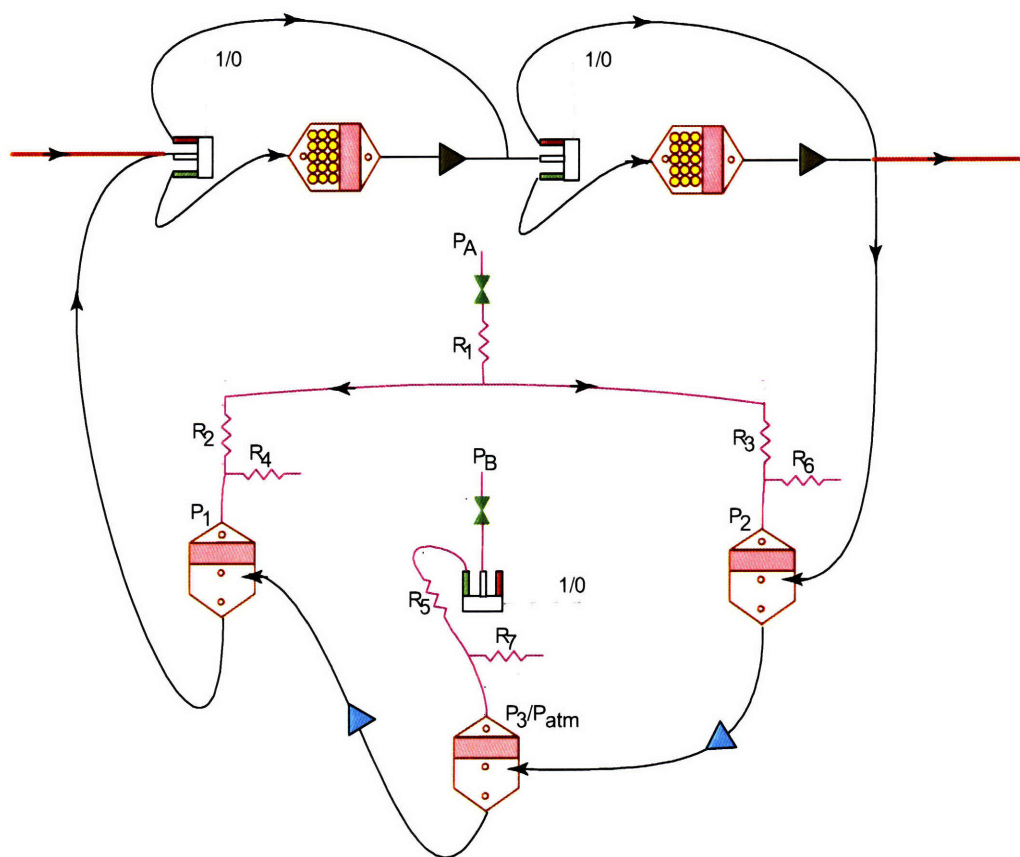
Figure 5.11 Peptide synthesis system with two chips simultaneously using different solid supports for the synthesis.

5.4.4 Results

Figure 5.12 shows the pictures of the two chips after each coupling step. The increase in volume observed is due to the growth of the peptide chain on the support. During cleavage, all protective groups come off the peptide. Leuenkephalin's molecular weight is 505. Leukenkephalin is a negatively charged peptide, and therefore it finds common positive ions such as hydrogen, sodium and potassium to bind. These counter-ions add to the molecular mass and show up on the results of the two microchips, shown in Figure 5.13 as additional peaks. The MALDI results demonstrate successful synthesis of

Leuenkephalin because the desired peptide synthesis is confirmed without any side product formation.

(a)   (b)
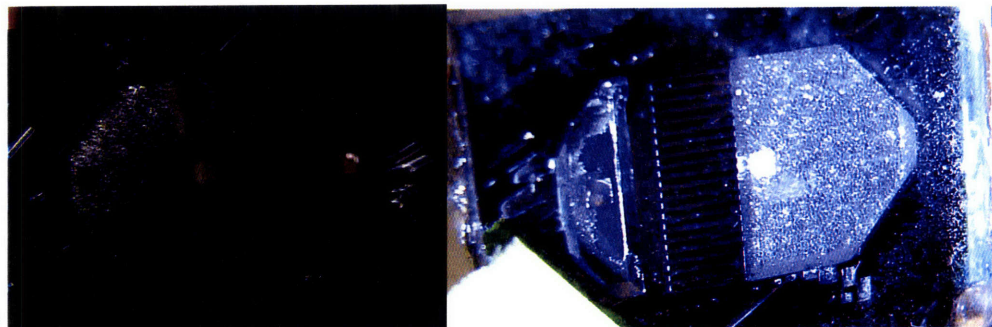
Figure 5.12 (a) Packed bed for both the microchips after loading and swelling the beads but before starting the peptide synthesis. It shows some areas that are free and not occupied by the beads. (b) Packed bed after peptide synthesis. Note that the bed has expanded to cover the free volume available before.
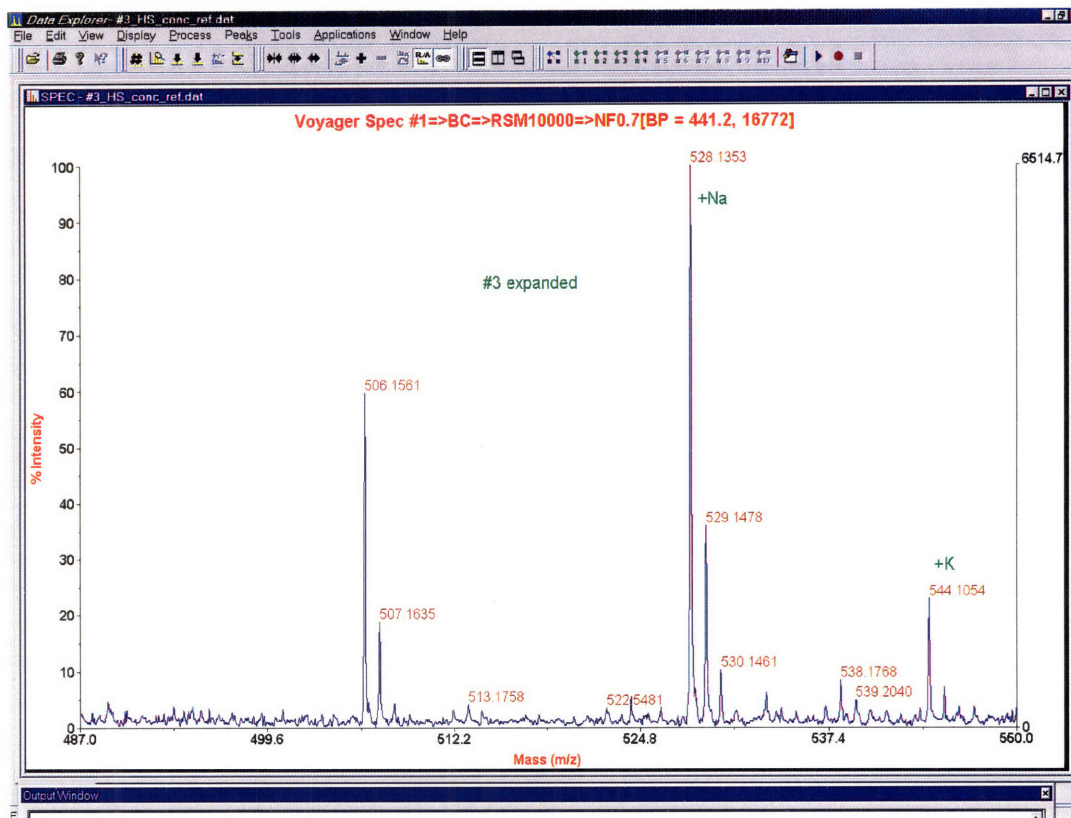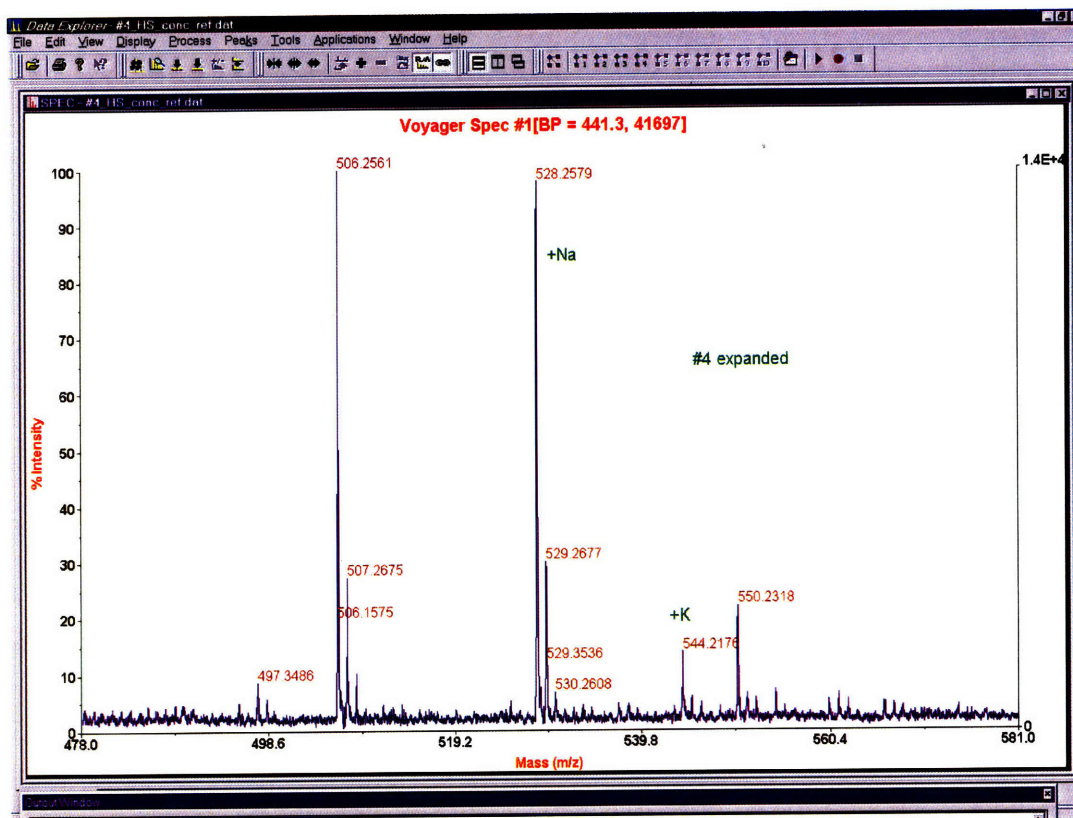
Figure 5.13 MALDI results confirming presence of the desired peptide. Peak at 506 mass is desired product. Peaks at 507, 528 and 544 mass show association with H$^+$, Na$^+$ and K$^+$.

5.5 Click Chemistry

The "click chemistry"[107-112] is an example of a popular synthetic step in the manufacture of important chemical compounds that have pharmaceutical relevance. The packed bed reactor described earlier in the chapter was used to demonstrate the click chemistry reaction for synthesis of triazoles. This work was performed in collaboration with Eamon Comer and Sarathy Kesavan from the Chemical Biology Platform at the Broad Institute, along with Jonathan McMullen.

5.5.1 Chemistry

As shown in Figure 5.14, the click chemistry comprises of the triazole ring formation from the azide and triple bond. The experiments performed in this study were Cu(I) catalyzed, shown in Figure 5.15. The catalyst (Figure 5.16) was solid phase polystyrene

resin with Cu immobilized along with basic groups required for the reaction. The desired product was the result of the intramolecular reaction while the dimers formed as a result of intermolecular reaction (Figure 5.17) were undesired. The two substrates studied are shown in Figure 5.19.
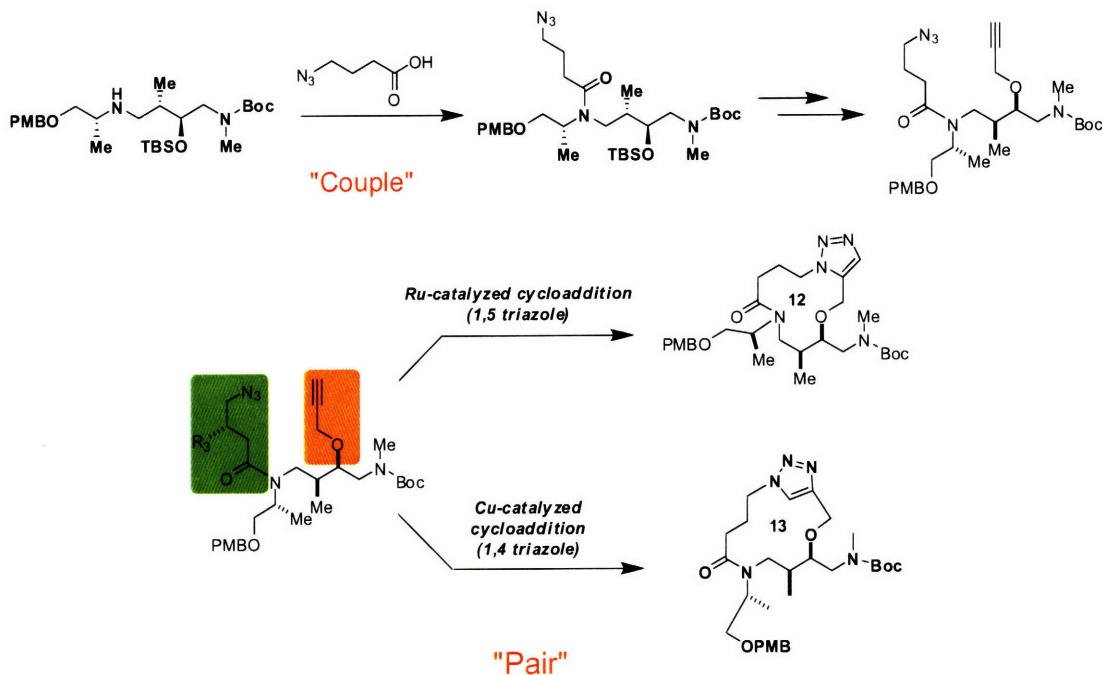
Figure 5.14 Triazole formation using click chemistry
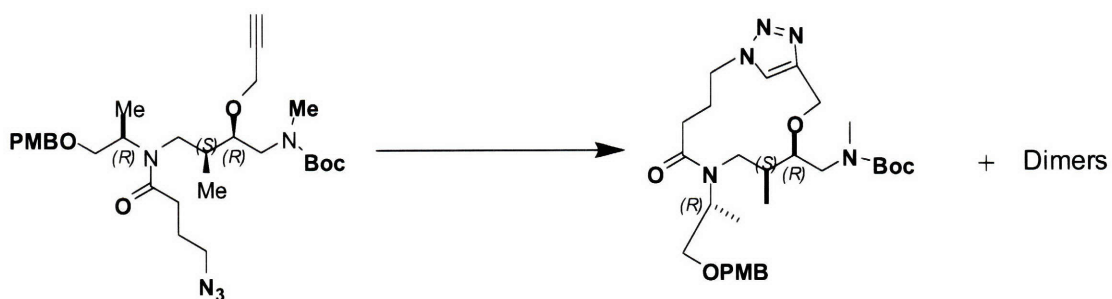
Figure 5.15 Reaction studied in this work

PS-CuPF$_6$
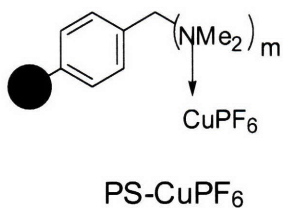
Figure 5.16 Solid phase Cu(I) catalyst used for the experiments

110

Desired Reaction - Intramolecular Coupling
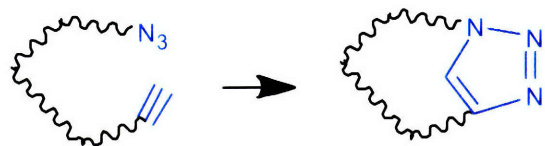
Undesired Reaction - Intermolecular coupling
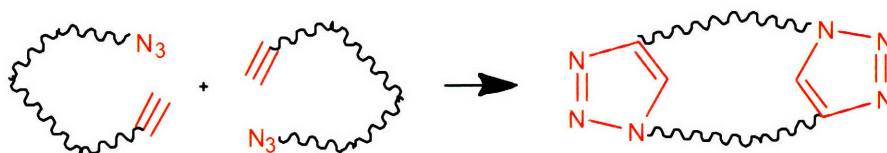
Figure 5.17 Schematic representation of desired and undesired reactions

5.5.2 Experimental

The microdevice was prepared by crushed catalyst beads and sieving to get particles between 250 μm and 300 μm size range. 62 mg of this sieved catalyst was loaded in microchip having cavity volume of 118 μl by design. The catalyst density (ρ) was measured to be 1 mg/μl, so the volume occupied by the catalyst particles was 62 μl, providing liquid volume in the packed region as $118 - 62/\rho = 56$ μl. When the continuous flow experiments were performed at a flowrate of 2 μl/min (as in the temperature studies), the reaction time for catalysis was $56/2 = 28$ min. The packed bed microreactor is shown in Figure 5.18.
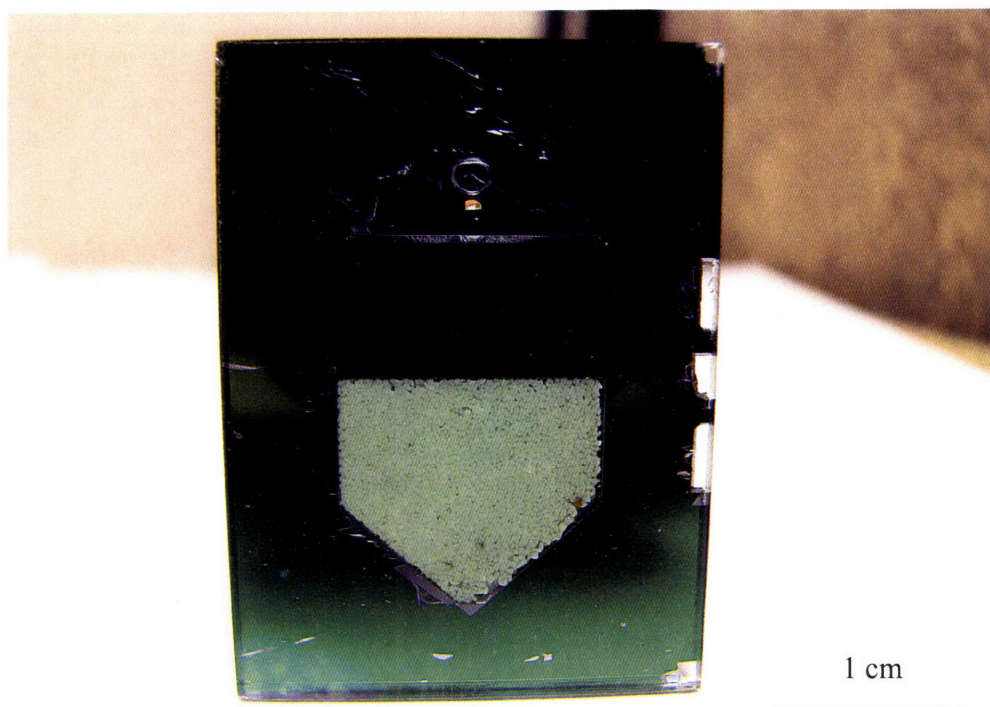
Figure 5.18 Microreactor with 62 mg supported Cu(I) catalyst packed., and solvent (toluene).
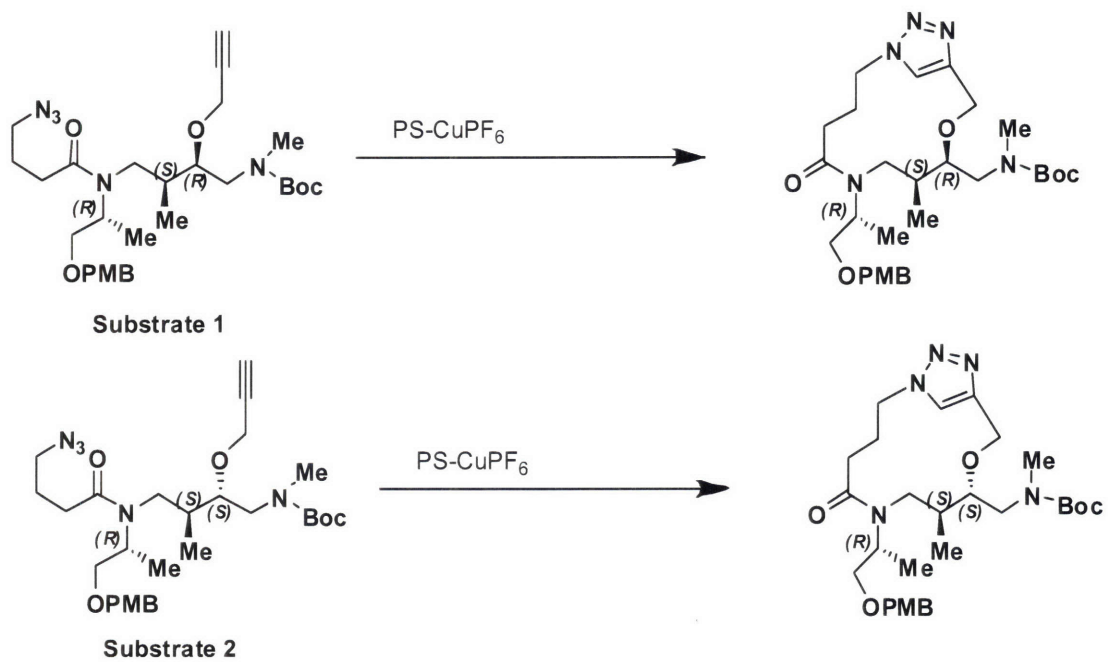
Figure 5.19 Different substrates studied

5.5.3 Results and Discussion

The solid-phase catalyzed reaction takes several hours on the batch scale. The microsystem based method of reaction differed from the batch method in that the relative concentration of catalyst was always higher in the microreactor experiment as only a small amount of reagent saw the catalyst at any given time due to the continuous flow mode of operation. Rates will also be higher if reaction is mass-transfer controlled because the microdevices offer improved mass transfer rates compared to large scale batch systems.

The advantages of using a continuous flow, packed bed plug flow microreactor over stirred batch experiments was seen in experiments with substrate 1. Substrate 1 achieved full conversion in about 16 hours in batch experiments at 60 ^{O}C. Microreactor based experiments achieved similar conversions in a little over 2 hours, as seen in Figure 5.21. The ease of performing multiple experiments quickly in microreactors was demonstrated by performing temperature studies on a similar reactant, substrate-2 at temperatures from 50-110 ^{O}C. The results are shown in Figure 5.22. The continuous flow mode of operation meant that performing new experiments only required changing the temperature set point, and collect after 4 residence times to ensure steady state results. This is a big improvement from batch systems that need to be completely replaced and restarted for each new experiment. The faster rates in microreactors also help performing more experiments in given time. The selectivity in the second set of experiments is higher because the site concentration on the catalyst is lower. As seen in Figure 5.17, dimerization requires two coupling steps, and hence two reaction sites. Lower site density reduces the probability of dimerization, thus improving selectivity.

For future experiments, the recirculation setup could be used to operate at higher flowrates to obtain higher production rates. The concentration measurements after each loop would provide reaction kinetics data, as in a differential reactor. An alternative to recirculation is to flow at very small flowrates to achieve same overall residence times – the extreme example of this is the stop-flow experiments. However, these approaches do not provide intermediate concentrations, hence kinetics, and the low flowrates fail to capture the mass transfer advantages in microreactors that generally scale with increasing flowrates.
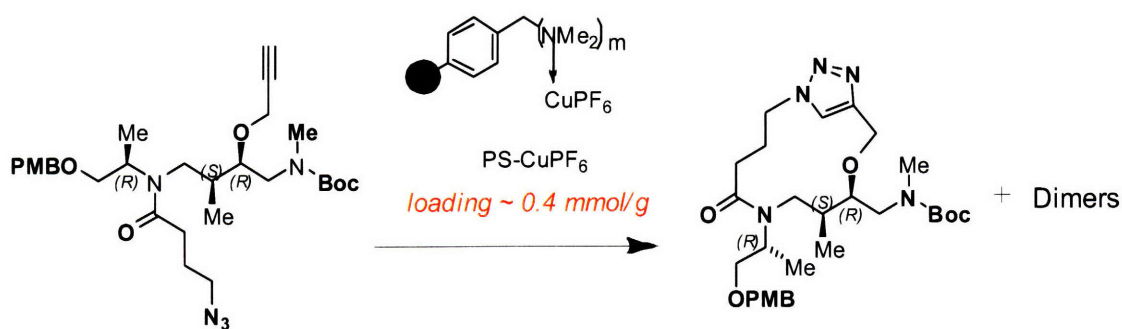
Entry	Conditions	Temperature	Monomer/Dimer (conversion)
1	PS-CuPF$_6$ Toluene, 0.01 M, Residence time = 35 min	RT	NR
2	PS-CuPF$_6$ Toluene, 60°C, 0.01 M Residence time= 35 min	60 °C	4:1 (40 %)
3	PS-CuPF$_6$ Toluene, 60°C, 0.01 M Residence time= 2h 20 min	60 °C	4:1 (95 %)

Figure 5.20 Results from experiments with Substrate-1
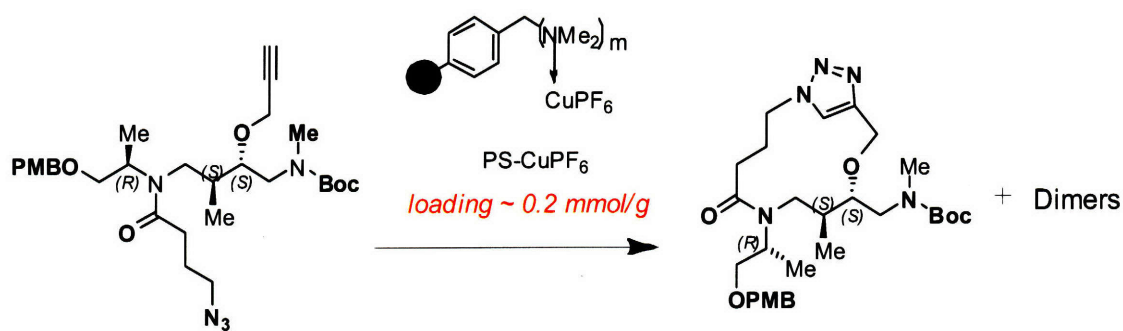
PS-CuPF$_6$

loading ~ 0.2 mmol/g

\+ Dimers

Entry	Conditions	Temperature	Monomer/Dimer (conversion)
1	PS-CuPF$_6$ Toluene, 0.01 M, Residence time = 28 min	50 °C	15:1 (50 %)
2	PS-CuPF$_6$ Toluene, 60°C, 0.01 M Residence time= 28 min	60 °C	15:1 (95 %)
3	PS-CuPF$_6$ Toluene, 60°C, 0.01 M Residence time= 28 min	70 °C	15:1 (100 %)
4	PS-CuPF$_6$ Toluene, 60°C, 0.01 M Residence time= 28 min	90 °C	15:1 (100%)
5	PS-CuPF$_6$ Toluene, 60°C, 0.01 M Residence time= 28 min	100 °C	15:1 (100%)

Figure 5.21 Results from experiments with Substrate-2

5.6 Conclusion

The constant flow recirculation technique is advancement over other approaches as it provides very constant flow for a wide range of flowrates. The development of recirculation techniques has enabled long residence time reactions such as the peptide synthesis and the click chemistry reactions. These are also the first demonstrations for a growing bed microchip design that overcomes limitations of standard packed channels. The microchip permitted synthesis of very small amounts of peptides, while the recirculation system allowed simultaneous synthesis of multiple peptides on different chips in the recirculation loop. The inline pump thus enabled study of new, interesting and varied systems such as the solid phase peptide synthesis and the click chemistry.

6 Multistep Synthesis with Reactions and Separations

6.1 Introduction

Chapter 1 discussed in detail how microreactors enhance chemical synthesis through advantages offered by continuous operation at small length scales in closed systems such as reduced reaction volumes, enhanced heat and mass transfer, and protection from air and moisture.[5, 24, 113-120] Typical chemical synthesis involves multiple reaction steps with separations (work-up) between two successive reaction steps. However, the majority of microchemical demonstrations have been limited to a single reaction step,[5, 24, 113-120] multiple reaction steps without intermediate separations,[121, 122] or multiple steps with solid phase capture and off-line work-up.[44, 47] As an example of the latter, the first demonstration of the complete synthesis of the natural product oxomaritidine used solid phase reactants and capture as well as offline manual solvent switch.[47] The total synthesis of ^{18}F labeled fluorodeoxyglucose in an integrated microfluidic chip built in poly(dimethylsiloxane) (PDMS) combined five sequential steps: ^{18}F ion concentration on solid capture agent, water evaporation through the PDMS, radiofluorination, solvent exchange by evaporation through the PDMS and replacement, and hydrolytic deprotection in sequential sub μL batch quantities[46]. These studies elegantly demonstrate the potential of microreactors in multistep synthesis, but the need for integration of continuous work-up with reactions remains. Solvent compatible microreactor systems combined with separation units would allow continuous multistep synthesis ranging from nanoliter to milliliter quantities with potential for scale-up to larger amounts through parallel operation. Moreover, avoiding the use of solid phase capture agents reduces costs and the need for replacing/regenerating the solid phase.

The dominance of surface tension forces over gravity in microfludidic devices[123] means that microfluidic extraction is typically based on immiscible fluid contacting.[91, 92] By exploiting the laminar flow characteristics of microfluidic devices, extraction can be realized by side-by-side contacting of immiscible fluids in co-current and counter-current flow arrangements.[91] Such devices offer the potential for more than one equilibrium

extraction stage, but often have relatively low interfacial surface area to microchannel volume ratios with corresponding modest separation capacity (throughput) and in the case of counter-current modest operating range.[51, 56-58, 61, 91, 124, 125] Phase separation in these systems is usually achieved by having a small interfacial area to preserve sufficient capillary pressure to counter balance the imposed driving pressure or by modifying wetting characteristics to stabilize interfaces. The life time of the later approach can be limited by degradation of the surface modification over time either through gradual dissolution of the coating into the solvent flowing through the device or via susceptibility to chemical attack. Efficient (ml/min), surface tension based continuous microfluidic techniques for separating immiscible fluids such as gas-liquid[126] and organic-aqueous phases[92] was developed in chapter 2 and demonstrated for applications in multistage extraction in chapter 4.
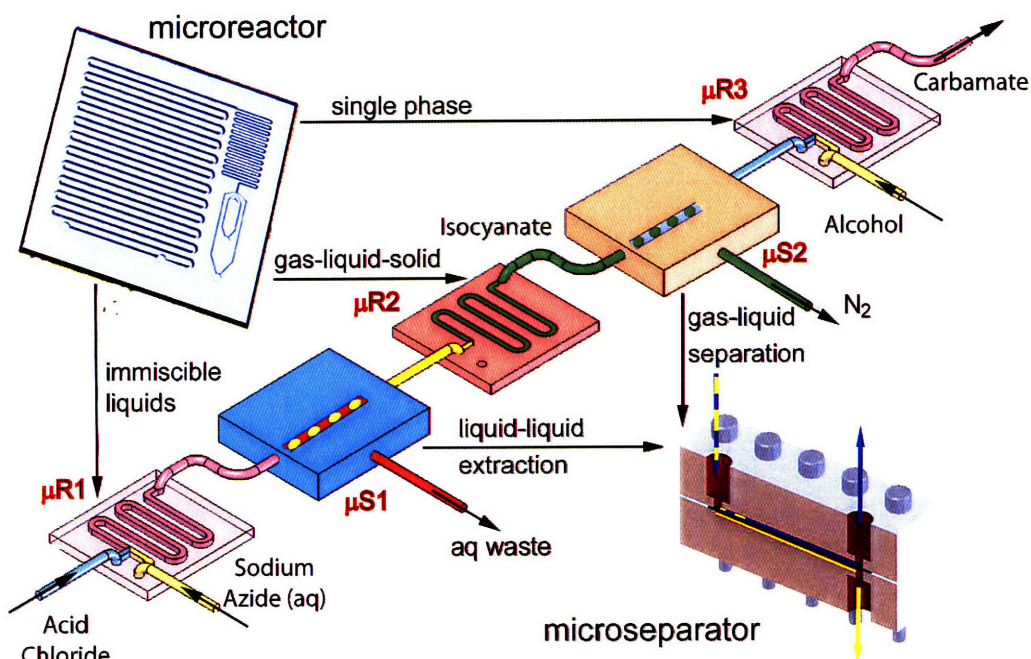
Figure 6.1 Schematic of the experimental setup for carbamate synthesis. μR_1 microreactor for conversion of acid chloride to organic azide; μS_1 quantitative separation of organic and aqueous streams; μR_2 microreactor load with solid acid catalyst for conversion of organic azide to isocyanate; μS_2 quantitative separation of gaseous N_2 from liquid stream; μR_3 microreactor for reaction of isocyanate and alcohol to carbamate.

118

In this contribution, these microfluidic extraction systems, and inline pumps developed in chapter 3 were integrated with microreactors[9, 127] in a continuous multistep synthesis system (Figure 6.1) that enabled sequential reactions without leaving the microreactor environment and created the potential for synthesis of varying amounts of analogous structures.

6.2 Model chemistry

The synthesis of carbamates using the Curtius rearrangement of isocyanates[128] serves as the model chemistry (Figure 6.2) for demonstrating the multi-step microchemical synthesis. Carbamates are interesting because they show biological activity[129, 130]. Moreover, isocyanates and organic azides are important intermediates that serve as a starting material for a variety of reactions in synthetic chemistry[131, 132]. This choice of the model chemistry is further motivated by the intermediates azide and isocyanate being potentially hazardous and difficult to scale-up in conventional batch chemistry. Continuous flow synthesis offers *in situ* generation and consumption of the intermediates, which eliminates the need to store intermediates and thus makes the synthesis scheme safer. Furthermore, the use of glass coated silicon-based microreactors provides the chemical inertness of glass with the excellent heat transfer characteristics of silicon.[119]
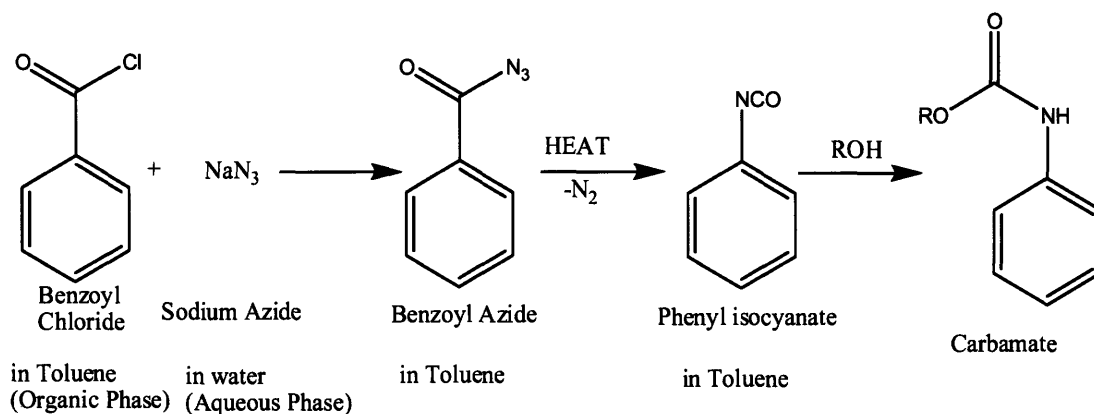
Figure 6.2 Carbamate synthesis scheme as case study.

6.3 Experimental Setup and Devices

The first step, the phase transfer reaction between aqueous azide and acid chloride to produce the organic azide, was performed in a silicon based microreactor (μR_1)

119

previously described.[9, 126] The formation of isocyanates in the second reaction step was first performed by heating the organic azide in a standard microreactor (μR_2) and then by packing this reactor with a solid acid catalyst (H-mordenite solid acid catalyst, HS-690, Wako Chemicals) to achieve high conversions at lower temperatures. Subsequent removal of the generated nitrogen was achieved in the separator unit (μS_2) by the liquid wetting and flowing through the membrane while preventing gas penetration.[126] Carbamate was formed in the third step by contacting the generated isocyanate with alcohol in the third microreactor (μR_3). As a demonstration of using *in situ* generated potentially hazardous intermediates in subsequent parallel reactions, a small vial replaced the second gas liquid separator and served as a liquid supply for three concurrent carbamate reactions (Figure 6.9). Figure 6.3 shows the experimental setup photographed inside a chemical hood. Three silicon microreactor and two modular phase-separators are seen. The details of the devices and the packaging schemes used are discussed below-
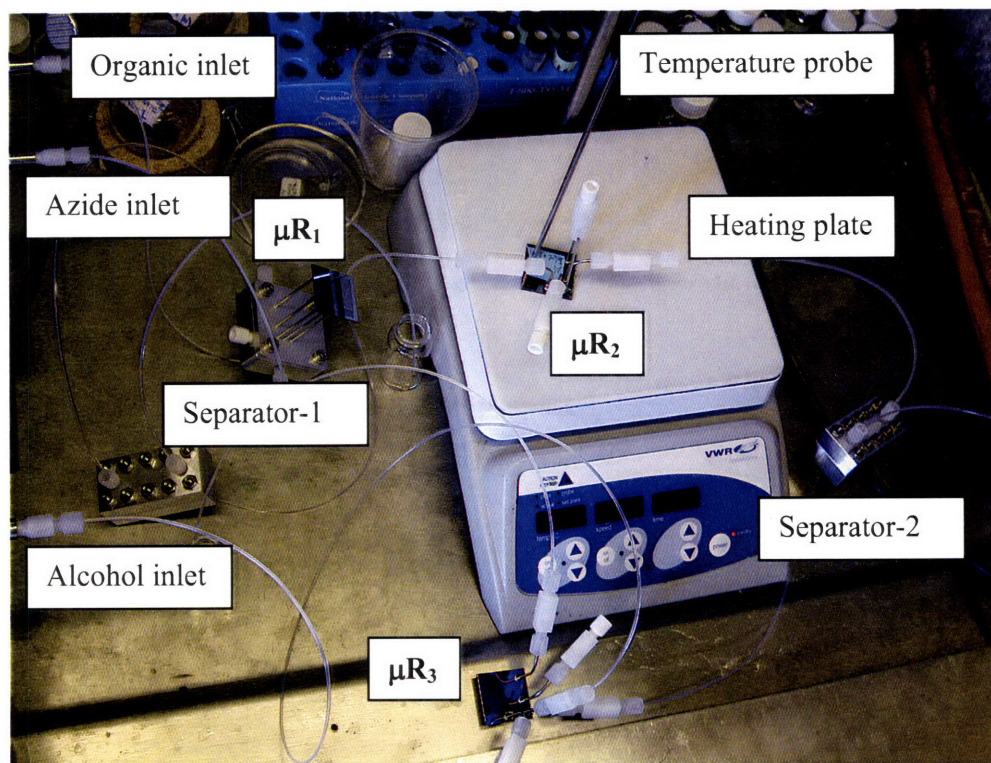
Figure 6.3 Experimental setup with three microreactors and two microseparators

6.3.1 Solder-based packaging for chip-to-tube bonding

The microreactors used in the study have been described before.[9, 32] They were packaged (Figure 6.4) for inlet-outlet connections by soldering 1/16" SS tubes using brass ferrules. The detailed process is described in Murphy *et. al.*[33] Reversible quick connect manifolds were designed as shown in Figure 6.5 to quickly replace microdevices with fresh ones if need be. μR_1 in Figure 6.3 is attached using this technique.
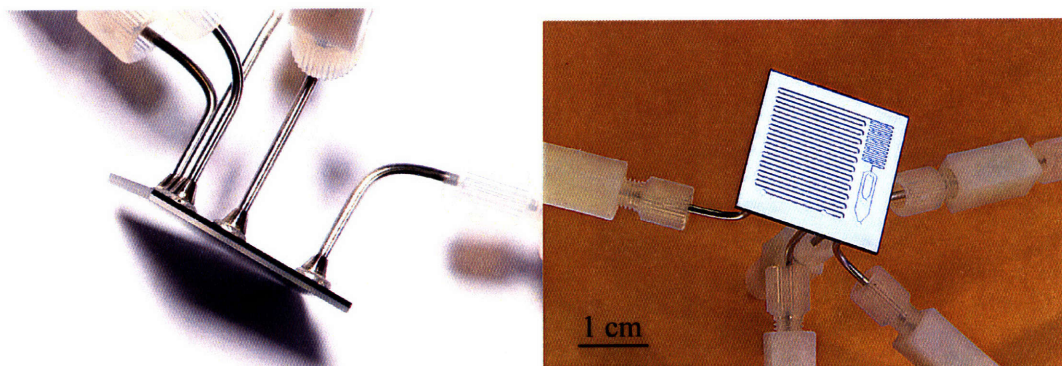
Figure 6.4 Tubes soldered to a microchip
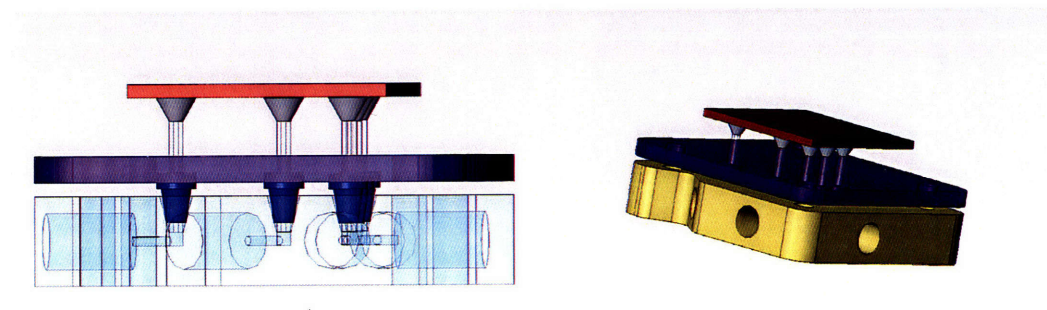
Figure 6.5 Quick-connect reversible packaging

6.4 Separators

6.4.1 Separator-1 (μS_1)

μS_1 is a two-phase liquid-liquid separator. Standalone separators were machined from stainless steel with device assemble similar to that described in chapter 2. Figure 6.6 shows the details of these separator modules. The continuous separation of the aqueous and organic mixture was realized in a microseparator (μS_1) based on preferential wetting characteristics.[92] The device has a thin porous fluoropolymer membrane that is selectively wetted by the organic solvent. The membrane has pore sizes in the 0.1-1 μm

range (giving high capillary pressures), and a high pore density providing high throughput. The wetting by the organic phase prevents the aqueous phase from passing through the membrane while an imposed pressure drives the organic phase through the membrane holes resulting in quantitative separation of the two phases. The throughput increases with imposed pressure difference across the membrane with the maximum pressure limited by the capillary pressure. The first reaction and separation steps were also combined into a single device[92] (Figure 6.7) integrating contacting of the organic and aqueous reactants and subsequent phase separation of the reaction products.
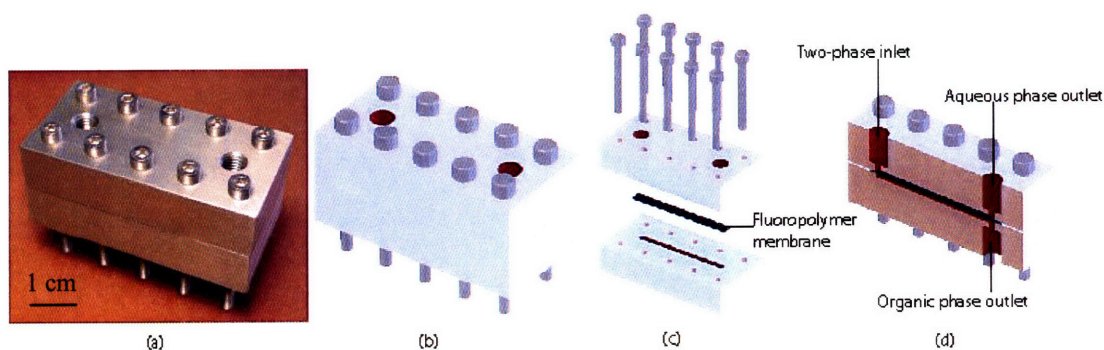
Figure 6.6 (a) Phase-separation device (b) Schematic (c) Exploded view (d) Sectional view. The flow channels for both, aqueous and organic phases were 4 cm long, 2 mm wide and 1 mm deep.
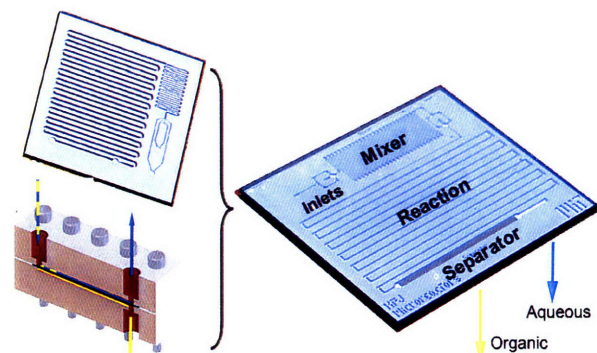
Figure 6.7 Combined reaction and work-up into a single device

6.4.2 Separator-2 (μS_2)

μS_2 is a two-phase gas-liquid separator. Three different approaches were used. In one approach, μS_2 was a similar unit as that for μS_1. As gas-liquid interfacial tension differences are greater than liquid-liquid differences, these separators worked under lesser constraints of operating pressures. Another way of accomplishing gas-liquid

separation after the second reaction was to use a degasser (Figure 6.8). Semi-permeable tubing (Teflon® AF, Biogeneral, San Diego, CA) was enclosed inside a chamber connected to vacuum. The two-phase gas-liquid flow entered the vacuum chamber where the pressure difference between the interior and exterior of the tubing drove out the gas from the flow channel resulting in gas-liquid separation.
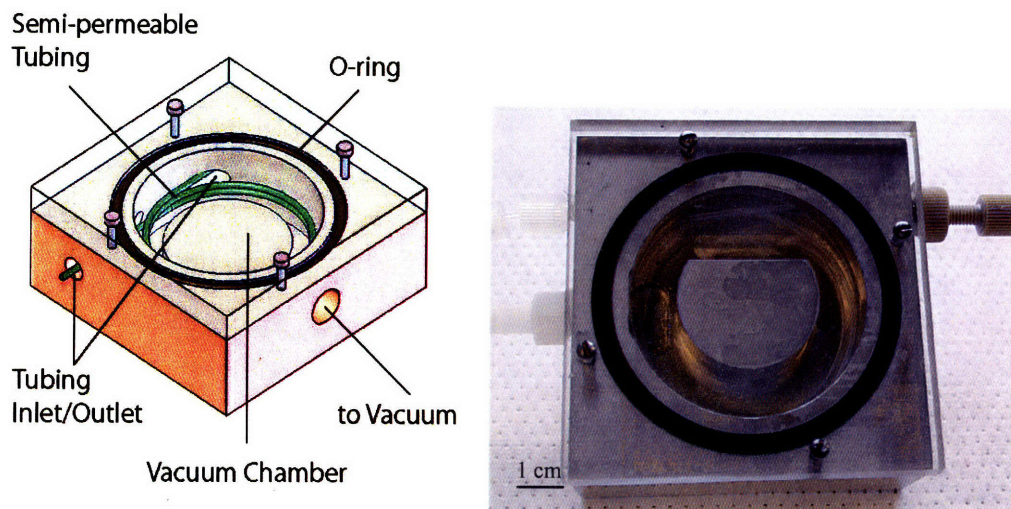
Figure 6.8 Schematic, and actual device using coiled semipermeable tubing inside of a vacuum chamber.

The flowrate across the membrane is described by-

$$q = p\frac{A}{T}\Delta P$$

Where q is the total permeate flowrate, p is the permeability, A the surface area, T the wall thickness, and ΔP the difference in pressure across the membrane. High permeate materials, such as PDMS[133] and Teflon AF®[134], have a permeability of $\sim 10^{-14}$-10^{-15} m^2/s·Pa, while most other materials are several orders of magnitude less permeable. Permeability of common gases generated by chemical or biological reactions such as H_2, O_2, CO_2 and N_2 are within an order of magnitude and tend to be higher compared with other larger organic molecules. Assuming complete conversion, and knowing initial concentration, the maximum amount of gas evolved can be calculated. The length of tubing required was estimated knowing the flowrate. The amount of tubing provided in the degasser was far more than necessary, as all gas evolved was removed within the first

two inches of tubing length. The excess tubing was provided to enable coiling and to have the degasser be used as a general gas-liquid separator. The advantage of using these degassers was that start-up was easier as the two-phases could not cross-flow as in μS_l resulting in failed separations. A challenge using theses degassers was the high pressure drop they offered, narrowing the operable flowrate range for the system. For most experiments, gas-liquid separation was performed using the third method described next. When parallel synthesis was performed, gas-liquid separation was driven by the differences in gas and liquid density as in conventional separation schemes. This branching method, which could also be applied to the organic azide stream, allowed simultaneous synthesis of multiple compounds in the same run. Using this scheme, parallel synthesis of methyl phenyl carbamate, ethyl phenyl carbamate and benzyl phenyl carbamate was performed. Two different pressure-driven flow schemes were used to flow liquid out of the vial. (1) The vial was pressurized with an inert gas (helium) while allowing a small leak for the generated nitrogen to escape. Tube diameters and lengths were adjusted to control the flow rates in the three systems. (2) The vial was kept open, and three syringe pumps were connected independently to the three final microreactors. The syringe pumps were operated in withdrawal mode. The latter was the easier of the two methods as it did not pressurize the upstream devices, and no adjustment of tubing lengths/diameters was needed. However, this method required the use of three additional syringe pumps making the experimental setup bulkier and more expensive than the active pressure-driven scheme.
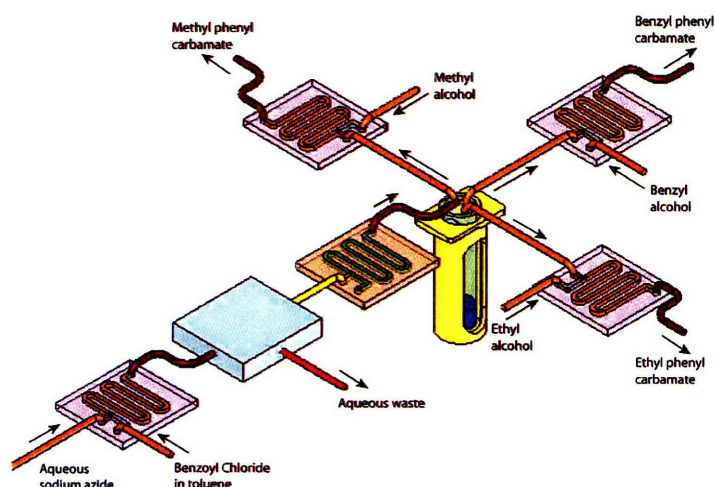
Figure 6.9 Reaction scheme for parallel synthesis of three analogous carbamates.

6.5 Experimental

The organic and aqueous phases were loaded in separate 10 ml syringes (GasTight, Hamilton) and connected to the inlets of the first reactor (Figure 6.1). The outlet from the third reactor was used directly for analysis without any further treatment. The flowrates used ranged from 1 to 5 $\mu L \cdot min^{-1}$ with a 1:1 ratio of aqueous and the organic reagents. The ports of reactors not in use were closed using plugs (Upchurch). To facilitate better two phase contact, a T-mixer (Upchurch) was added upstream of the first reactor, and tubing (1/16" OD, 0.01" ID Teflon, Upchurch) was provided for additional residence time before the first reactor. The overall two-phase contacting residence time was varied in this manner from 90 min to 200 hours. The second reactor was heated using a hotplate directly in contact with the reactor. A 5% w/v aqueous sodium azide solution (VWR) was diluted with MilliQ water and sodium hydroxide solution (made using sodium hydroxide pellets from Mallinckrodt and MilliQ water) to give 0.4 M sodium azide solution of pH 9. Benzoyl chloride solution was prepared by adding commercial benzoyl chloride (Sigma Aldrich) directly to toluene (Sigma Aldrich) to give 0.36 M benzoyl chloride in toluene; resulting in the azide being in 11% molar excess.

6.5.1 Sample Analysis

NMR was used to identify the final product. GCMS was used to quantify the concentration of benzoyl chloride, phenyl isocyanate and the final carbamate, while HPLC was used to quantify the aqueous phase concentration of azide in the feed stream to the first reactor as well in the aqueous waste from the first separator.

6.6 System Startup

The multistep synthesis when started goes from the initial state of rest through increasing flowrates, concentrations and pressures until all three reach a steady state, i.e. invariant in time. The start-up procedure should be such that at all times during the unsteady state, i) the separator pressure conditions are satisfied and ii) the flowrate directions are maintained as desired for synthesis. Examples of cases when condition (i) is not held is when the start-up is done dry, i.e. with air in the devices and tubes. In this case, the aqueous outlet offers significantly smaller backpressure due to orders of

magnitude lower viscosity of gas over liquid, causing the organic phase to flow out the aqueous outlet, resulting in failed separation. Condition (ii) is challenged when the alcohol inlet to μR_3 starts flowing up the scheme into the separator-2 and flows out the aqueous outlet of separator-2 immediately after the scheme is started. Any failure occurring in the system takes a long time to correct. Therefore, to ensure proper start-up, the entire system was primed with liquid phases that would be expected in those sections of the system at steady state. So the aqueous outlet was primed with aqueous phase, and the organic lines were primed with toluene. This technique helped offer correct backpressures right from the start of the system. The backflow in the network was prevented by calculating pressure drops and adjusting tubing lengths and diameters to match pressures at the junctions, and to offer favourable pressure drops in desired flow directions. Thus, the alcohol inlet was made of a tube with flow resistance equivalent of the upstream system with two reactors and two separators so that when the alcohol meets the isocyanate, the pressures are similar. Also, the alcohol flow was not started until the isocyanate started flowing out μR_3. The start-up process was:
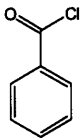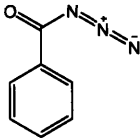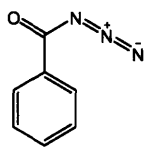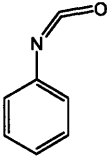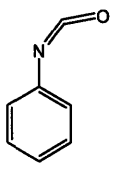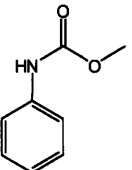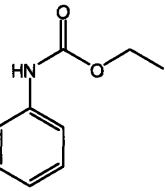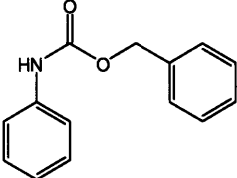
i)   Prime all lines

ii)   Start the azide and azoyl chloride flows

iii)   Start the alcohol flow after the fluid-flow out the μR_3 outlet is seen.

iv)   Wait four residence times for concentration steady state to collect samples.

This start-up process is very similar to large scale continuous start-up. Once the system reached steady state, it could be run indefinitely till all the reagents got consumed. Using larger reservoir (bigger syringes) of reagents in the beginning allowed for longer run times. The system was shown to run for 6-7 days continuously without change in concentrations of the products. For large residence time reactions (200 minutes), the start-up time was 14 hours. In such experiments, the system was started and steady state allowed to be reached overnight. Sample collection started the next day.

6.7 Results and Discussion

Uniform liquid-liquid segmented flow was observed in the first microreactor when contacting benzoyl chloride in toluene (0.36 M) with a basic (pH 9) solution of sodium azide (0.4 M). The conversion of benzoyl chloride to benzoyl azide was a function of the residence time, 65% conversion at a residence time of 90 minute and 98% conversion after 200 minute. To facilitate better two phase contact, a T-mixer (Upchurch) was added upstream of the first reactor, and tubing (1/16" OD, 0.01" ID Teflon, Upchurch) provided for additional residence time before the first reactor. Liquid recirculation within the liquid segments enhanced mass transfer[123] beyond diffusive rates and increased surface/volume ratio at the microscale eliminated the need for phase transfer catalyst. As a result, the final carbamate was obtained without having to remove any contaminants such as phase transfer catalysts. The liquid-liquid separator (μS_1) provided complete separation of the organic and aqueous phases. The conversion of benzoyl azide to phenyl isocyanate in the second reactor was a function of the heating temperature (Table 6.3) consistent with reported kinetic data.[135, 136] The decomposition temperature of benzoyl azide is reported to be between 50-80°C.[132] In batch operation, the azide is typically heated gently not much beyond the decomposition temperature to prevent uncontrolled release of energy. The microreactor enables higher temperatures reducing the time needed to achieve complete conversion.

Table 6.1 Conversion after each step of the multistep scheme

Reactant	Product	Conversion
		98.0
		99.0
	Parrallel Synthesis[a]	
		99.5
		99.9
		95.7

[a] This was performed according to the scheme shown in Figure 6.9

Table 6.2 Conversion as a function of residence time for the two phase reaction

(PhCOCl → PhCON₃)

Residence time (min)	Temperature (°C)	Flowrate ratio (Org : Aqueous phase)	Conversion (%)
90	20	1:1	65
200	20	1:1	98

Table 6.3 Conversion as a function of temperature for the decomposition reaction

PhCON₃ → PhNCO, without catalysis

Temperature (°C)	Residence time (min)	Average Conversion ± Std. Dev. (%)
60	60	7.0 ± 0.8
90	60	91.2 ± 1.4
105	60	99.0 ± 1.3

The conversion of the azide to isocyanate in the second reactor proved to be the limiting step in increasing the overall system productivity. This limitation can be mitigated by adding a second heated reactor and operating at double the flowrate while keeping the same overall residence time. Another approach would be to use higher temperatures by (i) pressurizing the system and using the same solvent[127] or ii) by replacing toluene with a higher boiling solvent, such as xylene. Yet another possibility is to speed up the decomposition using acid catalysis.[137] The latter approach was demonstrated by loading the microreactor with 12.13 mg of H-mordenite solid acid catalyst (HS-690, Wako

Chemicals) and operating at the same flowrate. At 90°C, 99.9% conversion of the azide into the isocyanate was obtained, as compared to the 91.2% conversion in the non-catalyzed case. The higher boiling point (167°C) of phenyl isocyanate compared to toluene (108°C) should also make it possible to remove the toluene by a 'solvent-stripping' operation. This process could be done by heating the gas-liquid separator vial (Figure 3) above the boiling point of toluene to obtain neat phenyl isocyanate and to remove toluene vapors along with nitrogen in the gas phase. The gas-liquid separators operated as designed, and removed all of the evolved gas. The final reaction between an alcohol and phenyl isocyanate was fast[138] yielding 96-99% of the carbamate. With a flowrate of 1 µl/min each of aqueous (0.4 M) and organic reagents (0.36 M), the productivity ranged from 80-120 mg per day depending on the type of carbamate synthesized. Achieving high productivity was not the target of this investigation. Productivity can be increased by optimization of the microreactor design and the operating conditions. In typical runs, the continuous multistep synthesis setup was operated for 6-7 days without any interruption until the all the reagents were used. There was no change in system performance over the long-term continuous operation of the microreactors and separators. It was also feasible to use only the first two reactors and corresponding phase separator to produce isocyanate on-demand.
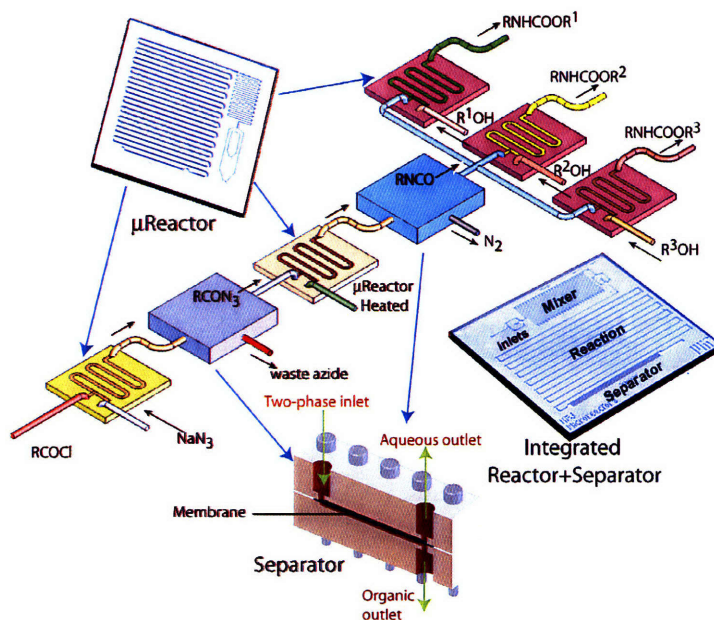
Figure 6.10 Series and parallel reactions with separation

130

6.8 Conclusion

The Curtius rearrangement served as a case study with reactive and potentially hazardous intermediates (azide and isocyanate). However, the technique of combining microreactors and separators apply broadly to continuous multi-step synthesis. When needed, the general microreactors can be replaced by specialized devices such as packed bed catalytic microreactors,[38, 39] as illustrated by introducing solid acid catalyst in the second transformation. Monitoring and optimization of reaction yields become feasible when combining the microreaction system with analytic techniques as already demonstrated for individual microreactors.[120] Introducing branching after the formation of an intermediate provides for continuous synthesis of multiple, analogous compounds as demonstrated with the addition of multiple alcohols to the benzoyl isocyanate to form different carbamates. Moreover, different reagent solutions could be run in succession to further expand the number of compounds synthesized. The continuous operation implies that the amounts of particular interesting products could be scaled up by increasing the run time or the number of systems. In conclusion, a continuous multi-step microchemical synthesis consisting of three transformations with in-between separation steps using the Curtius rearrangement as a model system was performed, as shown in Figure 6.10. The work demonstrated the simultaneous use of a network of microreactors and separators for parallel synthesis of a family of compounds, *in situ* generation and consumption of hazardous intermediates such as isocyanates, safe operation of microreactor systems for reactive compounds such as azides, and small-scale synthesis of chemicals for screening and optimization purposes.

7 Conclusion and Future Outlook

7.1 Summary of Thesis Contributions

This thesis focused on advancing the microchemical field from single device based demonstrations to systems that can perform multi-step series and parallel synthesis. Packed bed microreactors, micro-separators and micro-pumps suited for miniaturized lab-on-a-chip systems for organic syntheses were developed in the first half of this thesis, while the second half demonstrated different multistep microchemical operations enabled by these systems.

In chapter 2, inline continuous separation devices were developed that enabled removal of unreacted reagents/byproducts, making it possible to realize a series of reactions without leaving the microreactor environment. Differences in surface forces and preferential wettability characteristics of fluoropolymers were used for phase separation. Such microseparators were used to demonstrate 100% separation of two phase flows of hexane and water, toluene and water, dichloromethane and water, and hexane and methanol. Integrated liquid-liquid extraction devices were microfabricated that performed two-phase contacting by segmented flow, followed by separation – resulting in single stage extraction. Single stage extraction of N,N-dimethylformamide from dichloromethane to water, and from diethyl ether to water was demonstrated.

In chapter 3, pressure-driven flow was used as the basis for operations of micropumps. An enclosure with the liquid was pressurized with helium gas, causing the liquid to flow. The dynamics of pressurizing and de-pressurizing an enclosure were modeled and confirmed by experiments. Active and passive control schemes to provide constant flowrate of the liquid were developed and implemented. Different schemes were developed to use the gas pressure to manipulate the flow path of liquids. In one scheme, two enclosures were used together to perform as an inline pump. The inline pumps also acted as a buffer to prevent any disturbance propagation, and allowed the upstream and downstream to operate at different flowrates. The pump was demonstrated at two scales – 1) microfabricated silicon chips of 40 microliter volume and 2) using glass shell vials of 10000 microliter volume. In chapter 4, these pumps were used along

132

with two microseparators to demonstrate two-stage countercurrent and cross-flow liquid-liquid extraction of N,N-dimethylformamide from dichloromethane to water starting with 4.4 mole percent mixture. The inline pumps also allowed recirculation with a constant flowrate that enabled long residence time reactions. As an example, peptide synthesis starting from the amino acids, using the Merrifield technique was demonstrated in chapter 5. The pentapeptide, Leu-Pro-Gly-Gly-Tyr (Leuenkephalin, a type of endorphin) was synthesized on different resins simultaneously as an example.

A new design for the silicon microreactor for packed bed reactions was developed in chapter 5 that permitted larger catalyst loadings, and offered manageable pressure drops across the packed bed even when the solid loading increased in volume during operation, as was the case with the peptide synthesis experiments. These microchips were also used to study click chemistry reactions to synthesize drug-candidate molecules. The packed bed microreactor experiments gave higher conversions and better selectivities than batch experiments after the same amount of reaction time as the microreactor experiments provided increased relative catalyst concentration, and prevented background reactions that otherwise reduce selectivity.

As an example of multi-step synthesis involving reactions and separations, the synthesis of carbamates starting from azoyl chloride and sodium azide, using the Curtius rearrangement of isocyanates was demonstrated in chapter 6. Parallel synthesis of analogous carbamates by introducing branching in the synthesis sequence after the isocyanate production to form microreactor networks was also demonstrated. The second reaction involved heat decomposition of the organic azide, and was shown to perform faster when catalyzed using solid acid zeolite catalyst in a packed bed microreactor. Continuous operation of the microdevice network for ~ 7-10 days at flowrates of 1-5 μl/min showed no change in performance. The microreactor based synthesis was run at higher temperatures than conventional batch scale reactions due to the inherent safety in microreactor based production. The multiple-carbamate-synthesis microreactor network consisted of five microreactors and two separators, with the second one used pressure driven flow. This demonstration was the first multi-step organic synthesis involving reactions and separations, and showcased the major contributions from this thesis.

The development of micro-unit-operations in this thesis has advanced the microchemical field from single device based demonstrations to systems that can perform continuous-flow multi-step series and parallel chemical synthesis.

7.2 Specific directions for future work

The packed bed reactor, two-phase separator, and inline pump developed in this thesis could be used in demonstrations of several chemical systems that cannot be otherwise performed in microdevices. Such examples may include multiple reaction steps, systems with large pressure drop, system with large reaction times, systems with multiple separation steps, and packed bed reactions. Complete synthesis scheme optimization could be performed over multiple reactors and separators to provide optimum conditions to satisfy an objective such as maximize yield or minimize side-products.

The pressure driven flow techniques developed for the pump and recirculation could be extended to replace syringe pumps entirely. The dynamics for flow control from one reservoir were developed – it could be extended to multiple reservoirs pumping simultaneously, thereby replacing all syringes and providing constant flow. The ability to generate large pressures also allows for a larger range of flowrates and reactions with solid supports or catalysts.

Distillation operations separating a single phase mixture could be developed by heating the single-phase to form vapor-liquid two-phase flow which can be separated using the two-phase separator. The gas phase enriched in the more volatile component, upon condensation yields an enriched mixture. This represents one stage of an enrichment operation which could be performed over more stages to provide desired purity.

Early work on integrated silicon board with sensors for temperature, pressure, and concentration presented two challenges – the fluidic network was susceptible to change in flow directions when bad packaging resulted in leaks. The leaks changed the flow resistance and hence the flow paths. This can be corrected by incorporating jumpers or redundancies in design to make the network more robust. Another challenge was the incorporation of electrical connections in a reliable manner, especially with the pressure sensor chips. At that point, gold-wire bonds, similar to the ones used for IC packaging

were used. However, as microsystems handle harsher chemical environment, more robust packaging methods need to be developed. New techniques have appeared since the initial approaches. For example, wireless pressure sensors (CardioMEMS Inc, Atlanta, GA) that work on radio frequency communication can be used to make the electrical integration simpler.

7.3 Future Outlook

The contributions of this thesis are a step towards the development of robust and elegant microsystems. The devices and techniques developed in this thesis although aimed at chemical synthesis; also find applications in other areas of microreactor application, namely, biological studies, nanoparticle synthesis, fuel-cell development, and energy research.

The opportunity is ripe at this point for contributions at many levels – either direct continuation of this work or related work branching out in other disciplines. The further development of microsystems for chemistry research will benefit from inter-disciplinary contributions, such as the development of smart electrical interfacing with the fluidics/pneumatics, not only for electrical power and sensing, but also for advanced techniques such as distributed control systems for decentralized control.

The biggest advantages of using microsystems for chemistry research will not come from simple miniaturizations of existing processes – it will come about from a rethinking of process design accompanied by a change in operating parameters suited more for the microsystems. The key is to achieve the desired results without having to replicate each single step of a traditional process. For example, solids handling is often cited as a challenge for microsystems. However, there may be no need to crystallize the product after each reaction step in microsystems. Change in operating temperature or concentration from batch conditions may also avoid solids formation during synthesis.

Continuous workup methods are vital to realizing robust multistep microsystems. One form of continuous workup in microsystems was developed in this thesis. Differences between other physical or chemical properties significant at the microscale could be used to develop more ways to perform separation. Mature technologies such as distillation could be adapted for the microscale to offer more tools for multistep operations. Any new

135

separation technology has the potential for important contribution and immediate impact to the further development of multistep microsystems.

The aim to develop elegant, but robust microsystems often springs up the question if the final systems should be modular – comprised of multiple independent units, or integrated systems – all in one boards, similar to integrated circuits in the computer industry. While each approach has its pros and cons, there is no one answer. Multiple in-between hybrid systems are possible, and the answer also depends on the final application. The objective has to be to minimize total development times while delivering required performance. For example, all-in-one-systems are attractive from a usability perspective; however, a small change in design requirements could mean spending a lot more time fabricating. In one example, lack of redundancy in flow network design caused a silicon board to cease operating whenever leaks occurred. Such systems could be tested in modular arrangements before finalizing the design for the integrated board. In modular systems, the connections between devices take up a substantial portion of the system volume. When the system has to go through a period of startup, these connection volumes matter. The excess volume also means additional material in the system, and increases the wait between successive experiments under different conditions. As all-in-one boards take a long time to develop, ideas could first be tried out in modular systems, and when perfected, integrated to form unified systems. An example is the development of the two-phase microseparator. Initial studies were performed in simple separator devices, and when the operation was understood, they were integrated with residence time units in silicon microchip to form integrated liquid-liquid extraction devices.

Appendix A – Governing equations for In-line Pumps

A.1 Derivation of charging and discharging equations

In this section, the equations for pressure (P_2) in the enclosure are derived in the transient and steady state operation.

Assumptions made-

1) The gas follows the ideal gas law ($PV = nRT$)

2) The liquid flow out from the enclosure is governed by the Hagen Poiseuille equation.

$$Q \, (volume \, / \, time) = \frac{\Delta P}{R_1}, \, R_1 = \frac{8\mu L}{\pi r^4}$$

3) All gas-phase flowrate - pressure drop relationships are modeled using the equation

$$Q \, (moles \, / \, time) = \frac{\Delta P}{R_2}, \, R_2 = \frac{8\mu L M}{\pi r^4 \rho}$$

4) Gas flow is incompressible (ρ = constant). Previous work[139] on compressible laminar flow in a capillary supports this assumption.

Referring to Figure A-1 below, let Q represent the molar flowrate at the gas inlet and q represent the molar flowrate out from the leak to the atmosphere.
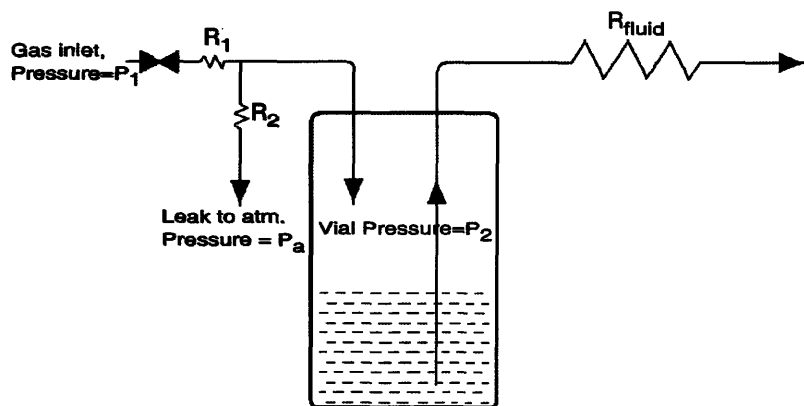
Figure A-1 Pressure Driven Flow Setup

The pressure in the vial (P_2) as a function of time after the instant the gas inlet is opened is derived below-

When gas flow is open,

$$Q = \frac{P_1 - P_2}{R_1} \tag{1}$$

$$q = \frac{P_2 - P_a}{R_2} \tag{2}$$

$$q_{in} = Q - q \tag{3}$$

Using (1) and (2) in equation (3)

$$q_{in} = \frac{P_1 - P_2}{R_1} - \frac{P_2 - P_a}{R_2} \tag{4}$$

$$q_{in} = \frac{P_1 R_2 + P_a R_1 - P_2 (R_1 + R_2)}{R_1 R_2} \tag{5}$$

$$q_{in} = \frac{dn_{in}}{dt} = \frac{d}{dt}\left(\frac{P_2 V}{RT}\right) \tag{6}$$

Assuming the rate of change in volume is very small, one can approximate

$$V \sim \text{constant} \left(\frac{dV}{dt} \approx 0, \text{when compared with} \frac{dP_2}{dt}\right)$$

$$k_1 \frac{dP_2}{dt} = \frac{P_1 R_2 + P_a R_1 - P_2 (R_1 + R_2)}{R_1 R_2} \qquad \left(k_1 = \frac{V}{RT}\right) \tag{7}$$

Solving equation (7),

$$P_2(t) = \frac{P_1 R_2 + P_a R_1 - (P_1 R_2 + P_a R_1 - P_2^0 (R_1 + R_2))\exp\left(-\frac{t}{\tau_1}\right)}{R_1 + R_2} \qquad \left(\tau_1 = \frac{k_1 R_1 R_2}{R_1 + R_2}\right) \tag{8}$$

Setting the reference as $P_a = 0$, equation (8) becomes

$$P_2(t) = \frac{P_1 R_2 - (P_1 R_2 - P_2^0 (R_1 + R_2))\exp\left(-\frac{t}{\tau_1}\right)}{R_1 + R_2} \qquad \text{(Charging equation)} \tag{9}$$

At steady state ($t > 4\tau_1$),

$$P_2(\infty) = P_1\left(\frac{R_2}{R_1 + R_2}\right) \tag{10}$$

The assumption $\left(\dfrac{dV}{dt} \approx 0, \text{when compared with} \dfrac{dP_2}{dt}\right)$ enabled analytical solution as equation (10).

In a more rigorous treatment of the problem, $\dfrac{dV}{dt} \neq 0$ but

$$\frac{dV}{dt} = \frac{\pi r_{fluid}^4}{8\mu} \frac{(P_2 - P_a)}{L_{fluid}}, \text{ the flowrate of the fluid out of the vial.} \tag{11}$$

Thus, the pressure profile as a function of time is calculated by solving equations (5), (6) & (11) numerically.

Figure A-2 shows a comparison of the numerical solution with the analytical solution given by equation (10), and the agreement of the two profiles supports the approximation made for equation (7).
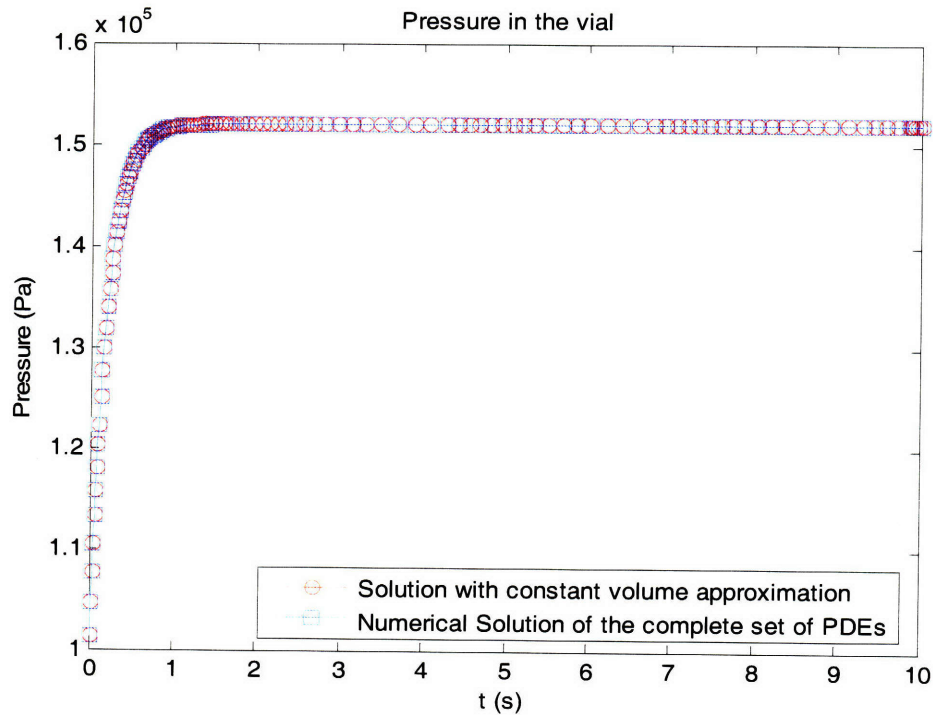
Figure A-2 Comparison of the numerical solution with the analytical solution having constant volume approximation.

When gas inlet is tuned off by closing inlet valve,

$$q_{out} = \frac{P_2 - P_a}{R_2} \tag{12}$$

$$-k_1 \frac{dP_2}{dt} = \frac{P_2 - P_a}{R_2} \tag{13}$$

Solving,

$$P_2(t) = P_a + \left(P_2^0 - P_a\right)\exp\left(-\frac{t}{\tau_2}\right) \quad (\tau_2 = k_1 R_2) \qquad \text{(Decay equation)} \tag{14}$$

$$P_2(t) = P_2^0 \exp\left(-\frac{t}{\tau_2}\right) \qquad \text{(using reference as } P_a = 0) \tag{15}$$

At steady state,

$$P_2(\infty) = P_a = 0 \tag{16}$$

The time constants, τ_1 and τ_2 are respectively, $\dfrac{V}{RT}\dfrac{R_1 R_2}{R_1 + R_2}$ and $\dfrac{V R_2}{RT}$. Therefore, for given gas, the system volume, V, tubing length L and diameter d are used as handles to affect the fluidic resistances, and hence the time constants. For as small time constants as possible, V and L must be small and diameter, d should be as large as practically possible. For most of the applications, V varied from 10 μl to 10 ml, L varied from 5 cm to 100 cm and d varied from 100 to 1000 μm. As a result, time constants ranged from 1 ms to 10 s.

A.2 MATLAB program used for the simulation results

```
function main=comparison;
% Program to compare the Numerical solution and Psuedo steady state
% approximation
% Hemant Sahoo (hemants@mit.edu)
% 12 February 2007
% data-
V0 = 1e-6; % initial volume, in m3
P0 = 101325; % initial pressure, 1 atm = 101325 Pa
PV0= 101325*1e-6;

T = 295; % constant operating temperature, in K
R = 8.314e-3; % Universal gas constant, in J/kmol.K
Pa = 101325; % Ambient pressure, in Pa
P1 = 2*101325; % Constant High pressure from gas cylinder

muLiq=1.2e-3; % Liquid = Ethanol, Gas = Helium
muHe=2.0113e-5;

densityHe=0.178;
densityLiq=789;

radius1=500e-6;
radius2=500e-6;
radiusL=75e-6;

L1=0.1;
L2=0.1;
LLiq=0.5;

R1=8*muHe*L1*2e-3/(3.14*radius1^4*densityHe); % 2e-3 = kg/moles of He
R2=8*muHe*L2*2e-3/(3.14*radius2^4*densityHe);

alpha=(3.14*radiusL^4)/(8*muLiq*LLiq);
a=(R*T)*(P1*R2+Pa*R1)/(R1*R2);
b=-R*T*(R1+R2)/(R1*R2);
c=(P1*R2+Pa*R1);
tau=-V0/b;

y0=[PV0,V0];

options = odeset('RelTol',1e-15);
[t,y] = ode45(@diff_eqn_solver111,[0,10],y0,options,a,b,PV0,alpha,Pa);

for j=1:length(t);
approx(j)=(c-(c-P0*(R1+R2))*exp(-t(j)/tau))/(R1+R2);
numerical(j)=y(j,1)/y(j,2);
end

% y(:,1)/y(:,2)
figure;
plot(t,approx,'-ro',t,numerical,'-bs');
```

```matlab
xlabel('t (s)');
ylabel('Pressure (Pa)');
title('Pressure in the vial');
h = legend('Solution with constant volume approximation','Numerical
Solution of the complete set of PDEs',4);

function f = diff_eqn_solver111(t,y,a,b,PV0,alpha,Pa);

f = zeros(size(y));

f(1) = a+b*y(1)/y(2);
f(2) = alpha*((y(1)/y(2))-Pa);

return;
```

A.3 Generalized Governing Equations

Referring to Figure A-1, consider the general case when the flow resistance between the leak to the atmosphere and the inlet to the enclosure is not zero but has a value equal to R_3. The charging and discharging equations in such a general case are derived using arguments similar to section A.1

Case (i) when the valve is open – enclosure charging.

$$q_{total} = \frac{P_1 - P^*}{R_1} \tag{17}$$

$$q_{out} = \frac{P^* - P_a}{R_2} \tag{18}$$

$$q_{in} = \frac{P^* - P_3}{R_3} \tag{19}$$

$$q_{total} = q_{in} + q_{out} \tag{20}$$

Solving equations (17)-(20) together for P^*,

$$P^* = \frac{P_2 R_1 R_2 + P_1 R_2 R_3 + P_a R_3 R_1}{R_1 R_2 + R_2 R_3 + R_3 R_1} \tag{21}$$

Solving equations (6), (19) and (21)

$$P_2 = \frac{P_a R_1 + P_1 R_2}{R_1 + R_2} + \left(P_a - \frac{P_a R_1 + P_1 R_2}{R_1 + R_2} \right) \exp(-t/\tau_1), \ \tau_1 = \frac{V}{RT} \left(\frac{R_1 R_2 + R_2 R_3 + R_3 R_1}{R_1 + R_2} \right) \tag{22}$$

This equation is identical to equation (6), except that τ_1 is different, and has terms due to R_3.

Following a similar line for the equation for case (ii), when the valve is close – enclosure discharging, the pressure profile as a function of time is-

$$P_2 = P_a + (P_2^0 - P_a) \exp(-t/\tau_2), \tau_2 = \frac{V}{RT}(R_2 + R_3) \tag{23}$$

143

Appendix B – Supporting Information on Recirculation System design

B.1   Design of peptide synthesis setup

The following shows a MAPLE program used to solve the network shown in Figure 5.6 and Figure 5.11. The gas side network was solved to estimate the pressures in the three enclosures, which were then used to estimate the flowrate through the peptide synthesis chip. The experimental measurement of the flowrate is shown in Figure 5.7 showing good agreement between prediction and actual flow. The observed difference is attributed to the existence of extra flow resistance offered by the fittings.

```
> restart;
> eqns := {(P0-P3)/R1=((P3-P4)/R2)+((P3-P5)/R3), (P3-
P4)/R2=(P4-Pa)/R4, (P3-P5)/R3=(P5-Pa)/R6};
```

$$eqns := \left\{ \frac{P0 - P3}{R1} = \frac{P3 - P4}{R2} + \frac{P3 - P5}{R3}, \frac{P3 - P4}{R2} = \frac{P4 - Pa}{R4}, \frac{P3 - P5}{R3} = \frac{P5 - Pa}{R6} \right\}$$

```
> abc:=simplify(solve(eqns,{P3,P4,P5}));
```

$$abc := \left\{ P5 = \frac{R4\,R6\,P0 + R4\,R1\,Pa + R2\,R1\,Pa + R4\,R3\,Pa + R1\,R3\,Pa + R6\,R2\,P0 + R6\,R1\,Pa + R2\,R3\,Pa}{R1\,R4 + R6\,R4 + R2\,R3 + R1\,R3 + R1\,R6 + R1\,R2 + R6\,R2 + R3\,R4}, \right.$$

$$P4 = \frac{R2\,R1\,Pa + R2\,R3\,Pa + R6\,R2\,Pa + R4\,R6\,P0 + R1\,R3\,Pa + R4\,R1\,Pa + R4\,R3\,P0 + R6\,R1\,Pa}{R1\,R4 + R6\,R4 + R2\,R3 + R1\,R3 + R1\,R6 + R1\,R2 + R6\,R2 + R3\,R4},$$

$$\left. P3 = \frac{R4\,R3\,P0 + R2\,R1\,Pa + R1\,R3\,Pa + R2\,R3\,P0 + R4\,R1\,Pa + R6\,R2\,P0 + R6\,R1\,Pa + R4\,R6\,P0}{R1\,R4 + R6\,R4 + R2\,R3 + R1\,R3 + R1\,R6 + R1\,R2 + R6\,R2 + R3\,R4} \right\}$$

```
>
> rho:=8.17e-2;M:=2e-3;mu:=1.9e-5;
```

$$\rho := 0.0817$$

$$M := 0.002$$

$$\mu := 0.000019$$

```
>
> L1:=0.8;L2:=0.1;L3:=0.1;L4:=0.564;L6:=0.10;d1:=1e-
3;d2:=0.25e-3;d3:=0.25e-3;d4:=0.25e-3;d6:=0.25e-3;
```

$$L1 := 0.8$$

$$L2 := 0.1$$

$$L3 := 0.1$$

$$L4 := 0.564$$

$$L6 := 0.10$$

$$d1 := 0.001$$

$$d2 := 0.00025$$

$$d3 := 0.00025$$

$$d4 := 0.00025$$

$$d6 := 0.00025$$

```
>
>
R1:=8*mu*M*L1/(3.14*(d1/2)^4*rho);R2:=8*mu*M*L2/(3.14*(d2/2
)^4*rho);R3:=8*mu*M*L3/(3.14*(d3/2)^4*rho);R4:=8*mu*M*L4/(3
.14*(d4/2)^4*rho);R6:=8*mu*M*L6/(3.14*(d6/2)^4*rho);
```

$$R1 := 1.516812324 \; 10^7$$

$$R2 := 4.853799435 \; 10^8$$

$$R3 := 4.853799435 \; 10^8$$

$$R4 := 2.737542883 \; 10^9$$

$$R6 := 4.853799435 \; 10^8$$

```
> Pa:=101325;
```

$$Pa := 101325$$

```
> P0:=101325+(10*101325/14.6959488);
```

$$P0 := 1.702725728 \; 10^5$$

```
> assign(abc);P3;P4;P5;eval(P4-P5);
```

$$1.688987097 \; 10^5$$

$$1.587219461 \; 10^5$$

$$1.351118548 \; 10^5$$

$$23610.0913$$

```
> Lliq:=0.40;Dliq:=0.1e-3;muliq:=1e-3;P5psi:=(P5-
101325)/101325*14.6959488;P4psi:=(P4-
101325)/101325*14.6959488;P3psi:=(P3-
101325)/101325*14.6959488;delPpsi:=(P4-
P5)/101325*14.6959488;
```

$$Lliq := 0.40$$

$$Dliq := 0.0001$$

$$muliq := 0.001$$

$$P5psi := 4.90036900$$

$$P4psi := 8.32472323$$

$$P3psi := 9.80073801$$

$$delPpsi := 3.42435423$$

```
> Q[liq-ulmin-1]:=3.14*(Dliq/2)^4*(P4-
P5)/(8*muliq*Lliq)*1e9*60;
```

$$Q_{liq - ulmin - 1} := 8.687775783$$

B.1.1 MATLAB program used for the simulation of flowrate constancy.

(The graphs are shown in Figure 5.5)

```matlab
function flownumexpt=theRealConstantFlow;
    y0(1)=10e-6;
    y0(2)=20e-6;
    y0(3)=20e-6;
    y0(4)=101325*10e-6;
    y0(5)=101325*20e-6;
    y0(6)=101325*20e-6;

    % solving the ODE system for steady state
    options = odeset('RelTol',1e-15);
    [t,y] = ode15s(@diffferential_eqns1,[0 16],y0,options);

    % noting the steady state values
    lastone=length(t);
    finalstate=y(lastone,:);
    p(:,1)=y(:,4)./y(:,1);
    p(:,2)=y(:,5)./y(:,2);
    p(:,3)=y(:,6)./y(:,3);
    flow=p(:,1)-p(:,2);
    z=y;
    time=t;
    fin=t(lastone);

% figure;
% plot(t,flow,'-r');
% % plot(t,flow,':ro',w1,z1,':bs');
% xlabel('Time');
% ylabel('deltaP through device');

% figure;
% plot(t,y(:,1),'-r',t,y(:,2),'-b',t,y(:,3),'-g');
% xlabel('Time');
% ylabel('volumes');

options = odeset('RelTol',1e-15);
[t,y] = ode15s(@diffferential_eqns2,[0 20],finalstate,options);
alpha=fin.*ones(size(t));
t=alpha+t;
z=[z' y']';
time=[time' t']';
    lastone=length(t);
    finalstate=y(lastone,:);
    p1(:,1)=z(:,4)./z(:,1);
    p1(:,2)=z(:,5)./z(:,2);
    p1(:,3)=z(:,6)./z(:,3);
    flow=p1(:,1)-p1(:,2);

figure;
plot(time,flow,'-r');
% plot(t,flow,':ro',w1,z1,':bs');
```

```matlab
xlabel('Time');
ylabel('deltaP through device');

% figure;
% plot(time,z(:,1),'-r',time,z(:,2),'-b',time,z(:,3),'-g');
% xlabel('Time');
% ylabel('volumes');
return;

function f = diffferential_eqns1(t,y);

f = zeros(size(y));

% constants
R=8.314;
T=293;

% external pressures
Pa=101325;
P01=3*101325;
P02=2*101325;
P03=4*101325;

% Gas side constants
L11=0.2;
L12=0.2;
L21=0.2;
L22=0.2;
L31=0.2;
L32=0.2;
rho1g=101325*28e-3/(8.314*293);     % nitrogen gas
rho2g=101325*28e-3/(8.314*293);     % nitrogen gas
rho3g=101325*28e-3/(8.314*293);     % nitrogen gas
M1=28e-3;                           % kg/mol, nitrogen gas
M2=28e-3;                           % kg/mol, nitrogen gas
M3=28e-3;                           % kg/mol, nitrogen gas
% r11=250e-6;
% r12=250e-6;
% r21=250e-6;
% r22=250e-6;
% r31=250e-6;
% r32=250e-6;
r11=500e-6;
r12=500e-6;
r21=500e-6;
r22=500e-6;
r31=500e-6;
r32=500e-6;
nug1=1.7e-5;            % air at 0C
nug2=1.7e-5;
nug3=1.7e-5;

% Liquid side constants
ra=500e-6;
rb=500e-6;
```

```matlab
rd=500e-6;
nuL=1e-3;                % viscosity of water; etahnol = 2
LL1=1;
LL2=1;
LL3=2;                   % this is device

% Gas phase resistances
R11=8*nug1*L11*M1/(3.14*rho1g*r11^4);
R12=8*nug1*L12*M1/(3.14*rho1g*r12^4);
R21=8*nug2*L21*M2/(3.14*rho2g*r21^4);
R22=8*nug2*L22*M2/(3.14*rho2g*r22^4);
R31=8*nug3*L31*M3/(3.14*rho3g*r31^4);
R32=8*nug3*L32*M3/(3.14*rho3g*r32^4);

% Liquid phase resistances
Ra=8*nuL*LL1/(3.14*ra^4);
Rb=8*nuL*LL2/(3.14*rb^4);
Rd=8*nuL*LL3/(3.14*rd^4);

% ----------------------------------------------------------------
----
% When valve open
% ----------------------------------------------------------------
----
p(1)=y(4)/y(1);
p(2)=y(5)/y(2);
p(3)=y(6)/y(3);


f(1) = ((p(1)-p(2))/Rd)-((p(3)-p(1))/Ra);
f(2) = -((p(1)-p(2))/Rd);
f(3) = ((p(3)-p(1))/Ra);
f(4) = R*T*(((P01-p(1))/R11)-((p(1)-Pa)/R12));
f(5) = R*T*(((P02-p(2))/R21)-((p(2)-Pa)/R22));
f(6) = R*T*(((P03-p(3))/R31)-((p(3)-Pa)/R32));

return;

function f = diffferential_eqns2(t,y);

f = zeros(size(y));

% constants
R=8.314;
T=293;

% external pressures
Pa=101325;
P01=3*101325;
P02=2*101325;
P03=4*101325;

% Gas side constants
L11=0.2;
L12=0.2;
L21=0.2;
```

```matlab
L22=0.2;
L31=0.2;
L32=0.2;
rho1g=101325*28e-3/(8.314*293);      % nitrogen gas
rho2g=101325*28e-3/(8.314*293);      % nitrogen gas
rho3g=101325*28e-3/(8.314*293);      % nitrogen gas
M1=28e-3;                            % kg/mol, nitrogen gas
M2=28e-3;                            % kg/mol, nitrogen gas
M3=28e-3;                            % kg/mol, nitrogen gas
% r11=250e-6;
% r12=250e-6;
% r21=250e-6;
% r22=250e-6;
% r31=250e-6;
% r32=250e-6;
r11=500e-6;
r12=500e-6;
r21=500e-6;
r22=500e-6;
r31=500e-6;
r32=500e-6;
nug1=1.7e-5;            % air at 0C
nug2=1.7e-5;
nug3=1.7e-5;

% Liquid side constants
ra=500e-6;
rb=500e-6;
rd=500e-6;
nuL=1e-3;              % viscosity of water; etahnol = 2
LL1=1;
LL2=1;
LL3=2;                 % this is device

% Gas phase resistances
R11=8*nug1*L11*M1/(3.14*rho1g*r11^4);
R12=8*nug1*L12*M1/(3.14*rho1g*r12^4);
R21=8*nug2*L21*M2/(3.14*rho2g*r21^4);
R22=8*nug2*L22*M2/(3.14*rho2g*r22^4);
R31=8*nug3*L31*M3/(3.14*rho3g*r31^4);
R32=8*nug3*L32*M3/(3.14*rho3g*r32^4);

% Liquid phase resistances
Ra=8*nuL*LL1/(3.14*ra^4);
Rb=8*nuL*LL2/(3.14*rb^4);
Rd=8*nuL*LL3/(3.14*rd^4);


% -----------------------------------------------------------------
----
% When valve closed
% -----------------------------------------------------------------
----
p(1)=y(4)/y(1);
p(2)=y(5)/y(2);
p(3)=y(6)/y(3);
```

```
f(1) = (p(1)-p(2))/Rd;
f(2) = -((p(1)-p(2))/Rd)+((p(2)-p(3))/Rb);
f(3) = -((p(2)-p(3))/Rb);
f(4) = R*T*(((P01-p(1))/R11)-((p(1)-Pa)/R12));
f(5) = R*T*(((P02-p(2))/R21)-((p(2)-Pa)/R22));
f(6) = -R*T*((p(3)-Pa)/R32);

% ---------------------------------------------------------------
----

return;
```

B.1.2 Matrix Assisted Laser Desorption Ionization (MALDI) peptide analysis details

User and sample information

Researcher:	Sahoo
Laboratory:	Jensen
Sample Name:	V8192_ samples #3,4
Sample Matrix:	DCM
Sample concentration:	0.52 mmol/g for sample 3, 0.24 mmol/g for sample 4
Amount submitted:	5 mg on a resin
Date analyzed:	7/16/08
Operator:	AL
MALDI Matrix:	Alpha-cyano acid
External standard used	C2 ABI

Brief description of the analysis performed:

~ 51 nG of "carrier" resin added to the sample,

- The sample was washed with DCM and methanol, and then dried down
- FMOC was removed with 20% Piperidine
- The sample was washed with DMF, DCM, Ethanol and dried down
- The sample was cleaved with TFA- cleavage mixture "A"
- precipitated in Ether
- centrifuged
- Ether removed and the sample was dried down
- reconstituted in 100 µl of 0.1% TFA
- 1uL of the sample was mixed with 1uL of matrix solution, spotted and analyzed on MALDI on negative and positive mode.

Operator comments:

Expected MW is 505 (506 with the proton)

Instrument Settings:

Mode of operation:	Reflector
Extraction mode:	Delayed
Polarity:	Positive
Acquisition control:	Manual
Accelerating voltage:	20000 V
Grid voltage:	66%
Mirror voltage ratio:	1.12
Guide wire 0:	0%
Extraction delay time:	250 nsec
Acquisition mass range:	400 -- 1500 Da
Number of laser shots:	100/spectrum

Laser intensity: 1855
Laser Rep Rate: 5.8 Hz
Calibration type: External -- D:\Maldi data\2008\July2008\071608\c2_p1-
refl.cal
Calibration matrix: a-Cyano-4-hydroxycinnamic acid
Low mass gate: 400 Da
Timed ion selector: Off
Digitizer start time: 29.335
Bin size: 0.5 nsec
Number of data points: 54724
Vertical scale 0:   1000 mV
Vertical offset: 0%
Input bandwidth 0:   750 MHz
Sample well: 75,76
Plate ID: BIOPOLY1
Serial number: 4219
Instrument name: Voyager-DE STR
Plate type filename: C:\VOYAGER\100 well plate.plt
Lab name: MIT BIOPOLYMERS
Absolute x-position: 27059
Absolute y-position: 11766.4
Relative x-position: 71.479
Relative y-posititon: 18.8553
Shots in spectrum: 52
Source pressure: 9.044e-007
Mirror pressure: 3.06e-008
TC2 pressure: 0.0137
TIS gate width: 8
TIS flight length: 1161

Appendix C – Microdevice Design and Fabrication

C.1 Microdevice as Small-scale Enclosure and Packed-bed Microreactor

C.1.1 Microchip Design

New silicon-based microchips were fabricated that permit volume change of the packed solid phase and were used for the peptide synthesis using flow recirculation. As shown in Figure C-2, there is a large cavity of 650 μm depth with a shallow 50μm deep bank of 50 μm wide capillaries at one end. The outlet was on the other side of the bank of capillaries. The small feature size at the outlet served as a filter to prevent beads, usually 100 μm in diameter from flowing out. The large cavity allowed for increase in volume when packed partially.
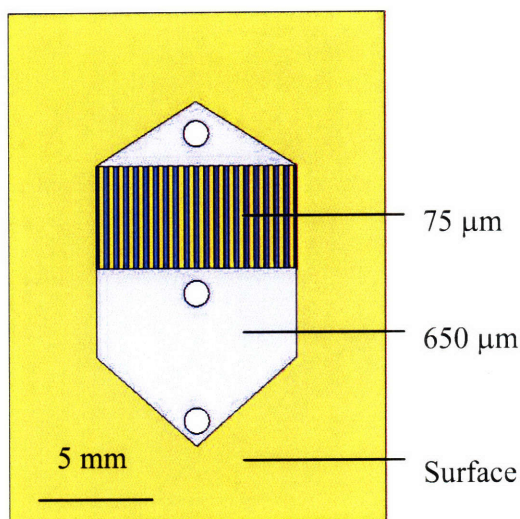

Figure C-1 Same color represents same depth from the surface. The microdevices were fabricated from a 1000 μm thick silicon wafer.
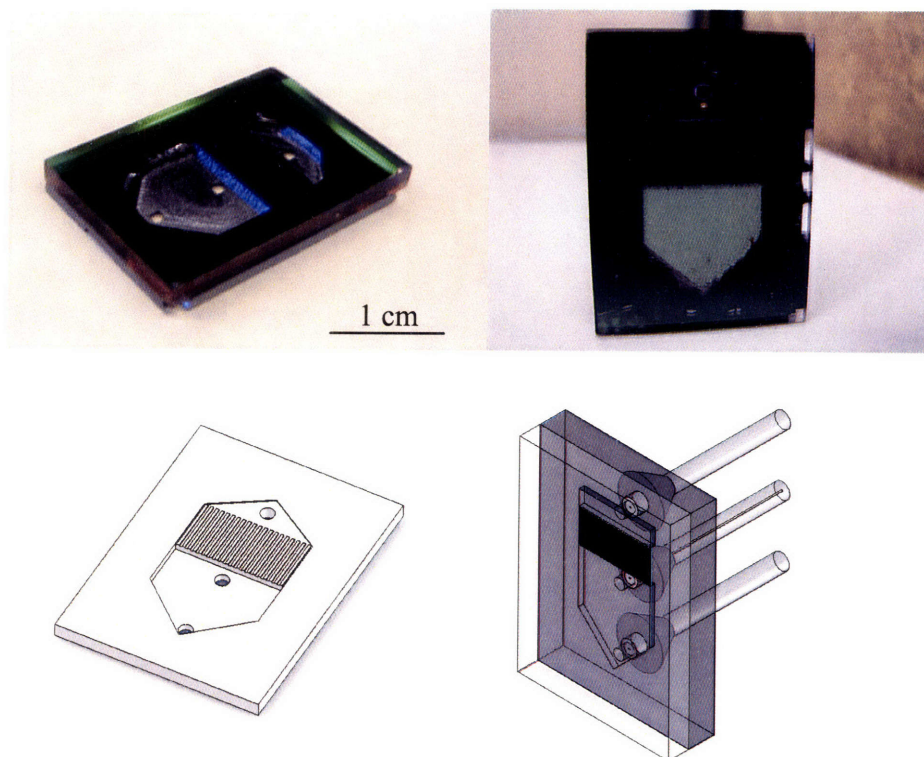
Figure C-2 Photograph and schematic of microchip and packaged microdevice. The photograph shows (left) a microdevice with no catalyst packed and (right) with 55 mg catalyst with support.

C.1.2 Microchip Fabrication

Fabrication process steps are discussed below without cleanroom machine details-

1) Start with 1 mm silicon wafer with 5000 A low-stress nitride.

2) Spin photoresist, expose mask 3, and develop

3) Etch away exposed nitride using RIE

4) Piranha clean wafer to remove photoresist.

5) Repeat steps 2-4 on the back side with mask 1

6) Etch in potassium hydroxide such that both sides get etched. Through holes are formed on the back, and the large cavity is formed on the frontside.

7) Spin photoresist, expose mask 2, and develop

8) Using handle wafer, DRIE the channels to connect the two large cavities to depth of 75 micrometer.

9) On the backside, Spin photoresist, expose mask 4, and develop

155

10) E-beam deposit chromium, followed by copper and gold

11) Anodically bond pyrex wafer

12) Die-saw individual devices.

Nitride

Silicon

Nitride

Starting wafer for step 1

Inlet/Outlet
Ports

Wafer after step 6 of fabrication process

Wafer after step 8 of fabrication process

Final chip
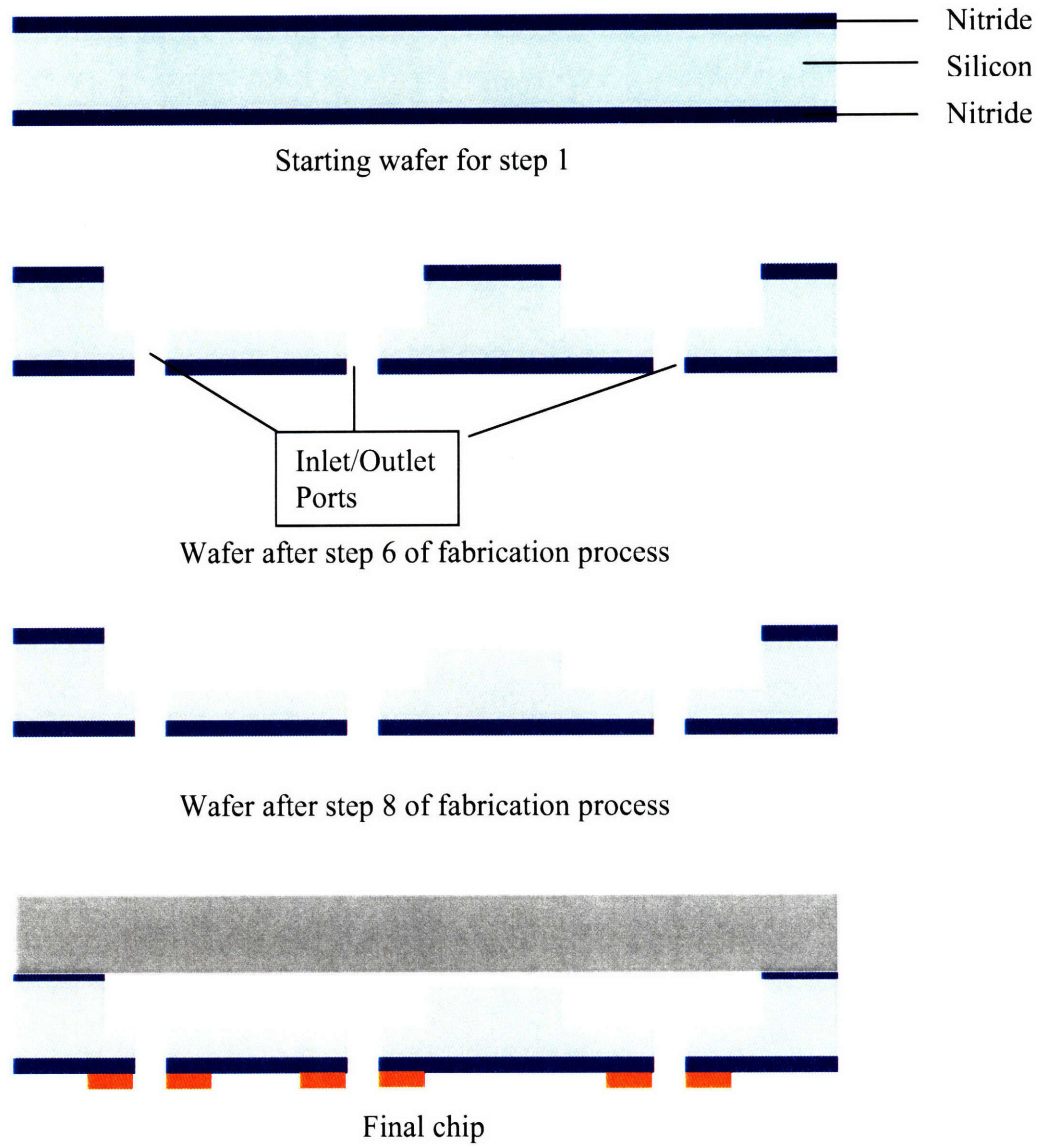
Figure C-3 Schematic of fabrication steps

As seen from Figure C-4, four different types of devices were fabricated from a single wafer. 26 devices of size 15 mm x 20 mm, and 2 devices of size 30 mm x 40 mm were the yield from a single wafer. The shallow pit connecting the deep cavities had channels

present in half the devices while they were absent in the other half. While the channels help increase the resistance for liquid to flow up the gas side, it makes matters worse for wetting liquids as the channels aid in wicking up the liquid. Therefore, both kinds of devices were fabricated to present an option to the user. The dimensions of the microchip are presented in Figure C-5.
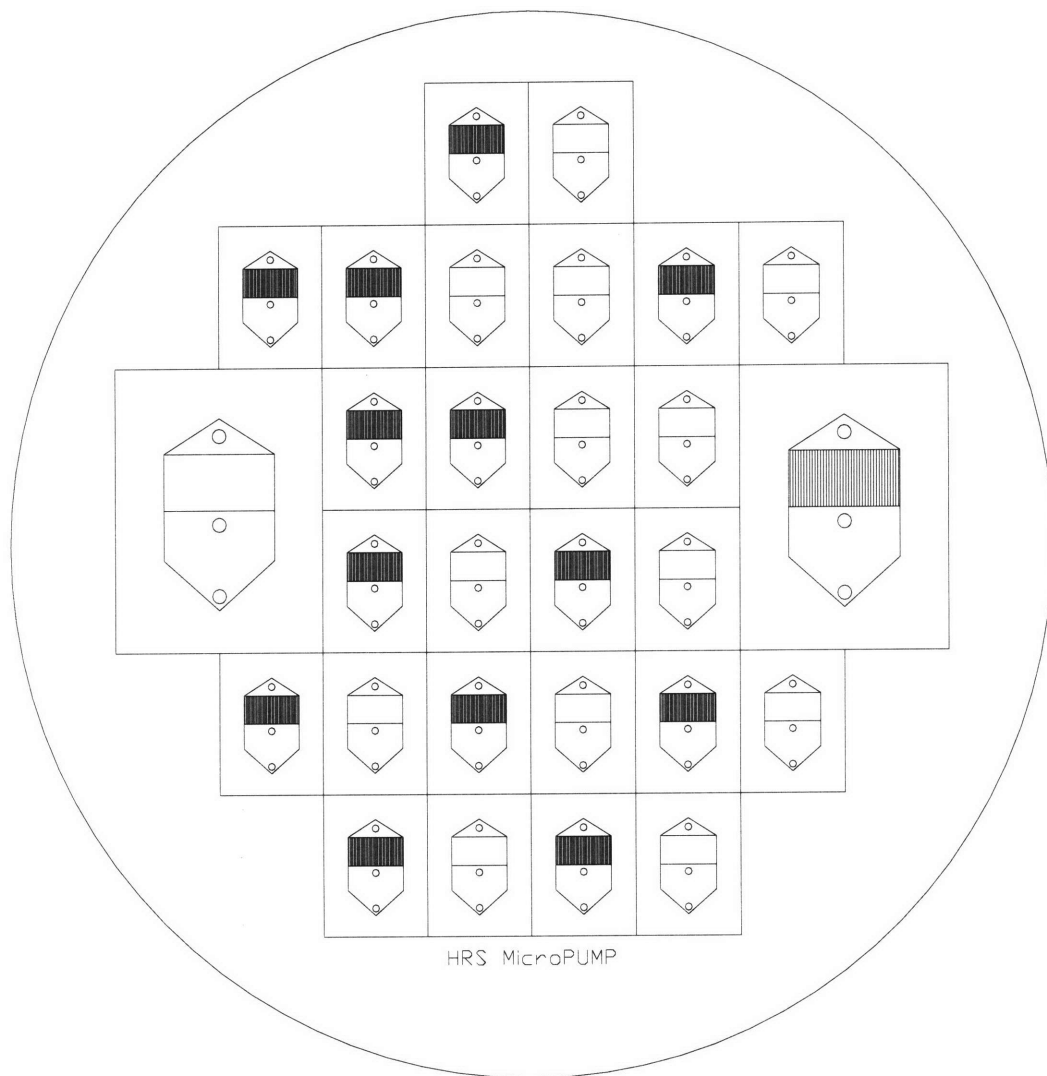
Figure C-4 Final device layout on a six-inch silicon wafer
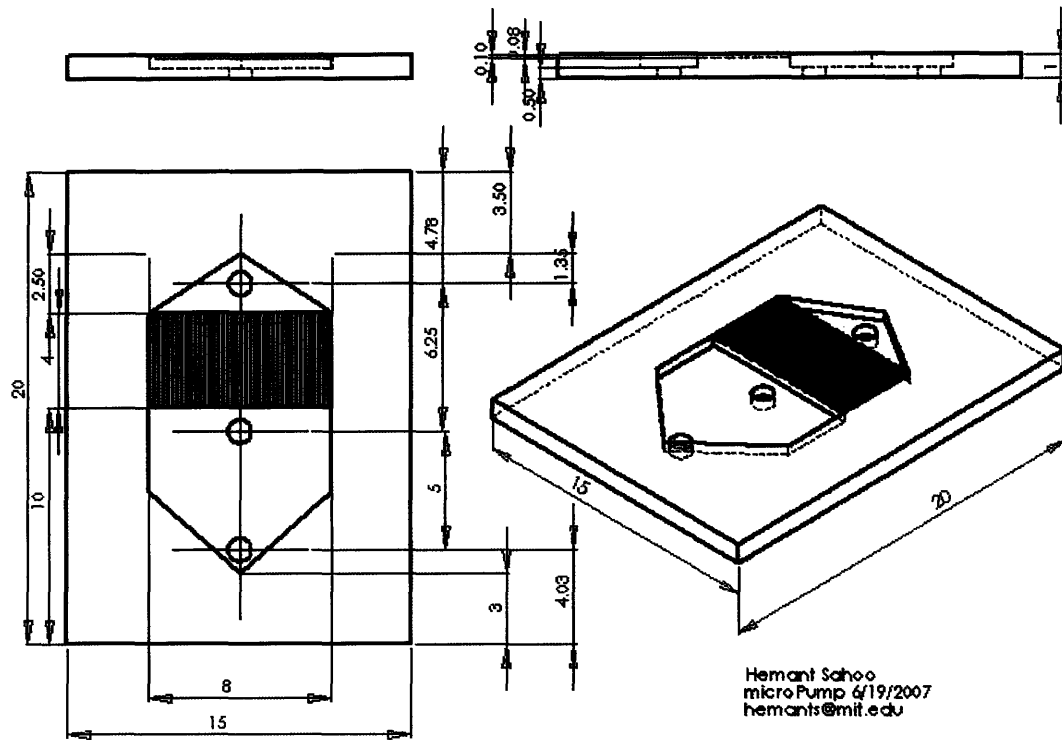
Figure C-5 Dimensions of the 15x20 mm microchip. The 30x40mm microchip has the same proportion except for the channel width and port size that are the same dimension. Units used is millimeter.

158

C.1.3 Masks

The masks used for the microchip fabrication are presented below. The dimensions are presented in Figure C-5

Figure C-6 Mask-1 for ports on the backside of a 150 mm diameter silicon wafer

Figure C-7 Mask -2 for etching shallow trench and channels.

Figure C-8 Mask-3 for etching deep cavity in microdevice.
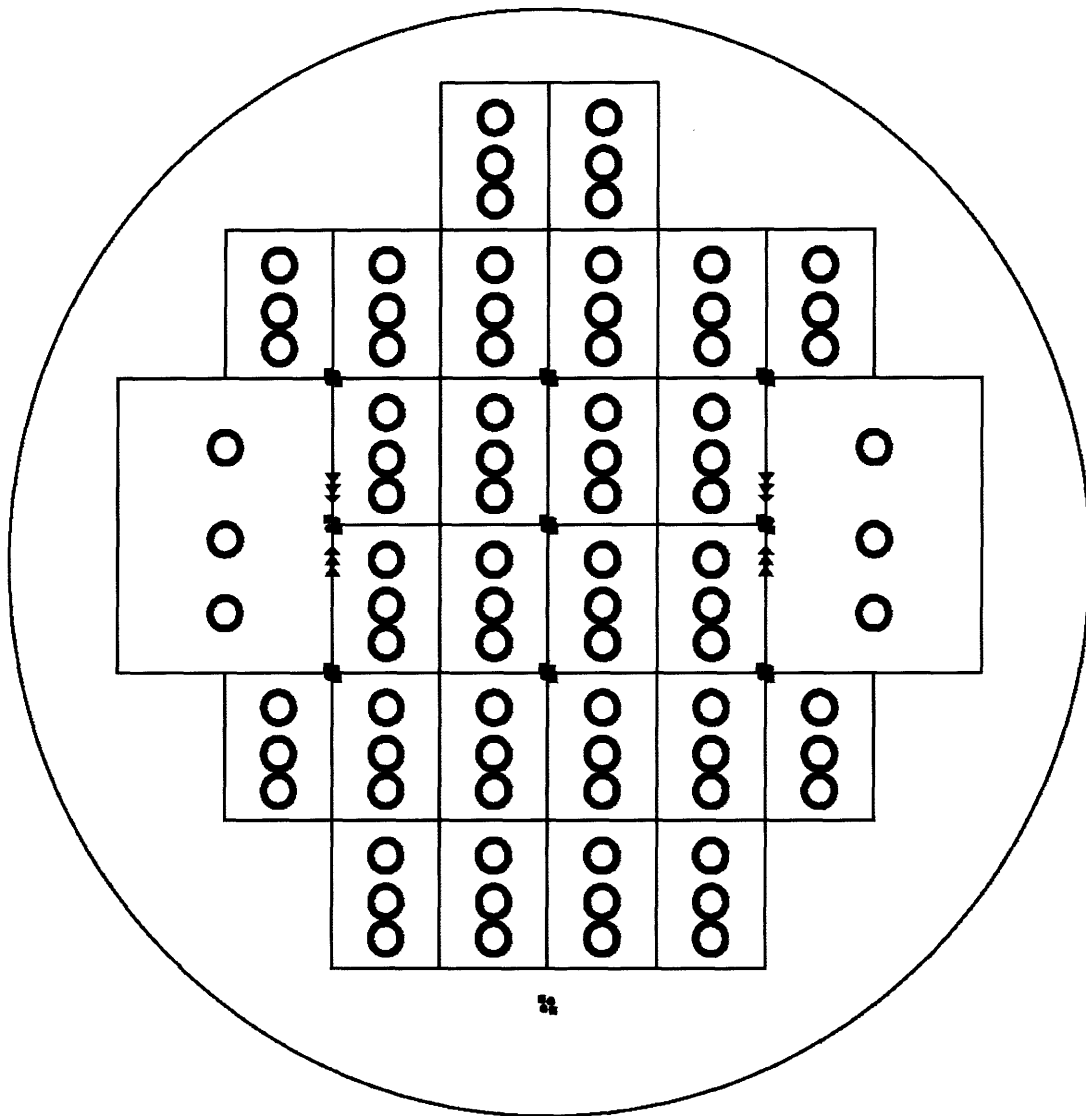
Figure C-9 Mask-4 for cavity on the frontside of a 150 mm diameter silicon wafer. Two different size devices are designed.

C.2 Microchip Packaging

C.2.1 Soldering

Tube to chip soldering was used to package the chips. A custom stand as shown in Figure C-10 was machined to align the tubes when the chip fitted in the space at the stand bottom. It is important to add weight at the top of the tubes to ensure proper contact and soldering of the tubes with the microchip.

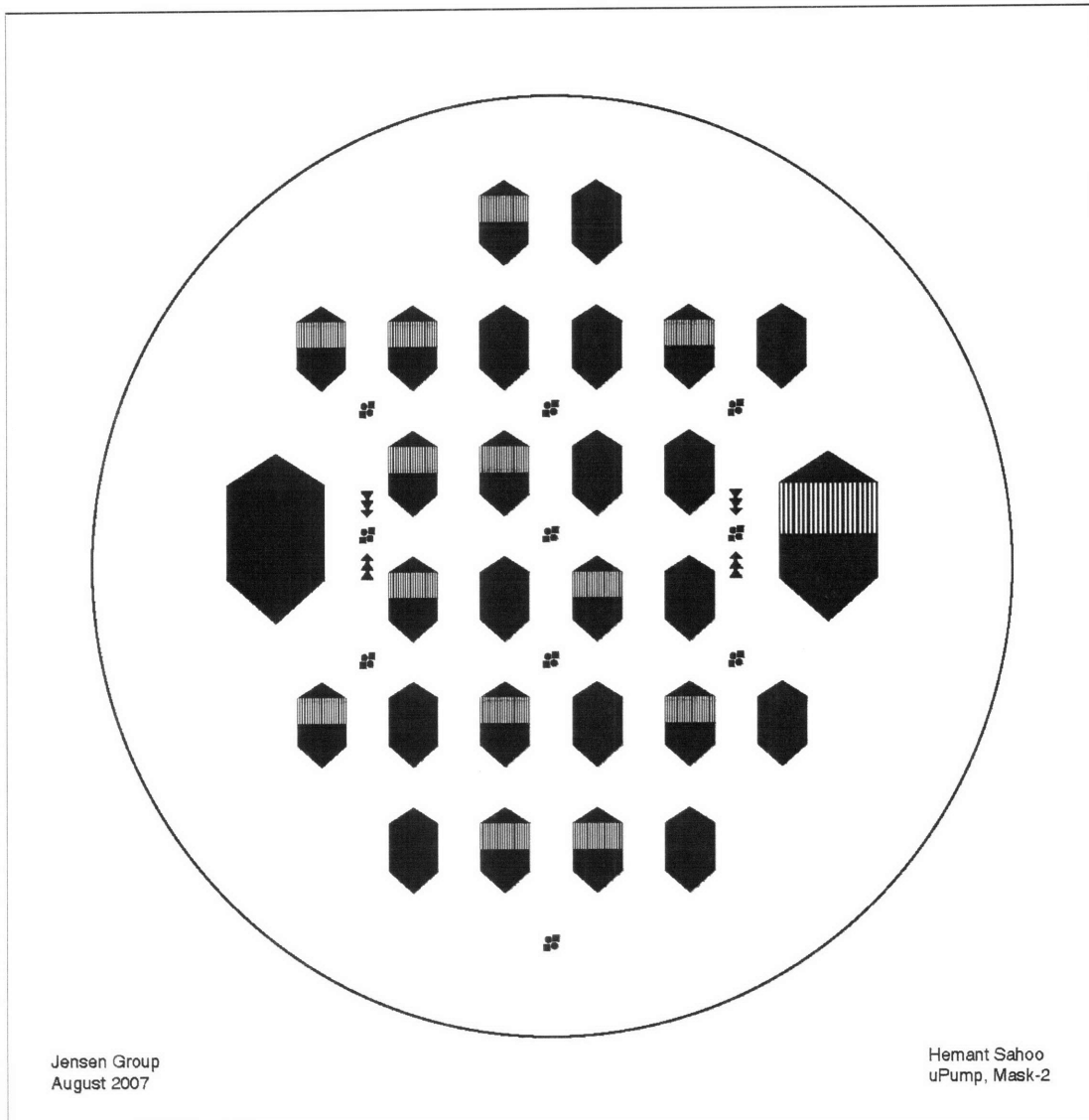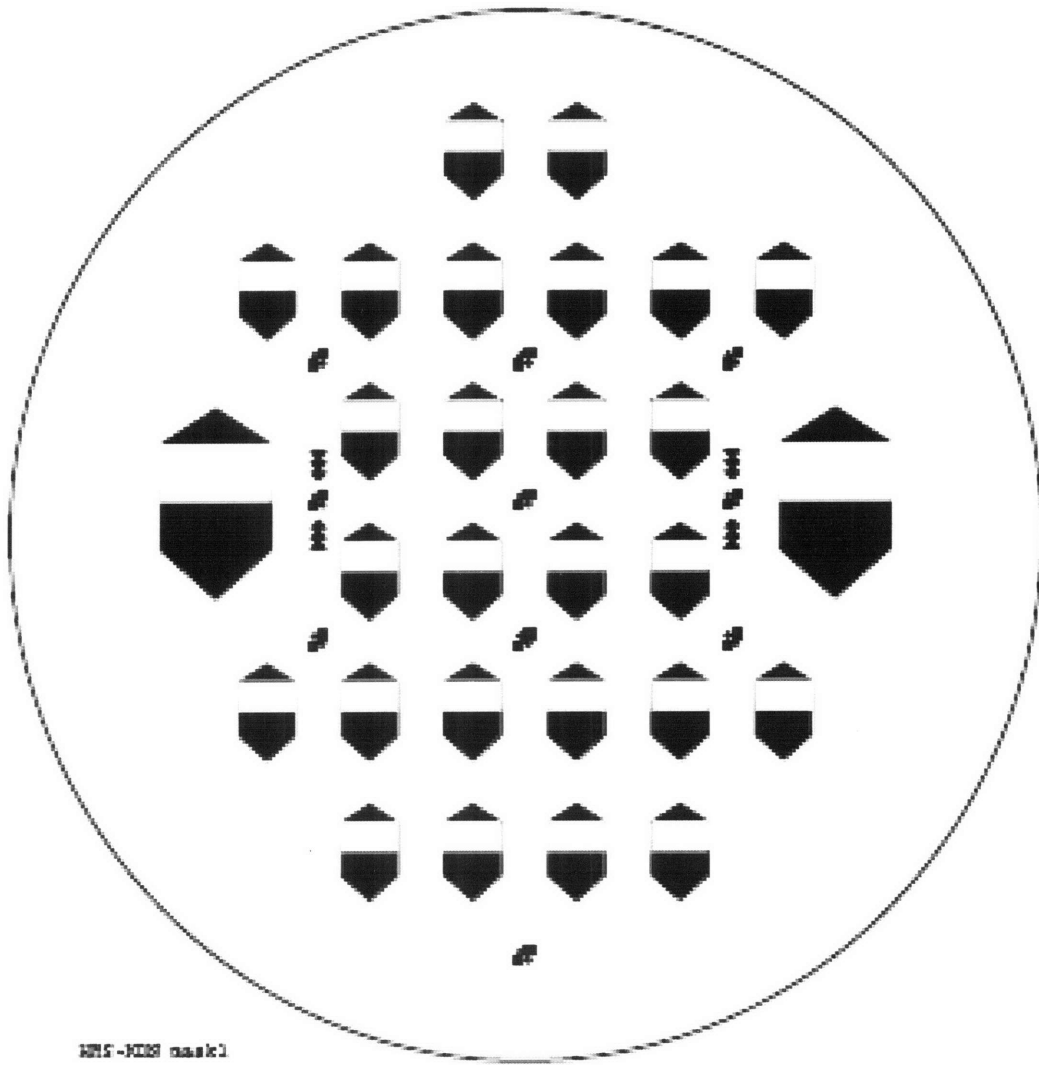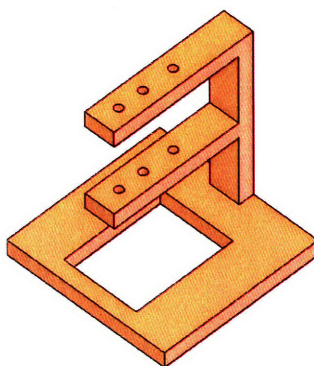**Figure C-10 Schematic of stand used to solder tubes to microdevice**

C.2.2 Compression method

The compression sealing method using standard O-rings made of either viton, silicone, PVDF or teflon (depending on chemical compatibility) was used when the soldering method was not possible, as when the tubing was too small to permit catalyst loading after packaging. Loading before packaging would damage the catalyst at the high temperature of soldering. The packaging needs to be done carefully to avoid the silicon devices from breaking. Compression methods are useful when the clearance between ports is too small to permit soldering or use of Nanotight fittings (discussed next).
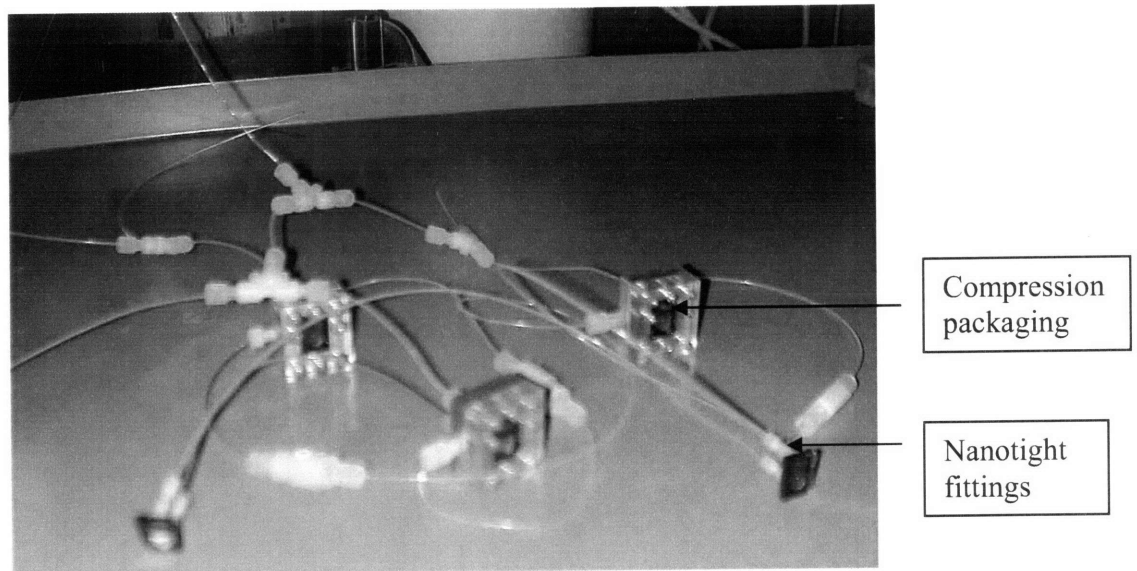
Figure C-11 Microchips with compression seal, as well as Nanotight packaging

C.2.3 Nanotight fittings

Nanotight fittings from Upchurch Scientific (part number N-333) were used to connect standard tubing to the inlet/outlet ports. It requires at least 9 mm clearance between ports for successful bonding.

Appendix D - Design of Vial Holder

The vial holder was designed to serve as pressure chamber to flow liquid out when pressurized, and have a quick connect feature to present the ability to easily change reagents. Glass was the only wetted material, besides the tubing that dipped in the liquid to flow in/out. An O-ring made a pressure-tight seal. A 90^0 turn disengaged the setup and freed the glass vial for refilling/replacement. The pressure setup was tested to consistently hold pressure up till 200 psi. It was also used to liquefy ammonia at 25 atmospheres. Beyond 200 psi, the pressure seal depended on how well the compression using nuts and bolts was performed. For experiments involving multiple pressurized chambers, a 4-vial setup was designed and machined, as shown in Figure D-2

1 cm
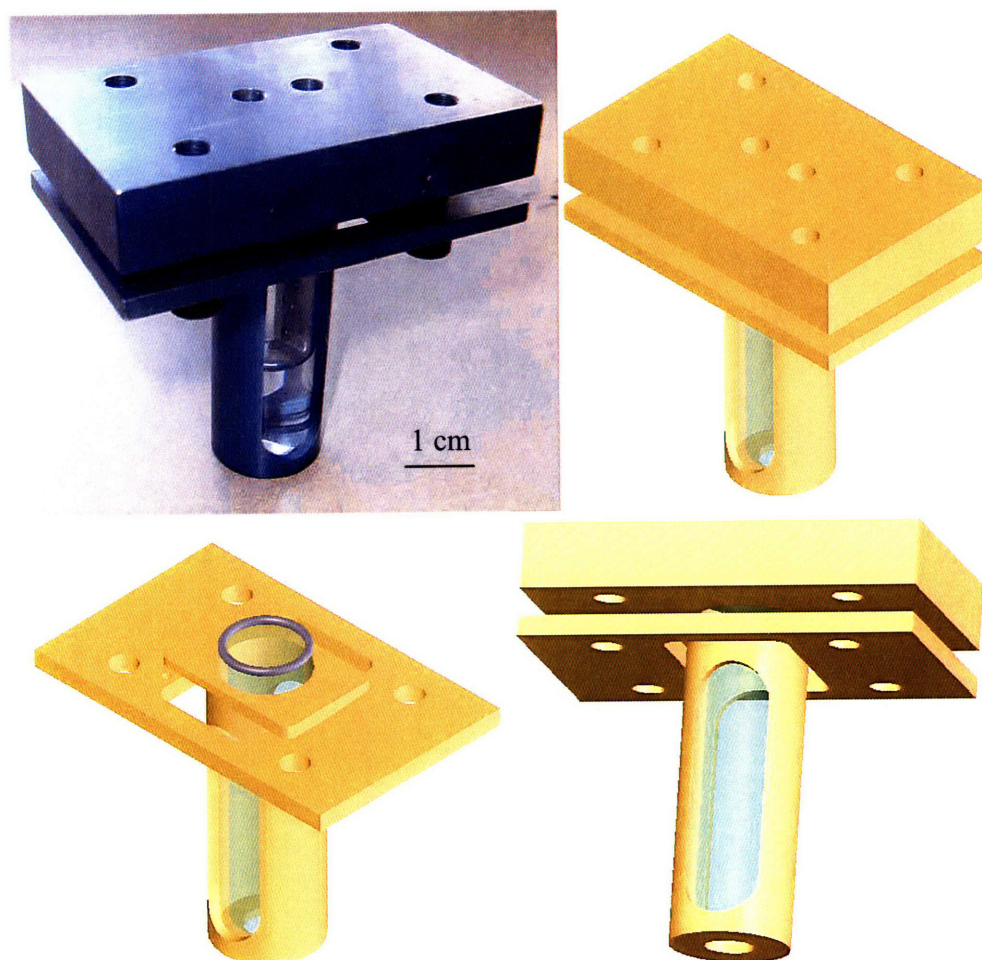
Figure D-1 Construction details with photograph of the vial holder
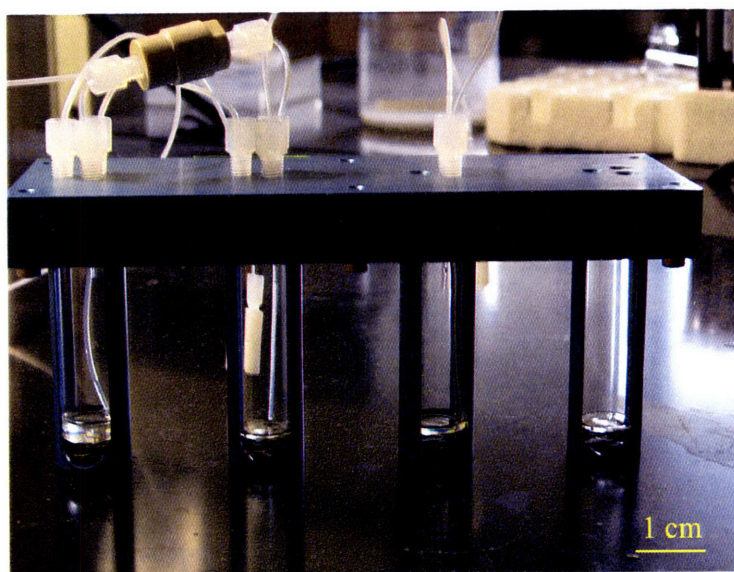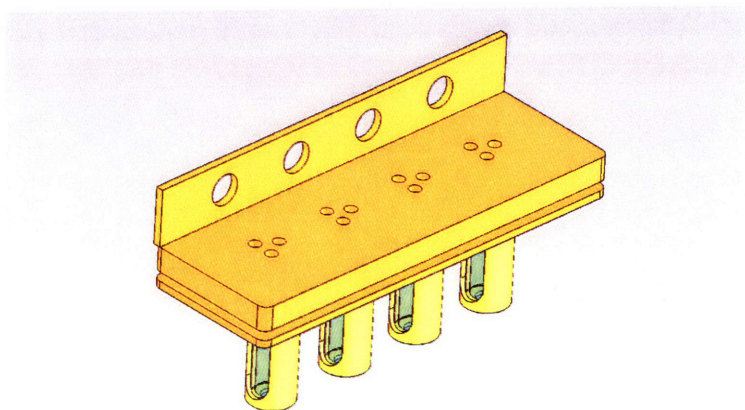
Figure D-2 Schematic and photograph of the 4-vial holder

Appendix E - Component Engineering Drawings

The CAD files used to machine the assembly components are presented next-

1) Vial-Holder
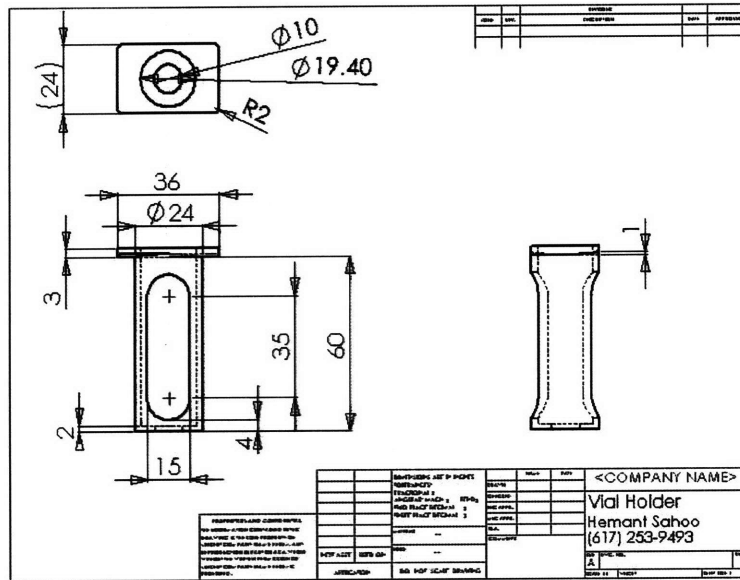
2) Bottom plate for Individual Holder
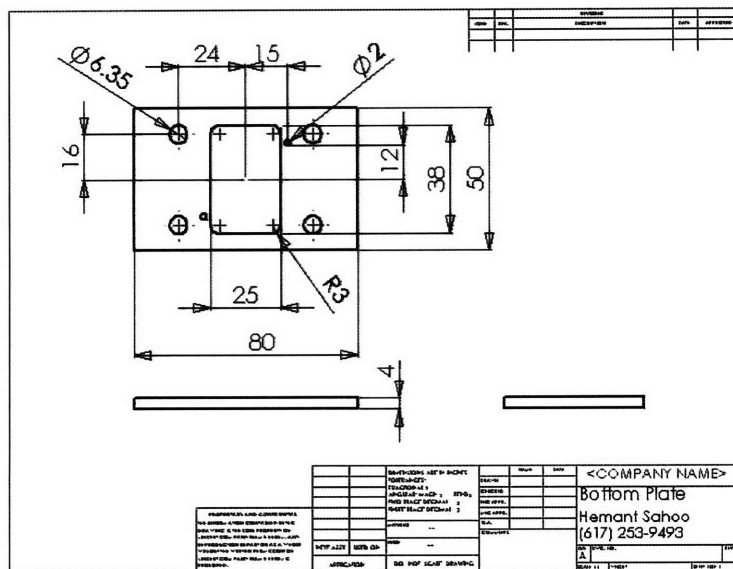
3) Glass Shell Vial, 3 dram

4) O-Ring for seal

168

5) Top Plate for Individual Vial Holder
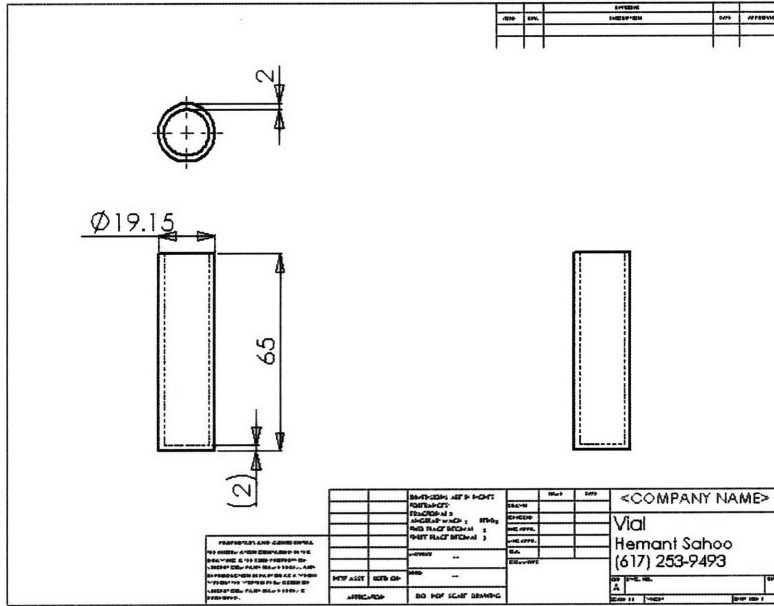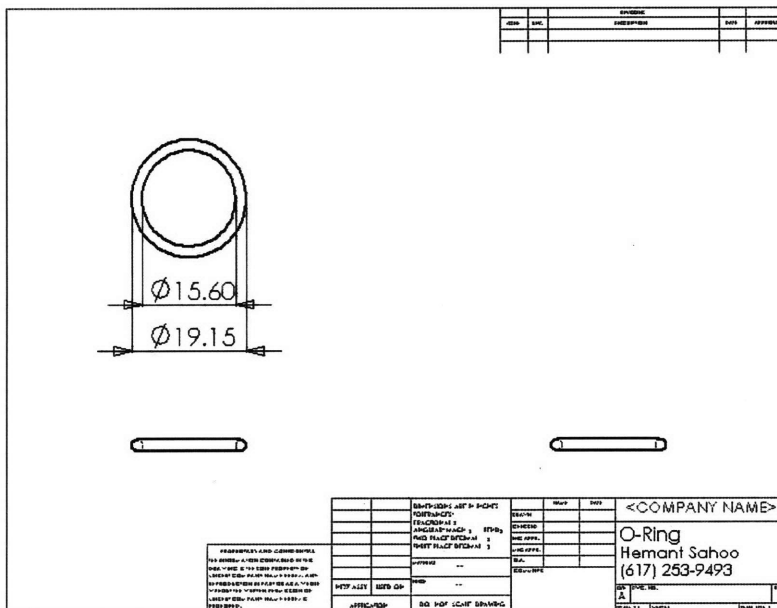
6) Top Plate for 4-Vial Holder
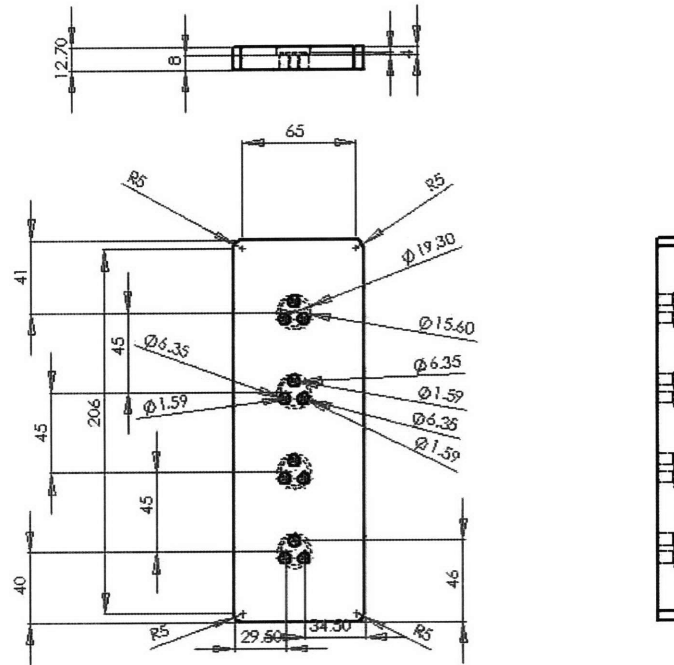
Hemant Sahoo
hemants@mit.edu
66-125; x21459
Chemical Eng., MIT

7) Bottom Plate for 4-Vial Holder
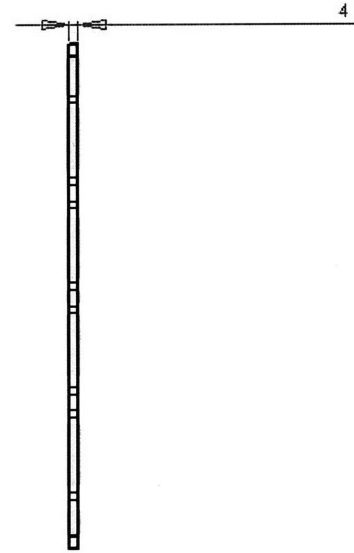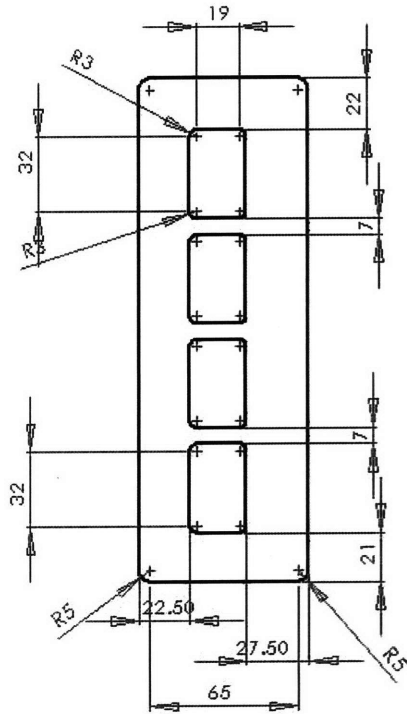
Hemant Sahoo
hemants@mit.edu
66-125; x21459
Chemical Eng., MIT

8) Modular Separator – Upper part
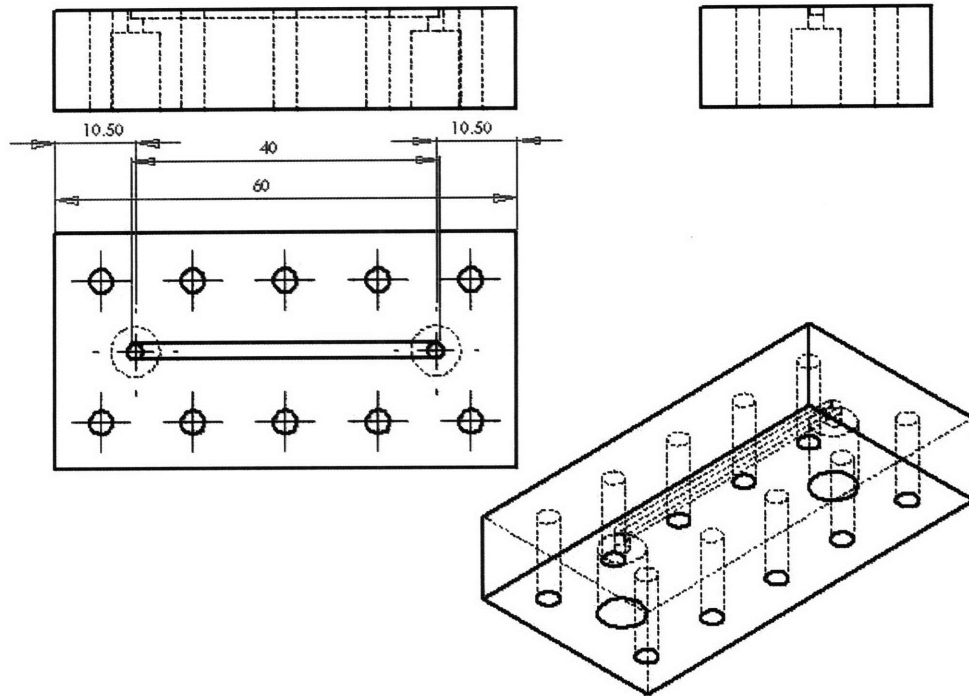
9) Modular Separator – Lower part
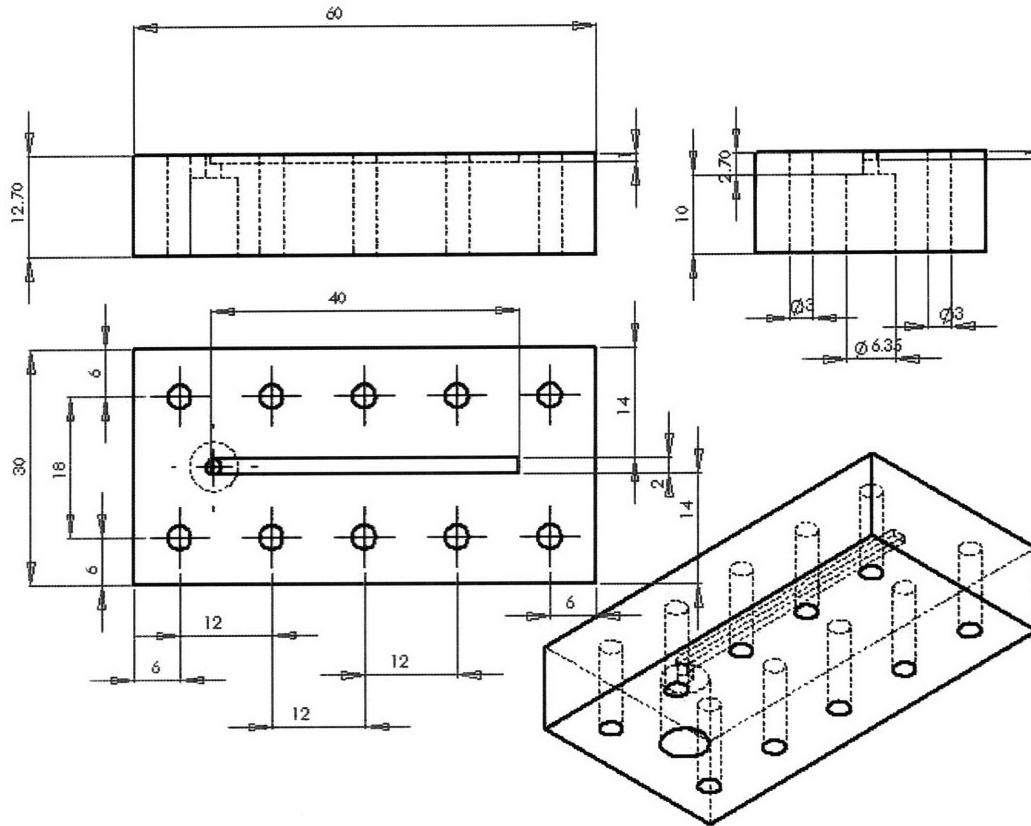
References

1. Service, R. F., Miniaturization Puts Chemical Plants Where You Want Them. *Science* **1998**, 282, (5388), 400.

2. Manz, A.; Graber, N.; Widmer, H. M., Miniaturized Total Chemical-Analysis Systems - a Novel Concept For Chemical Sensing. *Sensors and Actuators B-Chemical* **1990**, 1, (1-6), 244-248.

3. Manz, A.; Harrison, D. J.; Verpoorte, E. M. J.; Fettinger, J. C.; Ludi, H.; Widmer, H. M., Miniaturization of Chemical-Analysis Systems - a Look Into Next Century Technology or Just a Fashionable Craze. *Chimia* **1991**, 45, (4), 103-105.

4. Manz, A.; Miyahara, Y.; Miura, J.; Watanabe, Y.; Miyagi, H.; Sato, K., Design of an Open-Tubular Column Liquid Chromatograph Using Silicon Chip Technology. *Sensors and Actuators B-Chemical* **1990**, 1, (1-6), 249-255.

5. Ehrfeld, W.; Hessel, V.; Lowe, H., *Microreactors: New Technology for Modern Chemistry*. Wiley-VCH.: Weinheim, Germany, 2000.

6. Jensen, K. F., Microchemical systems: status, challenges, and opportunities. *AIChE Journal* **1999**, 45, (10), 2051-2054.

7. Bassous, E.; Taub, H. H.; Kuhn, L., Ink jet printing nozzle arrays etched in silicon. *Applied Physics Letters* **1977**, 31, (2), 135-137.

8. Terry, S. C.; Jerman, J. H.; Angell, J. B., A gas chromatographic air analyzer fabricated on a silicon wafer. *IEEE Transactions on Electron Devices* **1979**, ED-26, 1880-1886.

9. Ratner, D. M.; Murphy, E. R.; Jhunjhunwala, M.; Snyder, D. A.; Jensen, K. F.; P. H. Seeberger, Microreactor-based reaction optimization in organic chemistry - Glycosylation as a challenge. *Chem. Commun.* **2005**, 5, (5), 578-580.

10. http://www.syrris.com/category/3.aspx. *Syrris Ltd. 27 Jarman Way, Royston, Herts SG8 5HW, United Kingdom* **30 June 2008**.

11. http://www.micronit.com/. *Micronit Microfluidics BV, Colosseum 15, 7521 PV Enschede, Netherlands* **30 June 2008**.

12. Jensen, K. F., Silicon-based microchemical systems: Characteristics and applications. *Mrs Bulletin* **2006**, 31, (2), 101-107.

13. Hessel, V.; Lowe, H.; Stange, T., Micro chemical processing at IMM - from pioneering work to customer-specific services. *Lab on a Chip* **2002**, 2, (1), 14N-21N.

14. Meschke, F.; Riebler, G.; Hessel, V.; Schuerer, J.; Bairer, T., Hermetic gas-tight ceramic microreactors. *Chemical Engineering & Technology* **2005**, 28, (4), 465-473.

15. Whitesides, G. M.; Ostuni, E.; Takayama, S.; Jiang, X. Y.; Ingber, D. E., Soft lithography in biology and biochemistry. *Annual Review of Biomedical Engineering* **2001**, 3, 335-373.

16. Whitesides, G. M.; Stroock, A. D., Flexible methods for microfluidics. *Physics Today* **2001**, 54, (6), 42-48.

17. http://www.epigem.co.uk/. *Epigem Limited, Malmo Court, Kirkleatham Business Park, Redcar, TS10 5SQ, UK* **30 June 2008**.

18. Madou, M. J., *Fundamentals of Microfabrication: The Science of Miniaturization.* 2nd ed.; CRC Press: Boca Raton, Florida, 2002.

19. El-Ali, J.; Sorger, P. K.; Jensen, K. F., Cells on chips. *Nature* **2006**, 442, (7101), 403-411.

20. Khan, S. A.; Guenther, A.; Schmidt, M. A.; Jensen, K. F., Microfluidic Synthesis of Colloidal Silica. *Langmuir* **2004**, 20, (20), 8604-8611.

21. Yen, B. K. H.; Gunther, A.; Schmidt, M. A.; Jensen, K. F.; Bawendi, M. G., A microfabricated gas-liquid segmented flow reactor for high-temperature synthesis: The case of CdSe quantum dots. *Angewandte Chemie-International Edition* **2005**, 44, (34), 5447-5451.

22. Wilhite, B. A.; Schmidt, M. A.; Jensen, K. F., Palladium-based micromembranes for hydrogen separation: Device performance and chemical stability. *Industrial & Engineering Chemistry Research* **2004**, 43, (22), 7083-7091.

23. Hessel, V.; Hardt, S.; Löwe, H., *Chemical Micro Process Engineering : Fundamentals, Modelling and Reactions.* John Wiley and Sons: 2004.

24. Jensen, K. F., Microreaction engineering - is small better? *Chemical Engineering Science* **2001**, 56, (2), 293-303.

25. Jensen, K. F., Silicon-based microreactors. In *Microreactor Technology And Process Intensification*, 2005; Vol. 914, pp 2-22.

26. Floyd, T. M.; Schmidt, M. A.; Jensen, K. F., Silicon Micromixers with Infrared Detection for Studies of Liquid-Phase Reactions. *Industrial & Engineering Chemistry Research* **2005**, 44, (8), 2351-2358.

27. Lob, P.; Drese, K. S.; Hessel, V.; Hardt, S.; Hofmann, C.; Lowe, H.; Schenk, R.; Schonfeld, F.; Werner, B., Steering of liquid mixing speed in interdigital micro

mixers - from very fast to deliberately slow mixing. *Chemical Engineering & Technology* **2004,** 27, (3), 340-345.

28. Hessel, V.; Hardt, S.; Lowe, H.; Schonfeld, F., Laminar mixing in different interdigital micromixers: I. Experimental characterization. *Aiche Journal* **2003,** 49, (3), 566-577.

29. Bokenkamp, D.; Desai, A.; Yang, X.; Tai, Y. C.; Marzluff, E. M.; Mayo, S. L., Microfabricated silicon mixers for submillisecond quench-flow analysis. *Analytical Chemistry* **1998,** 70, (2), 232-236.

30. Haverkamp, V.; Ehrfeld, W.; Gebauer, K.; Hessel, V.; Lowe, H.; Richter, T.; Wille, C., The potential of micromixers for contacting of disperse liquid phases. *Fresenius Journal of Analytical Chemistry* **1999,** 364, (7), 617-624.

31. Hessel, V.; Lowe, H.; Schonfeld, F., Micromixers - a review on passive and active mixing principles. *Chemical Engineering Science* **2005,** 60, (8-9), 2479-2501.

32. Murphy, E. R.; Martinelli, J. R.; Zaborenko, N.; Buchwald, S. L.; Jensen, K. F., Accelerating Reactions with Microreactors at Elevated Temperatures and Pressures: Profiling Aminocarbonylation Reactions. *Angew. Chem. Int. Ed.* **2007,** 46, 1734-1737

33. Murphy, E. R.; Inoue, T.; Sahoo, H. R.; Zaborenko, N.; Jensen, K. F., Solder-based chip-to-tube and chip-to-chip packaging for microfluidic devices. *Lab on a Chip* **2007,** 7, 1309-1314.

34. Stankiewicz, A. I.; J.A. Moulijn, Process Intensification: Transforming Chemical Engineering. *Chem. Eng. Prog.* **2000,** (1), 22-34.

35. Internal Material Library of the Finite Element Method Simulation Software - FEMLAB 3.0

36. de Mas, N.; Guenther, A.; Schmidt, M. A.; Jensen, K. F., Microfabricated multiphase reactors for the selective direct fluorination of aromatics. *Industrial & Engineering Chemistry Research* **2003,** 42, (4), 698-710.

37. Hessel, V.; Ehrfeld, W.; Golbig, K.; Haverkam, V.; Lowe, H.; Storz, M.; Wille, C.; Guber, A.; Baerns, M. In *Gas/Liquid microreactors for direct fuorination of aromatics using elemental fluorine,* Third International Conference on Microreaction Technology, Frankfurt, Germany, 1999; Ehrfeld, W., Ed. Springer: Frankfurt, Germany, 1999.

38. Kobayashi, J.; Mori, Y.; Okamoto, K.; Akiyama, R.; Ueno, M.; Kitamori, T.; Kobayashi, S., A microfluidic device for conducting gas-liquid-solid hydrogenation reactions. *Science* **2004,** 304, (5675), 1305-1308.

39. Losey, M. W.; Schmidt, M. A.; Jensen, K. F., Microfabricated multiphase packed-bed reactors: Characterization of mass transfer and reactions. *Industrial & Engineering Chemistry Research* **2001**, 40, (12), 2555-2562.

40. Wada, Y.; Schmidt, M. A.; Jensen, K. F., Flow distribution and ozonolysis in gas-liquid multichannel microreactors *Ind. Eng. Chem. Res.* **2006** 45, 8036-8042.

41. Watts, P.; Haswell, S. J., Continuous flow reactors for drug discovery. *Drug Discovery Today* **2003**, 8, (13), 586-593.

42. Wiles, C.; Watts, P.; Haswell, S. J.; Pombo-Villar, E., The application of microreactor technology for the synthesis of 1,2-azoles. *Organic Process Research & Development* **2004**, 8, (1), 28-32.

43. Baumann, M.; Baxendale, I. R.; Ley, S. V.; Smith, C. D.; Tranmer, G. K., Fully automated continuous flow synthesis of 4,5-disubstituted oxazoles. *Organic Letters* **2006**, 8, (23), 5231-5234.

44. Baxendale, I. R.; Griffiths-Jones, C. M.; Ley, S. V.; Tranmer, G. K., Preparation of the neolignan natural product grossamide by a continuous-flow process. *Synlett* **2006**, (3), 427-430.

45. Hessel, V.; Lowe, H., Organic synthesis with microstructured reactors. *Chemie Ingenieur Technik* **2004**, 76, (5), 535-554.

46. Lee, C. C.; Sui, G. D.; Elizarov, A.; Shu, C. Y. J.; Shin, Y. S.; Dooley, A. N.; Huang, J.; Daridon, A.; Wyatt, P.; Stout, D.; Kolb, H. C.; Witte, O. N.; Satyamurthy, N.; Heath, J. R.; Phelps, M. E.; Quake, S. R.; Tseng, H. R., Multistep synthesis of a radiolabeled imaging probe using integrated microfluidics. *Science* **2005**, 310, (5755), 1793-1796.

47. Baxendale, I. R.; Deeley, J.; Griffiths-Jones, C. M.; Ley, S. V.; Saaby, S.; Tranmer, G. K., A flow process for the multi-step synthesis of the alkaloid natural product oxomaritidine: a new paradigm for molecular assembly. *Chemical Communications* **2006**, (24), 2566-2568.

48. http://www.cpc-net.com/. *Cellular Process Chemistry Systems* **30 June 2008**.

49. http://www.imm-mainz.de/seiten/en/index.php. *Institut für Mikrotechnik Mainz GmbH Carl-Zeiss-Strasse 18-20 55129 Mainz* **30 June 2008**.

50. http://www.thalesnano.com/. *ThalesNano Nanotechnology Inc, H-1031 Budapest, Záhony u. 7., Graphisoft Park, Hungary* **30 June 2008**.

51. Maruyama, T.; Matsushita, H.; Uchida, J.-i.; Kubota, F.; Kamiya, N.; Goto, M., Liquid Membrane Operations in a Microfluidic Device for Selective Separation of Metal Ions. *Analytical Chemistry* **2004**, 76, (15), 4495-4500.

52. Tokeshi, M.; Kikutani, Y.; Hibara, A.; Sato, K.; Hisamoto, H.; Kitamori, T., Chemical processing on microchips for analysis, synthesis, and bioassay. *Electrophoresis* **2003,** 24, (21), 3583-3594.

53. Tokeshi, M.; Minagawa, T.; Kitamori, T., Integration of a microextraction system on a glass chip: Ion-pair solvent extraction of Fe(II) with 4,7-diphenyl-1,10-phenanthrolinedisulfonic acid and tri-n-octylmethylammonium chloride. *Analytical Chemistry* **2000,** 72, (7), 1711-1714.

54. MIT-Novartis Center for Continuous Manufacturing. *http://web.mit.edu/newsoffice/2007/novartis-0928.html* **28 September 2007.**

55. Gunther, A.; Jensen, K. F., Multiphase microfluidics: from flow characteristics to chemical and materials synthesis. *Lab on a Chip* **2006,** 6, (12), 1487-1503.

56. Aota, A.; Nonaka, M.; Hibara, A.; Kitamori, T., Micro counter-current flow system for highly efficient extraction. *Proceedings, 7th Intl. Conf. on Miniaturized Chem. and Biochem. Anal. Systems* **2003,** 441-444.

57. Hisamoto, H.; Tokeshi, M.; Hibara, A.; Kitamori, T., Molecular transport and extraction in liquid microspace - a key to develop microchemical systems. *Journal of Ion Exchange* **2003,** 14, (1), 38-43.

58. Maruyama, T.; Kaji, T.; Ohkawa, T.; Sotowa, K.-i.; Matsushita, H.; Kubota, F.; Kamiya, N.; Kusakabe, K.; Goto, M., Intermittent partition walls promote solvent extraction of metal ions in a microfluidic device. *Analyst (Cambridge, United Kingdom)* **2004,** 129, (11), 1008-1013.

59. Tokeshi, M.; Minagawa, T.; Kitamori, T., Integration of a Microextraction System on a Glass Chip: Ion-Pair Solvent Extraction of Fe(II) with 4,7-Diphenyl-1,10-phenanthrolinedisulfonic Acid and Tri-n-octylmethylammonium Chloride. *Anal. Chem.* **2000,** 72, 1711-1714.

60. Tokeshi, M.; Minagawa, T.; Uchiyama, K.; Hibara, A.; Sato, K.; Hisamoto, H.; Kitamori, T., Continuous-Flow Chemical Processing on a Microchip by Combinging Microunit Operations and a Multiphase Flow Network. *Anal. Chem.* **2002,** 74, 1565-1571.

61. Wojik, A.; Marr, R., Mikroverfahrenstechnicsche Prinzipien in der Fluessig/Fluessig-Extraktion. *Chemie Ingenieur Technik* **2005,** 77, (6), 653-668.

62. Burns, J. R.; Ramshaw, C., The intensification of rapid reactions in multiphase systems using slug flow in capillaries. *Lab-on-a-chip* **2001,** 1, 10-15.

63. Gunther, A.; Jhunjhunwala, M.; Thalmann, M.; Schmidt, M. A.; Jensen, K. F., Micromixing of miscible liquids in segmented gas-liquid flow. *Langmuir* **2005,** 21, (4), 1547-1555.

64.   Song, H.; Tice, J. D.; Ismagilov, R. F., A microfluidic system for controlling reaction networks in time. *Angewandte Chemie-International Edition* **2003**, 42, (7), 768-772.

65.   Benz, K.; Jaeckel, K.-P.; Regenauer, K.-J.; Schiewe, J.; Drese, K.; Ehrfeld, W.; Hessel, V.; Loewe, H., Utilization of micromixers for extraction processes. *Chemical Engineering & Technology* **2001**, 24, (1), 11-17.

66.   Burns, J. R.; Ramshaw, C., A microreactor for the nitration of benzene and toluene. *Chemical Engineering Communications* **2002**, 189, (12), 1611-1628.

67.   Kralj, J. G.; Schmidt, M. A.; Jensen, K. F., Surfactant-enhanced liquid-liquid extraction in microfluidic channels with inline electric-field enhanced coalescence. *Lab on a Chip* **2005**, 5, (5), 531-535.

68.   Shaw, J.; Nudd, R.; Naik, B.; Turner, C.; Rudge, D.; Benson, M.; Garman, A., Liquid/liquid extraction systems using micro-contactor arrays. *Micro Total Analysis Systems 2000, Proceedings of the mTAS Symposium, 4th, Enschede, Netherlands, May 14-18, 2000* **2000**, 371-374.

69.   Ueno, M.; Hisamoto, H.; Kitamori, T.; Kobayashi, S., Phase-transfer alkylation reactions using microreactors. *Chemical Communications* **2003**, 936-937.

70.   Wenn, D. A.; Shaw, J. E. A.; Mackenzie, B., A mesh microcontactor for 2-phase reactions. *Lab on a Chip* **2003**, 3, (3), 180-186.

71.   US Patent 6666909. **2003**.

72.   Guenther, A.; Jhunjhunwala, M.; Thalmann, M.; Schmidt, M. A.; Jensen, K. F., Micromixing of Miscible Liquids in Segmented Gas-Liquid Flow. *Langmuir* **2005**, 21, 1547-1555.

73.   Mayer, G. K.; Offereins, H. L.; Sandmaier, H.; Kuhl, K., Fabrication Of Non-Underetched Convex Corners In Anisotropic Etching Of (100)-Silicon In Aqueous Koh With Respect To Novel Micromechanic Elements. *Journal Of The Electrochemical Society* **1990**, 137, (12), 3947-3951.

74.   Zhang, Q. X.; Liu, L. T.; Li, Z. J., A new approach to convex corner compensation for anisotropic etching of (100)Si in KOH. *Sensors And Actuators A-Physical* **1996**, 56, (3), 251-254.

75.   Kreutzer, M. T.; Kapteijn, F.; Moulijn, J. A.; Heiszwolf, J. J., Multiphase monolith reactors: Chemical reaction engineering of segmented flow in microchannels. *Chemical Engineering Science* **2005**, 60, 5895-5916.

76.   Kikutani, Y.; Tokeshi, M.; Sato, K.; Kitamori, T., Integrated chemical systems on microchips for analysis and assay. Potential future, mobile high-performance

detection system for chemical weapons. *Pure and Applied Chemistry* **2002**, 74, (12), 2299-2309.

77. Sorenson, J. M.; Arlt, W., *Liquid-Liquid Equilibrium Data Collection*. Frankfurt, 1979.

78. Karpenko, G. V.; Koshokov, A. B.; Koryakov, N. Y.; Poltoratskii, G. M.; Rogachev, V. L., Liquid-phase equilibrium in the water-dimethylformamide-organic solvent three-component systems. *Zhurnal Prikladnoi Khimii (Sankt-Peterburg, Russian Federation)* **1979**, 52, (9), 2109-12.

79. Treybal, R. E., *Mass-Transfer Operations*. 3rd ed.; McGraw-Hill: London, 1981.

80. Unger, M. A.; Chou, H. P.; Thorsen, T.; Scherer, A.; Quake, S. R., Monolithic microfabricated valves and pumps by multilayer soft lithography. *Science* **2000**, 288, (5463), 113-116.

81. Atencia, J.; Beebe, D. J., Steady flow generation in microcirculatory systems. *Lab on a Chip* **2006**, 6, (4), 567-574.

82. http://bartels-mikrotechnik.de/produkte/mikropumpe-lang-en.html?lang-en, Bartels Mikrotechnik GmbH, Emil-Figge-Str. 76a, D-44227 Dortmund, Germany. **30 June 2008**.

83. Futterer, C.; Minc, N.; Bormuth, V.; Codarbox, J. H.; Laval, P.; Rossier, J.; Viovy, J. L., Injection and flow control system for microchannels. *Lab on a Chip* **2004**, 4, (4), 351-356.

84. de Mas, N.; Günther, A.; Kraus, T.; Schmidt, M. A.; Jensen, K. F., Scaled-out multilayer gas-liquid microreactor with integrated velocimetry sensors. *Industrial & Engineering Chemistry Research* **2005**, 44, (24), 8997-9013.

85. The resolution in flowrate units is dependant on the system and is affected by the resistances in the system, and the calibration curve between measured voltage signal (proportional to pressure) and flowrate.

86. Thorsen, T.; Maerkl, S. J.; Quake, S. R., Microfluidic large-scale integration. *Science* **2002**, 298, (5593), 580-584.

87. Fuerstman, M. J.; Garstecki, P.; Whitesides, G. M., Coding/decoding and reversibility of droplet trains in microfluidic networks. *Science* **2007**, 315, (5813), 828-832.

88. Whitesides, G. M., The origins and the future of microfluidics. *Nature* **2006**, 442, (7101), 368-373.

89. Prakash, M.; Gershenfeld, N., Microfluidic bubble logic. *Science* **2007**, 315, (5813), 832-835.

90. Dendukuri, D.; Gu, S. S.; Pregibon, D. C.; Hatton, T. A.; Doyle, P. S., Stop-flow lithography in a microfluidic device. *Lab on a Chip* **2007**, 7, (7), 818-828.

91. Aota, A.; Nonaka, M.; Hibara, A.; Kitamori, T., Countercurrent Laminar Microflow for Highly Efficient Solvent Extraction. *Angew. Chem. Int. Ed.* **2007**, 46,, 878 -880.

92. Kralj, J. G.; Sahoo, H. R.; Jensen, K. F., Integrated Continuous Microfluidic Liquid-Liquid Extraction *Lab Chip* **2007**, 7, 256 - 263.

93. Wankat, P. C., *Equilibrium Staged Separations*. 1st ed.; Prentice Hall Professional Technical Reference: 1988.

94. Schindler, M.; Ajdari, A., Droplet traffic in microfluidic networks: A simple model for understanding and designing. *Physical Review Letters* **2008**, 100, (4).

95. Jousse, F.; Farr, R.; Link, D. R.; Fuerstman, M. J.; Garstecki, P., Bifurcation of droplet flows within capillaries. *Phys Rev E Stat Nonlin Soft Matter Phys* **2006**, 74, (3 Pt 2), 036311.

96. Garstecki, P.; Fuerstman, M. J.; Whitesides, G. M., Oscillations with uniquely long periods in a microfluidic bubble generator. *Nature Physics* **2005**, 1, (3), 168-171.

97. Jousse, F.; Lian, G. P.; Janes, R.; Melrose, J., Compact model for multi-phase liquid-liquid flows in micro-fluidic devices. *Lab on a Chip* **2005**, 5, (6), 646-656.

98. Stark, J.; Manga, M., The motion of long bubbles in a network of tubes. *Transport in Porous Media* **2000**, 40, (2), 201-218.

99. Wael, S.; Asterios, G.; Panagiota, A., On the Formation of Taylor bubbles in small tubes. *Chemical Engineering Science* **2006**, 61, 6653-6666.

100. Hong, J. W.; Studer, V.; Hang, G.; Anderson, W. F.; Quake, S. R., A nanoliter-scale nucleic acid processor with parallel architecture. *Nature Biotechnology* **2004**, 22, (4), 435-439.

101. Watts, P., Solution phase synthesis of peptides using micro reactors. *Biopolymers* **2003**, 71, (3), 347-347.

102. Watts, P.; Wiles, C.; Haswell, S. J.; Pombo-Villar, E., Solution phase synthesis of beta-peptides using micro reactors. *Tetrahedron* **2002**, 58, (27), 5427-5439.

103. Lee, K.; Rouillard, J. M.; Pham, T.; Gulari, E.; Kim, J., Signal-amplifying conjugated Polymer-DNA hybrid chips. *Angewandte Chemie-International Edition* **2007**, 46, (25), 4667-4670.

181

104. Gao, X. L.; Zhou, X. C.; Gulari, E., Light directed massively parallel on-chip synthesis of peptide arrays with t-Boc chemistry. *Proteomics* **2003**, 3, (11), 2135-2141.

105. Komolpis, K.; Srivannavit, O.; Gulari, E., Light-directed simultaneous synthesis of oligopeptides on microarray substrate using a photogenerated acid. *Biotechnology Progress* **2002**, 18, (3), 641-646.

106. Pellois, J. P.; Zhou, X. C.; Srivannavit, O.; Zhou, T. C.; Gulari, E.; Gao, X. L., Individually addressable parallel peptide synthesis on microchips. *Nature Biotechnology* **2002**, 20, (9), 922-926.

107. Van der Eycken, E.; Sharpless, K. B., Click chemistry. *Qsar & Combinatorial Science* **2007**, 26, 1115-1115.

108. Hawker, C. J.; Pyun, J.; Nugent, A.; Frechet, J. M. J.; Voit, B.; Scheel, A.; Fokin, V. V.; Finn, M. G.; Feldman, A. K.; Yu, P.; Sharpless, K. B., Highly efficient approach to materials synthesis using click chemistry. *Abstracts of Papers of the American Chemical Society* **2004**, 227, U407-U407.

109. Kolb, H. C.; Sharpless, K. B., The growing impact of click chemistry on drug discovery. *Drug Discovery Today* **2003**, 8, (24), 1128-1137.

110. Kolb, H. C.; Finn, M. G.; Sharpless, K. B., Click chemistry: Diverse chemical function from a few good reactions. *Angewandte Chemie-International Edition* **2001**, 40, (11), 2004-+.

111. Sharpless, K. B.; Kolb, H. C., Click chemistry. A concept for merging process and discovery chemistry. *Abstracts of Papers of the American Chemical Society* **1999**, 217, U95-U95.

112. Wang, J. Y.; Sui, G. D.; Mocharla, V. P.; Lin, R. J.; Phelps, M. E.; Kolb, H. C.; Tseng, H. R., Integrated microfluidics for parallel screening of an in situ click chemistry library. *Angewandte Chemie-International Edition* **2006**, 45, (32), 5276-5281.

113. Pennemann, H.; Watts, P.; Haswell, S. J.; Hessel, V.; Lowe, H., Benchmarking of microreactor applications. *Organic Process Research & Development* **2004**, 8, (3), 422-439.

114. Jähnisch, K.; Hessel, V.; Lowe, H.; Baerns, M., Chemistry in microstructured reactors. *Angewandte Chemie-International Edition* **2004**, 43, (4), 406-446.

115. Hessel, V.; Lowe, H., Organic synthesis with microstructured reactors. *Chemical Engineering & Technology* **2005**, 28, (3), 267-284.

116. Fletcher, P. D. I.; Haswell, S. J.; Pombo-Villar, E.; Warrington, B. H.; Watts, P.; Wong, S. Y. F.; Zhang, X. L., Micro reactors: principles and applications in organic synthesis. *Tetrahedron* **2002**, 58, (24), 4735-4757.

117. Watts, P.; Wiles, C., Recent advances in synthetic micro reaction technology. *Chemical Communications* **2007**, (5), 443-467.

118. Watts, P.; Wiles, C., Synthesis of analytically pure compounds in flow reactors. *Chemical Engineering & Technology* **2007**, 30, (3), 329-333.

119. Jensen, K. F., Silicon-based microchemical systems: Characteristics and applications. *Mat. Res. Soc. Bulletin* **2006**, 31, (2), 101-107.

120. deMello, A. J., Control and detection of chemical reactions in microfluidic systems. *nature* **2006**, 422, 394-402.

121. Usutani, H.; Tomida, Y.; Nagaki, A.; Okamoto, H.; Nokami, T.; Yoshida, J.-i., Generation and Reactions of o-Bromophenyllithium without Benzyne Formation Using a Microreactor. *J. Am. Chem. Soc.* **2007**, 129, 3046-3047.

122. Belder, D.; Ludwig, M.; Wang, L. W.; Reetz, M. T., Enantioselective catalysis and analysis on a chip. *Angewandte Chemie-International Edition* **2006**, 45, (15), 2463-2466.

123. Günther, A.; Jensen, K. F., Multiphase microfluidics: From flow characteristics to chemical and materials synthesis. *Lab Chip* **2006**, 6, 1487-1503.

124. Tokeshi, M.; Minagawa, T.; Kitamori, T., Integration of a microextraction system - Solvent extraction of a Co-2-nitroso-5-dimethylaminophenol complex on a microchip. *Journal of Chromatography A* **2000**, 894, (1-2), 19-23.

125. Tokeshi, M.; Minagawa, T.; Uchiyama, K.; Hibara, A.; Sato, K.; Hisamoto, H.; Kitamori, T., Continuous-flow chemical processing on a microchip by combining microunit operations and a multiphase flow network. *Analytical Chemistry* **2002**, 74, (7), 1565-1571.

126. Günther, A.; Jhunjhunwala, M.; Thalmann, M.; Schmidt, M. A.; Jensen, K. F., Micromixing of Miscible Liquids in Segmented Gas-Liquid Flow. *Langmuir* **2005**, 21, 1547-1555.

127. Murphy, E. R.; Martinelli, J. R.; Zaborenko, N.; Buchwald, S. L.; Jensen, K. F., Accelerating Reactions with Microreactors at Elevated Temperatures and Pressures: Profiling Aminocarbonylation Reactions. *Angew. Chem. Int. Ed.* **2007**, 46, 1734-1737

128. Govindan, C. K., An Improved Process for the Preparation of Benzyl-N-vinyl Carbamate. *Org. Process Res. Dev.* **2002**, 6, (1), 74-77.

129. Pandey, R. K.; Dagade, S. P.; Dongare, M. K.; Kumar, P., *Synthetic Communications* **2003,** 33, 4019.

130. Angeles, E.; Martinez, P.; Keller, J.; Martinez, R.; Rubio, M.; Ramirez, G.; Castillo, R.; Lopez-Castanares, R.; Jimenez, E., *Journal of Molecular Structure-Theochem* **2000,** 504.

131. Patai, S., *Chemistry of Cyanates and Their Thio Derivatives (Chemistry of Functional Groups) Vol. 1, John Wiley and Sons Ltd, 1977.* Wiley: New York, 1977; Vol. 1 and 2.

132. L'Abbe, G., *Chemical Reviews* **1969,** 69, (3), 345.

133. Massey, L., *Permeability Properties of Plastics and Elastomers: A Guide to Packaging and Barrier Materials.* 2nd ed.; Norwich, NY, 2003.

134. Alentiev, A. Y.; Yampolskii, Y. P.; Shantarovich, V. P.; Nemser, S. M.; Plate, N. A., High transport parameters and free volume of perfluorodioxole copolymers. *Journal of Membrane Science* **1997,** 126, (1), 123-132.

135. Yasuhide, Y.; Tsuno, Y., *Journal of American Chemical Society* **1957,** 79, 5530.

136. Newman, M. S.; Lee, S. H.; Garrett, A. B., *Journal of American Chemical Society* **1947,** 69, 113.

137. Yukawa, Y.; Tsuno, Y., *Journal of American Chemical Society* **1959,** 81, 2007.

138. Sivakamasundari, S.; R. Ganesan, *Journal of Organic Chemistry* **1984,** 49, 720.

139. Vandenberg, H. R.; Tenseldam, C. A.; Vandergulik, P. S., Compressible Laminar-Flow in a Capillary. *Journal of Fluid Mechanics* **1993,** 246, 1-20.